DESIGN, ANALYSIS, AND THEORETICAL BOUNDS IN ACOUSTIC AND RF SENSOR NETWORKS

by

MIAO PENG

YANG XIAO, COMMITTEE CHAIR

XIAOYAN HONG
SUSAN V. VRBSKY
PU WANG
JINGYUAN ZHANG

A DISSERTATION

Submitted in partial fulfillment of the requirements
for the degree of Doctor of Philosophy
in the Department of Computer Science
in the Graduate School of
The University of Alabama

TUSCALOOSA, ALABAMA

2012

ABSTRACT

Wireless sensor networks (WSNs) have many important applications such as monitoring and tracking. Unlike traditional networks, a WSN has its own constraints, such as a limited amount of energy, short communication range, low bandwidth, and limited processing and storage in each sensor node. As a result, it is necessary to introduce new design concepts, create or improve existing protocols, and develop new algorithms in WSNs.

This dissertation addresses several important issues in wireless sensor network design and performance analysis. We first investigate the fundamental performance limits of medium access control (MAC) protocols for particular multi-hop, RF-based wireless sensor networks and underwater sensor networks. A key aspect of this study is the modeling of a fair-access criterion that requires sensors to have an equal rate of frame delivery to the base station. Next, we analyze the performance of network service in outdoor environment, such as coverage and network lifework. Due to the characteristics of random deployment in outdoor environment, a distribution-free method is proposed to evaluate these metrics. Finally, we consider the design of a WSN for indoor environment. In this design, reference structure is incorporated into sensor node to enhance sensor awareness.

DEDICATION

This dissertation is dedicated to my parents and my wife.

ACKNOWLEDGMENTS

First of all, I would like to thank my advisor, Dr. Yang Xiao, for all his enthusiastic support and patient guidance over the course of my research. His continuous guidance dramatically improved my research capabilities. He is the best advisor I could have asked for.

I am very grateful to all my committee members, Dr. Xiaoyan Hong, Dr. Susan Vrbsky, Dr. Pu Wang, and Dr. Jingyuan Zhang for reviewing and providing many thoughtful and constructive comments on this dissertation.

I would like to express my appreciation to all of my colleagues in W4-NET whose collaborative support was essential for the completion of my research. Especially, I offer my blessings to Mr. Nanxiang Li who collaborated with me to accomplish Section 5.4 of this dissertation. I also would like to thank Dr. Qi Hao at the University of Alabama for his discussions and suggestions, as well as providing the original source codes for Section 5. I need express my gratitude to the Computer Science Department which offered me an opportunity to study in the field of Computer Science.

Finally, I would like to express my deepest appreciation to my parents for their constant love and support. The special appreciation should be given to my wife, Hengxia, for her continuous encouragement throughout my studies.

This work is supported in part by the US National Science Foundation under grant numbers CNS-0737325, CNS-0716211, CCF-0829827, and CNS-1059265.

CONTENTS

LIST OF TABLES

LIST OF FIGURES

CHAPTER 1

INTRODUCTION

The development of low-cost, power-efficiency sensor nodes has enabled Wireless sensor networks (WSNs) become more and more popular in a wide range of applications. Making use of mobile nodes carried by animals [39] or automobiles [38] or deterministically deployed sensor nodes in fixed locations [37], many trials have demonstrated the potential of WSNs. Continuous miniaturization of sensor nodes can lead to future WSN applications where a large number of battery-powered sensor nodes are randomly and densely deployed and the network is left unattended to perform monitoring, tracking, and reporting functions [40-41]. Unlike traditional networks, a WSN has its own constraints, such as a limited amount of energy, short communication range, low bandwidth, and limited processing and storage in each sensor node. As a result, it is necessary to introduce new design concepts, create or improve existing protocols, and develop new algorithms in WSNs.

My dissertation first focuses on performance limitations of network protocol in WSNs. It is important to study the fundamental performance limitations of wireless sensor networks, as establishing the performance bounds of a network protocol is necessary for determining whether the protocol is appropriate for a particular network design choice. An inappropriate protocol can result in a network which cannot sustain expected traffic loads. The wireless sensor networks (either RF-based sensor networks or acoustic underwater sensor networks) considered in this proposal is multi-hop: each sensor node performs sensing, transmission, and relay. All data

frames are sent to a dedicated data-collection node, called the base station, which is responsible for relaying the frames to a dislocated command center over a radio or wired link.

For this study, we consider the linear network, a commonly used topology designed by researchers from UC Santa Barbara for moored oceanographic applications [1], in which an array of equally spaced underwater marine sensors is suspended from a mooring buoy. All data in the network flows to a base station above the water's surface which is responsible for storing and relaying all collected data to a command center via an aerial radio link. During an event of interest, (e.g., a storm), it is desirable for the command center to acquire near real-time readings from all of the sensors in order to calibrate them as the event progresses [1]. An equally appropriate employment would include a collection of seismic sensors, perhaps a long grid topology, along a potential tsunami path that would monitor the movement of the wave phenomena over a relatively short distance and relay the collected data samples through the base station to an observatory station, as the radio signal would travel nearly 200,000 times faster than an acoustic signal. For such real-world applicable networks, it is critical that the medium access control (MAC) protocol [4], [5], [6], [7], [8] ensure that each sensor has an equal opportunity to forward its local observations to the command system in order to establish trends or to detect anomalies.

Therefore, we introduce the notion of fairness for sensor data delivery to this environment and support the application of a fair-access criterion to the MAC protocols under consideration for use in both RF-based wireless sensor networks (WSNs) and Underwater Acoustic Sensor Networks (UASNs). Employing a fair-access MAC protocol, however, may have a negative impact on the network's performance in terms of reduced throughput of data delivery to the base station and increased average frame latency, as those stations furthest from

the base station must compete with nodes closer to the base station for the limited network capacity, while those closer to the base station incur a greater traffic load as they must relay all traffic received from the upstream (predecessor) nodes. This dissertation analyzes such an impact by deriving tight bounds on the network utilization and frame latency performance of fair-access MAC protocols for linear topology and for two-row grid topologies. The bounds are significant because they hold for any MAC protocol conforming to the fair-access criterion, such as contention-based protocols (e.g., Aloha or CSMA based) or contention-free protocols (TDMA, etc.) under both single-channel and half-duplex radios. We show that these bounds are tight by proving that they can be achieved by a particular TDMA scheduling algorithm. We also show how to obtain the performance bounds of more complex grid topologies using the analysis method employing by linear topology and two-row grid topologies.

Moreover, the design of MSNs is significantly based on the monitored environment. The environment plays a key role in determining the size of network, the deployment scheme, and the network topology [41]. In outdoor environments, WSNs typically consists of thousands of wireless sensor nodes which are randomly deployed into the target area. Fundamental issues related to network service in outdoor environments are coverage and network lifetime, which, in general, can be considered as a quality of service measurement of the WSNs [32].

The coverage problems have been widely studied in conjunction with energy efficiency and lifetime of WSNs. A sensor node can be in the off-duty cycle or can enter power-save mode to conserve battery power. We refer to a sensor node that is in duty to sense its surroundings as an active sensor node and to a sensor that is off duty or enters power-save mode as an inactive sensor node. In a densely deployed WSN, since multiple sensor nodes may cover a subarea or a

target, it may not affect the coverage to deactivate and activate sensor nodes alternatively; however, the lifetime of the WSN will be extended.

In recent work concerning network coverage and lifetime problems where sensor nodes are deployed randomly, researchers assume the spatial distributions of sensor nodes are known when evaluating their proposed algorithms or protocols. For instances, in [42], the coordinates of sensor nodes are generated using the pseudo-uniform distribution in an area; in [43], sensor nodes are deployed randomly with Poisson distribution in a barrier.

Previous work using given sensor node distributions provides deep insight into the performance of the WSNs. However, the sensor node distributions may either not hold true or be difficult to obtain beforehand in some applications. For example, for battle field surveillance, sensor nodes can be airdropped either by aircrafts or by rockets. The sensor nodes are distributed along the route of an aircraft when the sensors are dropped by the aircraft, while the sensors are usually within a circle centered under the location where the rocket releases the sensors when a rocket is used. In either of these two cases, sensor nodes will not distribute uniformly in the desired sensing field. Instead, more sensors are expected to be found along the route of the aircraft or close to the center of the circle. Moreover, due to wind and other factors, such as environmental, human, and mechanical factors, the distributions of sensor nodes can be difficult to determine beforehand.

There are a few potential disadvantages when sensor node distributions are assumed to be known beforehand. 1) It is very difficult to choose an accurate sensor node location distribution; 2) inaccurate distribution assumption will result in poor analysis of protocols or algorithms; and 3) changes in sensor node distributions may lead to variations in system performance and may sometimes even invalidate the whole analysis.

Motivated by this intuition, we propose a network service analysis approach in which no assumption on sensor location distribution is required beforehand. Thus, the approach is in effect a distribution-free approach. The approach is suitable to solve network service evaluation problems concerning a great number of sensors which are deployed randomly.

In indoor environments, sensor nodes can be strategically hand placed and replenished from an energy source by human. Therefore, more concerns come to sensing efficiency of sensor nodes other network coverage and lifetime issues. Sensor spatial response is a fundamental design characteristic of distributed sensor systems because sensor spatial response is a key metric in applications such as intrusion detection, tracking, and identification [48-52]. A novel technology called reference structure has been introduced into sensor systems to enhance sensor spatial awareness. The term "reference structure" was first proposed in computational imaging systems [53-54], where it was used to encode the mappings between radiating objects and measurements. From the application of reference structure in computation imaging systems, we know that the function of reference structure is to segment source space [55]. Taking advantage of the function of reference structure, researchers extended the application of reference structure into wireless sensor networks. With the help of reference structure, a wireless sensor network composed of simple binary pyroelectric sensors can be used for intrusion detection, tracking, and identification [56-58].

A binary pyroelectric sensor is very inexpensive compared to a high-resolution camera, and an array of such binary pyroelectric sensors is about $2 [58]. Each sensor produces a binary digit (0 or 1) for an observed object (intrusion), and the output of an array of such binary sensors is a sequence of binary digits. For example, 10101 means that:

- There are 5 sensors in the array;

- the object/target is visible to sensors 1, 3, and 5;
- and the object is invisible to sensors 2 and 4.

From the above example, we observe that the amount of data is much less than with a high-resolution camera, which typically senses billion of pixels in order to obtain just a few target state variables. Furthermore, the binary sequence can be further compressed. For sensing jobs such as intrusion tracking and identification, most data obtained from expensive monitors with a high resolution camera is unnecessary and requires a large amount of computer resources to be processed. The claim that more data implies better object tracking is not necessarily correct. Huge amounts of data from a high resolution camera are easy for human eyes to recognize, but they are more difficult for computers/sensors to comprehend in tracking and identification applications. In fact, these same sensing jobs can be done by low-cost pyroelectric binary sensors with reference structure. More important, the data generated by binary sensors excludes useless information. Thus, the technology of reference structure can enhance the data and computation efficiency of intrusion detection, tracking, and identification.

Reference structure technology can also enhance the sensing accuracy of a sensor network. In most of the previous work [26-30], the function of a sensor is to detect intrusions in its sensing range, but it is hard to detect the location and movement of the intrusion within its range. Through adding modulators, also known as reference structure, between the pyroelectric sensors and the monitoring space, the intrusion can be located more accurately by collaboration of these simple binary pyroelectric sensors. At first thought, reference structure brings down the sensibility of sensors because it blocks part of their visibility. However, the existence of reference structure enhances sensor spatial awareness. Thus, these simple, low-cost pyroecletric binary sensors can achieve the same or even better sensing performance as expensive monitors

with high resolution cameras. Thus, the issue of placement of sensors and reference structure plays an important role in the performance of a sensor system. P.K. Agarwal et al. [59] have done a significant work in this area. We will study the maximum number of signatures in a sensor system in my dissertation.

The rest of the dissertation is organized as follows: Chapter 2 investigates the fundamental performance limits of medium access control (MAC) protocols for particular multi-hop, RF-based wireless sensor networks and underwater sensor networks; Chapter 3 and Chapter 4 analyze WSNs services including coverage and lifetime in outdoor environments. Chapter 5 discusses the design of WSNs in indoor environments. Chapter 6 concludes the dissertation with a summary of results.

Each chapter of this dissertation has led to publications including conference papers and journal papers. The following table shows the publication records related to this dissertation.

Chapter2	Conference	1. "Upper Bound on Network Utilization under Fair-Access in Multi-hop Wireless Grid Sensor Networks with 3-4 Rows," Proceedings of 5th International Conference on Mobile Ad-hoc and Sensor Networks (MSN 2009). 2. "Performance Limits of Fair-Access in Underwater Sensor Networks," Proceedings of 38th International Conference on Parallel Processing (ICPP 2009). 3. "Energy Consumption of Fair-Access in Sensor Networks with Linear and Selected Grid Topologies," Proceedings of 4th International Conference on Wireless Algorithms, Systems, and Applications (WASA 2009).
	Journal	1. "Tight Performance Bounds of Multi-hop Fair-Access for MAC Protocols in Wireless Sensor Networks and Underwater Sensor Networks," IEEE Transactions on Mobile Computing, accepted and to appear.
Chapter 3	Conference	1. "Sensor Distribution on Coverage in Sensor Networks," Proceedings of 7th International ICST Conference on Heterogeneous Networking for Quality, Reliability, Security and Robustness (Qshine 2010).
	Journal	1. "Impacts of Sensor Node Distributions on Coverage in Sensor Networks," Journal of Parallel and Distributed Computing, accepted and to appear.
Chapter 4	Conference	1. "Error Analysis of Scheduling Sleeping Nodes in Wireless Sensor Networks," Proceedings of 6th International Conference on Embedded Software and Systems (ICESS 2009).
	Journal	1. "Error Analysis and Kernel Density Approach of Scheduling Sleeping Nodes in Cluster-Based Wireless Sensor Networks," IEEE

		Transactions on Vehicular Technology, Vol. 58, No. 9, Nov. 2009, pp.5105-5114.
Chapter 5	Conference	1. "Signature Maximization in Designing Wireless Binary Pyroelectric Sensors," Proceedings of IEEE Global Communications Conference (GlobeCom 2010).
	Journal	1. "A Survey of Reference Structure for Sensor Systems," IEEE Communications Surveys and Tutorials, accepted and to appear.

CHAPTER 2

TIGHT PERFORMANCE BOUNDS OF MULTI-HOP FAIR-ACCESS FOR MAC PROTOCOLS IN WIRELESS SENSOR NETWORKS AND UNDERWATER SENSOR NETWORKS

In this chapter, we introduce the concept of fair-access, which applies to both WSNs and UASNs. We then present a formal analysis of the utilization and delay bounds of specific linear or grid networks that require fair-access. The significance of these bounds is two-fold: First, they are universal (i.e., they hold for any MAC protocol) under both single-channel and half-duplex radios; second, they are provably tight (i.e., they can be achieved by a version of the time division multiple access (TDMA) protocol that is self-clocking and therefore does not require system-wide clock synchronization). In addition, this formal analysis provides a feasible way to estimate the performance bounds of more complex topologies. Therefore, in Section 2.6, we present the analysis results for general grid network. Furthermore, the performance bounds of underwater sensor networks are explored with the consideration of propagation delays. A tight upper bound on network utilization is derived for the case in which propagation delay is less than or equal to half of the frame transmission time, which demonstrates that the utilization in networks with propagation delays is larger than in networks without propagation delays. The challenge lies in the fact that the propagation delay impact on underwater sensor networks is difficult to model.

The rest of this chapter is organized as follows: Section 2.1 reviews the related work. Section 2.2 provides a problem formulation; Section 2.3 studies RF-based WSNs; Section 2.4 studies UASNs; Section 2.5 provides performance analysis for WSNs and USANs; Section 2.6

presents analysis of bounds in more complex topologies; Section 2.7 provides the simulation results; finally, we conclude this chapter in Section 2.8

2.1 Related Work

In many applications of sensor networks, data frames generated by every node need to reach the base station. In this scenario, the communication pattern is many-to-one also known as convergecast [9], [10]. Convergecast can be accomplished by employing either contention-based MAC protocols like CSMA or contention-free MAC protocols like TDMA. Contention-based MAC protocols usually consume more energy than TDMA protocols since they waste energy during collisions and idle listening [11]. For example, a traffic monitoring network using the TDMA protocol described in [12] has a lifetime of 1000 days, compared to ten days for a network using contention-based MAC protocols. Thus, many applications in sensor networks employ TDMA scheduling algorithms [2], [3]. These algorithms aim to minimize the number of timeslots required for each node to communicate once with all its neighbors. However, these algorithms might incur high latency in the Convergecast scenario.

The existence of a computationally traceable optimal fair-access protocol is interesting because it has been shown that the general problem of optimal scheduling for a multi-hop network is NP-complete [2]. This may be because we consider only the topology in which the routing structure is simple. The data forwarding paths of a linear or grid network can be modeled as a tree. While tree-based scheduling may be too restrictive for arbitrary ad hoc networks [3], such an approach seems appropriate for networks in which all traffic must flow to a collective base station, which essentially forms a root node. The flow of traffic along the branches of the tree must be de-conflicted with the flow of traffic along other branches so that collisions or

interference between branches is eliminated or minimized. Individual node transmission windows may be adaptive [4] or static, as described herein. While a multi-hop star topology may be of particular interest, a linear one is directly applicable to buoyed networks. Furthermore, if the branches of the star are non-interfering, then it is the final hop of the star by which each branch connects to the base station that must be carefully controlled in order to limit collisions.

The authors in [13], [14] proposed algorithms to obtain the minimum delays in collecting sensor data for networks of various topologies such as line, multiline, and tree. In these papers, they approached the problems from the way that base station sends frames to the sensor nodes. In addition, the algorithms proposed in [13], [14] are centralized such that the schedule is computed at the base station and requires cooperation between nodes. However, these requirements may not be practical in some sensor network applications. The authors in [9] proposed a distributed minimal time convergecast scheduling process in which each node computes its own schedule after the initialization phase. However, all of the scheduling algorithms for multiline topology networks in [9], [13], [14] assume that there is no interference between different routing routes. Furthermore, tree networks can be reduced into equivalent multi-line networks, as in [9], [13], [14], and thus the proposed algorithms for the tree topology also have implicit assumptions above.

As in [9], the optimal TDMA fair scheduling in our work is also distributed. Although the scheduling algorithm for linear topology in our work is similar to the line case in [9], we propose a novel method to place lower bounds on data collection times. Unlike in the previous work, the multiline topology networks referred to as grid topologies in our work assume that there exists interference between different routing routes; our scheduling algorithms for a grid topology are therefore more complicated. In addition, all previous works were focused on terrestrial wireless

sensor networks and have not considered the propagation characteristics of the underwater wireless medium. Many papers [4], [5], [6], [15], [16], [17], [18], [19], [20], [21] have addressed MAC in underwater sensor networks, but they have not considered our problems. This chapter addresses the impact of non-trivial propagation delays, a definitive characteristic of underwater acoustic networks. Considering non-trivial propagation delays, this problem is difficult to study, as shown in the approach presented in Section 2.4. For example, we demonstrate that the utilization in networks with propagation delay is larger than in networks with no propagation delay under certain conditions. Another difference of this work from the previous work is that we consider utilization under the fair-access criterion introduced in the next section.

Note that in this work the derived upper bounds hold for any MAC protocol (including CSMA, TDMA, Aloha, etc.) under both single-channel and half-duplex radios. For more information on upper limits for CSMA-like MAC proposals such as CSMA-CA, the readers may refer to [77], [78].

Just for the illustration purpose, if we do not consider the average performance and consider only one round of transmissions, a CSMA protocol could accidentally act as an optimal TDMA protocol for a short time; therefore, the tight bound could also be achieved by CSMA protocols for that short period of time.

2.2 Problem Formulation

In this section, we first present the sensor network model; then we give the fair-access criterion definition, based on which we formulize the optimization problem under a few assumptions. Lastly, we describe the linear and grid topologies on which we explore the tight upper bounds on network utilization.

Sensor Network Definition: Consider a wireless sensor network comprised of a base station (BS) and n sensor nodes, denoted as O_i; $i = 1,2,...,n$. Sensor nodes generate sensor data frames and send them to the BS. Some sensor nodes perform the additional task of forwarding/routing frames to the BS, (i.e., a frame may need to be relayed by several nodes in order to reach the BS).

Note that the above definition is not limited to a particular topology. Let $U(n)$ denote the utilization of the above network, (i.e., the fraction of time that the BS is busy receiving correct data frames). Let G_i denote the contribution of (i.e., data generated by) sensor O_i to the total utilization. The following holds: $U(n) = \sum_{i=1}^{n} G_i$. Implicit in the utilization is the impact of propagation delays. As noted, these delays can be significant for UASNs, especially when compared to more traditional RF-based wireless networks.

Suppose that the network is required to use a MAC protocol that ensures all hosts are provided with the capability to contribute equally to the composite throughput. The impacts of such a criterion on RF-based WSNs (negligible propagation) and UASNs (non-negligible propagation) are considered in this chapter. The criterion is presented as follows:

Fair-access Criterion Definition: A MAC protocol used by the sensor network satisfies the fair-access criterion if all sensor nodes contribute equally to the network utilization. In other words, if the following condition holds:

$$G_1 = G_2 = ... = G_n \qquad (2.1)$$

Optimization Objective and Assumptions: Consider a sensor network like the one described above. The optimization problem maximizes $U(n)$ under the fair-access criterion. In the remainder of this chapter, we investigate this problem under the following assumptions:

a. All data frames are of the same size.

b. All sensor nodes have the same transmission capacity.

c. Acknowledgments are either implicit via piggyback or are explicit and out-of-band.

d. In-network sensor data processing is not used.

e. If two sensor nodes are within one-hop, one sensor node's transmission will interfere with the other's reception.

f. Internal node processing delays, which are associated with frame storage and queuing within a node, are negligible. Propagation delay is negligible for WSNs, but not for USANs.

g. Other characteristics, such as variable propagation delay, frequency dependent path loss, fading, noise and Doppler spread of USANs are not discussed in this chapter.

Linear Topology: The topology is illustrated in Fig. 2.1. n sensor nodes and a BS are placed in a linear fashion. Assume that the transmission range of each node is just one hop and that the interference range is less than two hops. In other words, only neighboring nodes have overlapping transmission ranges. As shown in Fig.1, O_i generates sensor data frames and sends the frames to O_{i+1}. O_i also relays data frames received from O_{i-1} to O_{i+1}. Finally, O_n forwards data to the BS, which collects all of the data frames.

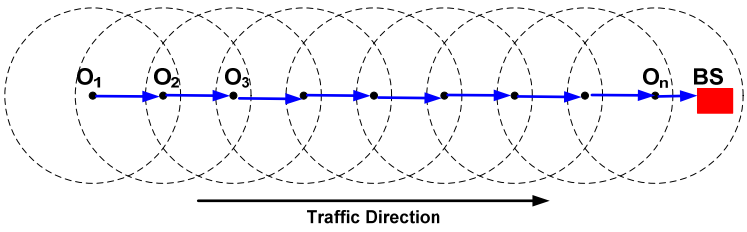

Fig. 2.1 A linear topology

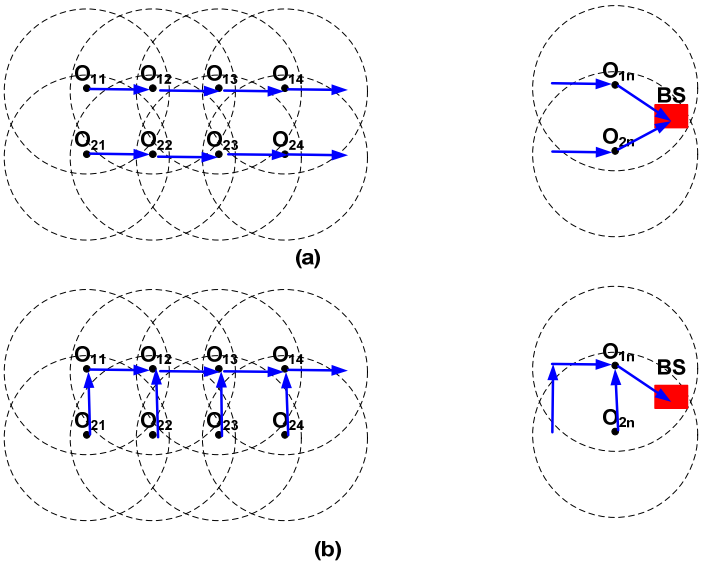

Fig. 2.2 Grid topology with two rows of sensors

2-row Grid Topology: The 2-row grid topology is illustrated in Fig. 2.2. The transmission ranges are such that horizontal or vertical neighbors can hear each other but two diagonal neighbors cannot. Two different routing patterns are considered: (i) the two rows forward data frames independently, as illustrated in Fig. 2.2(a), or (ii) the bottom sensors forward data to the top row first, as illustrated in Fig. 2.2(b). The results for this grid topology can be extended to grids with more rows which will be introduced in Section 2.6.

Different routing patterns behave differently since neighboring routing paths may interfere if the routing patterns are different. The number of routing patterns is exponentially large (with all kinds of combinations). Therefore, it is both impossible and unnecessary to study all of the routing patterns. Instead, we select some representative patterns.

2.3 RF-Based Wireless Sensor Network (WSNs) (Not Underwater)

In this section, we first derive upper bounds on network utilization for two specific topologies, linear and 2-row grid, under the fair-access criteria in RF-based wireless sensor

network. Then we show that derived upper bounds are indeed achievable by a particular TDMA scheduling algorithm.

2.3.1 Derivation of Utilization and Delay Bounds

In this subsection, we derive upper bounds on $U(n)$ and lower bounds on the effective inter-transmission delay of a node, that is, the time between samples for a given node for two specific topologies, linear and 2-row grid, under the fair-access criteria. We then present three theorems which establish the performance bounds. Finally, the proofs of the theorems are given for completeness.

Theorem 2.1: For the linear topology, under fair-access, $U(n)$ is upper bounded by the optimal utilization, $U_{opt}(n)$:

$$U(n) \le U_{opt}(n) = \begin{cases} n/\lfloor 3(n-1) \rfloor, & n > 1 \\ 1, & n = 1 \end{cases} \qquad (2.2)$$

An asymptotic lower limit for the optimal utilization exists and is equal to $1/3$.

Moreover, the inter-sample time for each node, denoted by $D(n)$, is lower bounded by the minimum effective transmission delay for the node, or minimum cycle time, $D_{opt}(n)$:

$$D(n) \ge D_{opt}(n) = \begin{cases} 3(n-1)T, & n > 1 \\ T, & n = 1 \end{cases} \qquad (2.3)$$

where T is the transmission time of one data frame.

Theorem 2.2: For the 2-row grid topology with the routing pattern as illustrated in Fig. 2.2(a), under fair-access, $U(2n)$ is upper bounded by the optimal utilization, $U_{opt}(2n)$:

$$U(2n) \le U_{opt}(2n) = 2n/(3n-1) \qquad (2.4)$$

The asymptotic lower limit for the optimal utilization is $2/3$.

Moreover, $D(2n)$ is lower bounded by the minimum inter-sampling time, $D_{opt}(2n)$:

$$D(2n) \geq D_{opt}(2n) = (3n-1)T \qquad (2.5)$$

where T is the transmission time of one data frame.

Theorem 2.3: For the 2-row grid topology with the routing pattern depicted in Fig. 2.2(b), under the fair-access criterion, $U(2n)$ is upper bounded by the optimal utilization, $U_{opt}(2n)$:

$$U(2n) \leq U_{opt}(2n) = \begin{cases} 2n/(6n-5), & n \geq 2 \\ 2/3, & n = 1 \end{cases} \qquad (2.6)$$

The asymptotic lower limit for the optimal utilization is $1/3$.

Moreover, $D(2n)$ is lower bounded by the minimum transmission delay, or time between samples, $D_{opt}(2n)$:

$$D(2n) \geq D_{opt}(2n) = \begin{cases} (6n-5)T & n \geq 2 \\ 3T & n = 1 \end{cases} \qquad (2.7)$$

where T is the transmission time of one data frame.

The significance of Theorems 2.1-2.3 is that they provide optimal bounds on utilization, regardless of the MAC protocol employed. In other words, no matter which MAC protocol is used, whether contention-free (TDMA, token passing, etc.) or contention-based (CSMA, aloha, etc.), the bounds hold as long as the protocol conforms to the fair-access criterion. In order to prove optimality, we must prove that (i) the bounds hold for any fair-access conforming MAC protocol and that (ii) the bounds are indeed achievable by at least one protocol.

Note that there are n nodes in Fig. 2.1, but $2n$ nodes in Fig. 2.2, as reflected in the notation for the network utilization and the minimum inter-sample time, or transmission delay.

Before showing the actual proofs, let us provide some of the intuition behind them. The fair-access criterion requires that $G_1 = G_2 = ... = G_n$ for the linear network. Let x denote the time period during which the BS successfully receives at least one original data frame from each sensor node in the network. It is clear that x is a random variable, that we can derive the minimum value of x, and that the maximum utilization is also achieved when the minimum value of x is achieved. During the time period x, the BS has busy time (denoted as b) receiving frames and idle time (denoted as y) when it is either blocked or waiting for its upstream neighbor to send. Thus, $x = b + y$. Note that x is the cycle time for the network under the fair-access criteria and that it determines the effective transmission delay for a node with a static ordering of relayed frames. For discussion purposes, we use a frame and the time period of transmitting/receiving a frame interchangeably in the following proofs. Since we assume no particular MAC protocol, frames may be lost, corrupted, or delayed due to collisions or queuing.

Proof of Theorem 2.1: For $n > 2$: During the time period x, the BS needs to receive at least n frames from O_n because frames may be lost or delayed as noted above. Thus, O_n transmits at least n frames (including $n-1$ relayed frames and one of its generated frames). We therefore have $b \geq nT$. Likewise, in order for O_n to receive $(n-1)$ frames from O_{n-1}, O_n needs to listen to at least $(n-1)$ frames, during which time the BS must be idle. Furthermore, when O_{n-2} transmits, O_n cannot transmit since they are within two-hops (i.e., O_n's transmissions will interfere with the frame reception by O_{n-1} from O_{n-2}). O_{n-2} needs to transmit at least $(n-2)$

frames to O_{n-1}, during which time O_n cannot transmit. Therefore, the total time in which O_n cannot transmit is $y \geq (n\text{-}1)T + (n\text{-}2)T$. Therefore, we have

$$x = b + y \geq nT + (n\text{-}1)T + (n\text{-}2)T$$

Since $D(n) = x$, we were able to derive equation (2.3) for the case of $n > 2$. During the time period x, the BS may receive more than n frames, but only n frames can be counted in the utilization under the fair-access criterion. Since we must minimize x to achieve the optimal utilization, we have

$$U(n) = nT/x \leq nT/\left[nT + (n-1)T + (n-2)T\right] = n/\left[3(n-1)\right]$$

which proves equation (2.2) for the case of $n > 2$.

Since $\lim_{n\to\infty} n/\left[3(n-1)\right] = 1/3$, $1/3$ is the asymptotic lower limit for the optimal utilization.

For $n = 2$: Since we want $G_1 = G_2$ during the time period x, O_2 transmits at least two frames (one relayed frame and its own). We have $b \geq 2T$. O_2 needs to listen to at least one frame from O_1. We have $y \geq T$ and thus $x = b + y \geq 3T$. Since $D_{opt} = x$, we were able to derive equation (2.3). Since we must minimize x to achieve the optimal utilization, $U(n) = 2T/x \leq 2T/3T = 2/3$, which proves equation (2.2) for this case.

For $n = 1$: Obviously, $U(1) \leq 1$, and $D(1) \geq T$. #

Proof of Theorem 2.2: For $n > 2$: under the fair-access criterion, during the time period x, the BS needs to receive at least n frames from O_{1n} because frames can collide, be corrupted, or be delayed (i.e., O_{1n} transmits at least n frames (including $n-1$ relayed frames and one of its generated frames) to the BS). Likewise, O_{2n} transmits at least n frames to the BS. We therefore have $b \geq 2nT$. In order for O_{1n} to receive $n-1$ frames from $O_{1(n-1)}$ and for O_{2n} to receive $n-1$

frames from $O_{2(n-1)}$, O_{1n} and O_{2n} need to listen for at least $(n-1)$ frames. Note that when $O_{1(n-2)}$ transmits, O_{1n} cannot transmit but O_{2n} can. Similarly, when $O_{2(n-2)}$ transmits, O_{2n} cannot transmit but O_{1n} can. So, the total time in which neither O_{1n} nor O_{2n} can transmit is $y \geq (n\text{-}1)T$. Thus, we have $x = b + y \geq 2nT + (n\text{-}1)T$. Since $D_{opt} = x$, we were able to derive equation (2.5) for this case. During the time period x, the BS may receive more than $2n$ frames, but only $2n$ frames can be counted in the utilization under the fair-access criterion. To achieve the optimal utilization, we minimize x, yielding

$$U(2n) = 2nT/x \leq 2nT/\left[2nT + (n-1)T\right] = 2n/(3n-1)$$

The rest of the proof is omitted for brevity. #

Proof of Theorem 2.3: For $n > 2$**:** under the fair-access criterion, during the time period x, the BS needs to receive at least $2n$ frames from O_{1n}, as shown above. We therefore have $b \geq 2nT$. In order for O_{1n} to receive $2(n\text{-}1)$ frames from $O_{1(n-1)}$ and one frame from O_{2n}, O_{1n} must listen for at least $2(n\text{-}1)+1$ frames. Furthermore, when either $O_{1(n-2)}$ or $O_{2(n-1)}$ transmits, O_{1n} cannot transmit. $O_{1(n-2)}$ must transmit at least $2(n\text{-}2)$ frames, and $O_{2(n-1)}$ must transmit at least one frame (if frames collide, are corrupted, or delayed more frames are needed). Thus, we have $y \geq 2(n-1)T + T + 2(n-2)T + T - T = (4n-5)T$. During this time the BS may receive more than $2n$ frames, but only $2n$ frames can be counted in the utilization under the fair-access criterion. Minimizing x to achieve the optimal utilization yields $U(2n) \leq \dfrac{2nT}{2nT + (4n-5)T} = \dfrac{2n}{(6n-5)}$.

The rest of the proof is omitted for brevity. #

From the proofs of Theorems 2.1, 2.2, 2.3; we can see that we only take use of the knowledge of the topology of sensor nodes within three hops of the base station and the number

of frames transferred by them to derive the upper bound of network utilization. Thus, we can extend this analysis method to complex topology network. In Section 2.6, we will explain it in detail

2.3.2 Bound Achievability via Optimal Fair Scheduling

In this subsection, we prove that the performance bounds introduced in Theorems 2.1, 2.2 and 2.3 are indeed achievable. Particularly, we present a TDMA scheduling algorithm that conforms to the fair-access criterion and show that it achieves the performance bounds. Note that herein the optimal utilization is under the constraint of the fair-access criterion. Otherwise, by simply allowing only O_n to transmit, the optimal utilization is 1. Recall that we assume a fixed data frame size and negligible propagation and processing delays. Thus, for the following discussion we divide the time into equal-duration timeslots with durations equal to the time needed to transmit one frame. The TDMA algorithm, which we term optimal fair scheduling, is described below.

Optimal Fair Scheduling for Linear Topology: Three tables containing the optimal schedules for the cases of $n = 1,2,3$, respectively, are shown in Fig. 2.3. Each row of the tables depicts node actions in a specific time slot. Consider the examples shown in the table of Fig. 2.3(b): at slot 1, O_1 transmits while O_2 receives and the BS is idle; at slot 2, O_2 relays the frame received in the previous slot to the BS; etc. It is not difficult to show that these schedules achieve the bounds for the cases of $n = 1,2,3$, respectively.

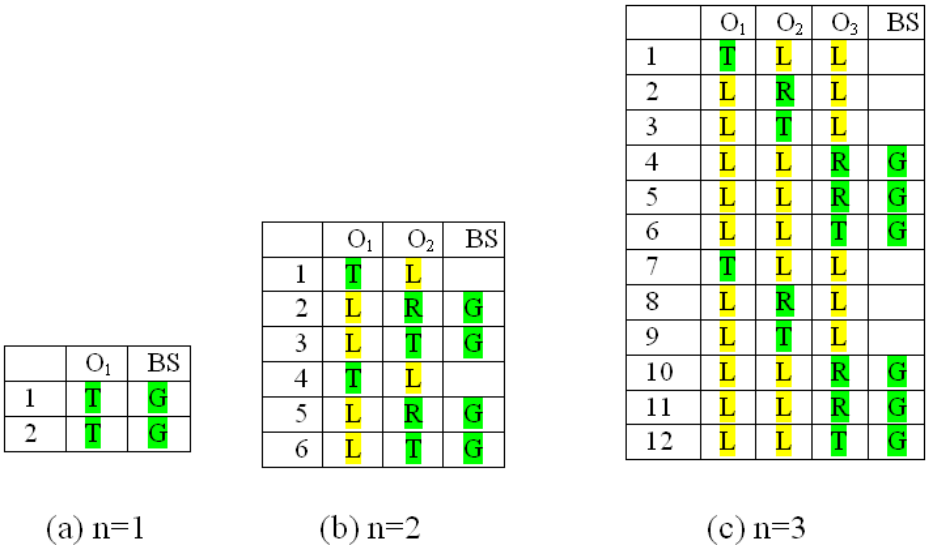

Fig. 2.3 Optimal schedules for small linear topologies (Legend: R: relay traffic; T: transmit own traffic; L: listening or receiving: G: frame received at BS)

For the general case of $n>3$, let $d=D_{opt}=3(n-1)$. A schedule with cycle d can be created as follows: O_1 transmits in timeslots $(d\cdot j)+1; j=0,1,...$; O_i ($i=2,...,n$) transmits relayed frames to O_{i+1} from timeslot $(d\cdot j)+f(i)$ to timeslot $(d\cdot j)+f(i)+i-2$ and transmits one of its own frames to O_{i+1} timeslot $(d\cdot j)+f(i)+i-1; j=0,1,...$, where $f(i)$ is recursively defined as follows:

$$f(i)=\begin{cases}1, & i=1\\ f(i\text{-}1)+(i\text{-}1), & i>1\end{cases} \qquad (2.8)$$

The proof of the schedule's optimality for arbitrary n is omitted for brevity.

Note that if we allow sensors to be self-clocking among sensors by listening to the wireless media, the above TDMA scheme can be implemented easily without requiring system-wide clock synchronization.

	O_{11}	O_{21}	BS
1	T	L	G
2	L	T	G
3	T	L	G
4	L	T	G

(a) n=1

	O_{11}	O_{12}	O_{21}	O_{22}	BS
1	T	L	T	L	
2	L	R	L	L	G
3	L	T	L	L	G
4	L	L	L	R	G
5	L	L	L	T	G

(b) n=2

Fig. 2.4 Optimal schedules for small Fig. 2.2(a) grid networks

Optimal Fair Scheduling for Fig. 2.2(a) Grid Topology: Before considering a general case, we must first consider some simple cases in which n is small. A schedule for $n=1$ is illustrated in Fig. 2.4(a). The utilization is 1. With $n=2$, when O_{11} transmits, O_{12} and O_{22} cannot transmit. A schedule is illustrated in Fig. 2.4(b). The utilization is $4/5$. These are consistent with Theorem 2.2 and are thus optimal.

	O_{11}	O_{21}	BS
1	L	T	
2	R	L	G
3	T	L	G

(a) n=1

	O_{11}	O_{12}	O_{21}	O_{22}	BS
1	L	L	T	T	
2	R	L	L	L	
3	T	L	L	L	
4	L	R	L	L	G
5	L	R	L	L	G
6	L	R	L	L	G
7	L	T	L	L	G

(b) n=2

	O_{11}	O_{12}	O_{13}	O_{21}	O_{22}	O_{23}	BS
1	L	L	L	T	T	T	
2	R	L	L	L	L	L	
3	T	L	L	L	L	L	
4	L	R	L	L	L	L	
5	L	R	L	L	L	L	
6	L	R	L	L	L	L	
7	L	T	L	L	L	L	
8	L	L	R	L	L	L	G
9	L	L	R	L	L	L	G
10	L	L	R	L	L	L	G
11	L	L	R	L	L	L	G
12	L	L	R	L	L	L	G
13	L	L	T	L	L	L	G

(c) n=3

Fig. 2.5 Optimal schedules for small Fig. 2.2(b) grid networks

Optimal Fair Scheduling for Fig. 2.2(b) Grid Topology: We first consider some simple cases where n is small. For Fig. 2.2(b), in which $n=1$, one scheme is shown in Fig.

2.5(a). The utilization is $2/3$. For $n=2$, O_{11} and O_{12} cannot transmit when O_{21} transmits. One possible scheme is shown in Fig. 2.5(b). The utilization is $4/7$. With $n=3$, the only nodes that can transmit at the same time are O_{21}, O_{22} and O_{23}. One scheme is shown in Fig. 2.5(c), and the utilization is $6/13$. Each of these is consistent with Theorem 2.3.

Now consider the general case. To fully utilize parallel transmissions, we let O_{2j} ($j=0,...,n$) transmit in the first slot. The second row waits for the remainder of the cycle while the first row forwards the traffic to the BS. This portion is simply a linear topology with double loads.

Therefore, the achievable utilization is $\frac{2n}{2n+2(n-1)+2(n-2)+1}=\frac{2n}{6n-5}$, which is consistent with Theorem 2.3. Since the bound is achievable, it is optimal. We can verify Fig. 2.5 when $n=1,2,$ or 3. Interestingly, when $n\to\infty$, the asymptotic limit for the upper bound of the optimal utilization is $1/3$, which is less than $2/3$, or the bound for traffic forwarded across the rows first, as in Fig. 2.2(a).

The optimal scheduling algorithms introduced above, though TDMA in nature, can be implemented without global clock synchronization. This is because a node's reception of a frame originated by its immediate upstream neighbor triggers that node's own transmission for the same cycle, thereby achieving self-clocking.

2.3.3 Traffic Load and Sensor Data Sampling Limit

This subsection addresses the impact of end-to-end performance bounds on the traffic load limitation of each sensor. Let ρ denote the traffic load generated by each sensor node. For the networks in Figs. 2.1, 2.2(a), and 2.2(b), since each node can transmit at most one original

frame, which requires a period of T in every $3(n-1)T$ time period, $(3n-1)T$ time period, and $(6n-5)T$ time period, respectively, we must have $\rho \le T/x = 1/[3(n-1)]$, $\rho \le T/x = 1/[(3n-1)]$ and $\rho \le T/x = 1/[(6n-5)]$, respectively, if $n > 2$. Furthermore, a data frame contains protocol overhead (because of headers and/or trailers). Thus, ρ must be adjusted to account for this overhead. Denote α to be the fraction of actual data bits in a frame. We have the following three theorems:

Theorem 2.4: For the linear topology illustrated in Fig. 2.1, under the fair-access criterion, the maximum feasible per node traffic load is

$$\frac{\alpha}{3(n-1)}, \text{ if } n > 2 \qquad (2.9)$$

Theorem 2.5: For the 2-row grid topology depicted in Fig. 2.2(a), under the fair-access criterion, the maximum feasible per node traffic load is

$$\frac{\alpha}{(3n-1)}, \text{ if } n > 2 \qquad (2.10)$$

Theorem 2.6: For the 2-row grid topology depicted in Fig. 2.2(b), under the fair-access criterion, the maximum feasible per node traffic load is:

$$\frac{\alpha}{(6n-5)}, \text{ if } n > 2 \qquad (2.11)$$

These three theorems not only tell us the traffic limitation of the sensor network, but they also provide lower bounds on the average sensor sampling rate/intervals (i.e., the minimum supportable time T/ρ between samples). The proofs are omitted.

2.4 Underwater Acoustic Sensor Networks (UASNs)

Consider an underwater sensor network in which the transmission medium is water and the carrier is an acoustic signal. We derive upper bounds on $U(n)$ and lower bounds on the minimum transmission delay, or time between samples, for the linear topology under the fair-access criterion. We consider the impact of non-negligible propagation delay. We denote transmission time and propagation delay as T and τ, respectively. As stated in the previous section, we let x denote the time period during which the BS successfully receives at least one original data frame from each sensor node in the network. We let b and y denote busy time and idle time, respectively. Thus, we have $x = b + y$. In Theorem 2.7, we study optimal utilization for underwater sensor networks.

Theorem 2.7: For the linear topology, under fair-access, $U(n)$ is upper bounded by the optimal utilization $U_{opt}(n)$ for all τ ($\tau \le T/2$):

$$U(n) \le U_{opt}(n) = \begin{cases} nT/[3(n-1)T - 2(n-2)\tau], & n > 1 \\ 1, & n = 1 \end{cases} \qquad (2.12)$$

and the maximum utilization $U_{opt}(n)$ can be achieved by a special case. An asymptotic lower limit for the optimal utilization exists and is $1/(3 - 2\tau/T)$. The inter-sample time for each node, denoted by $D(n)$, is lower bounded by the minimum effective inter-transmission delay for a node, or the minimum cycle time, $D_{opt}(n)$:

$$D(n) \ge D_{opt}(n) = \begin{cases} 3(n-1)T - 2(n-2)\tau, & n > 1 \\ T, & n = 1 \end{cases} \qquad (2.13)$$

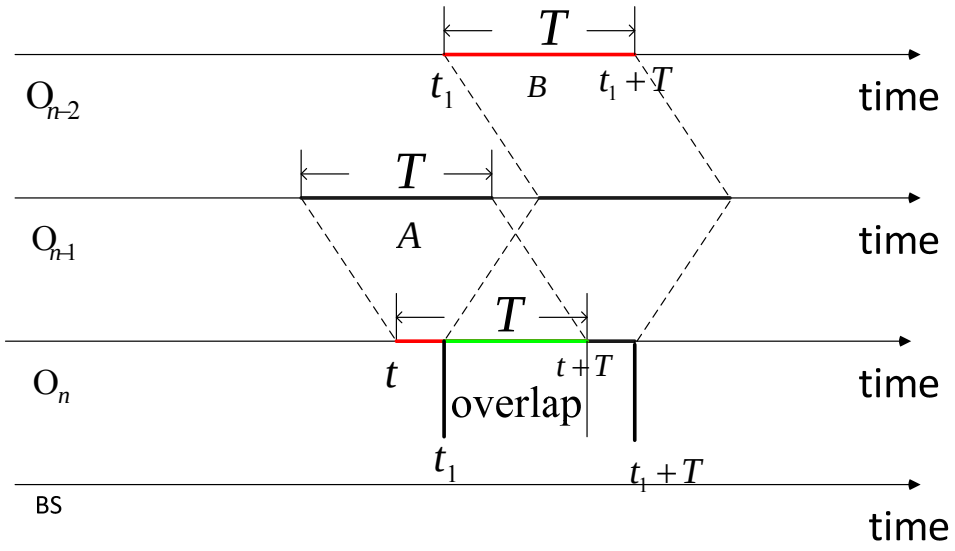

Fig. 2.6 Overlapping period

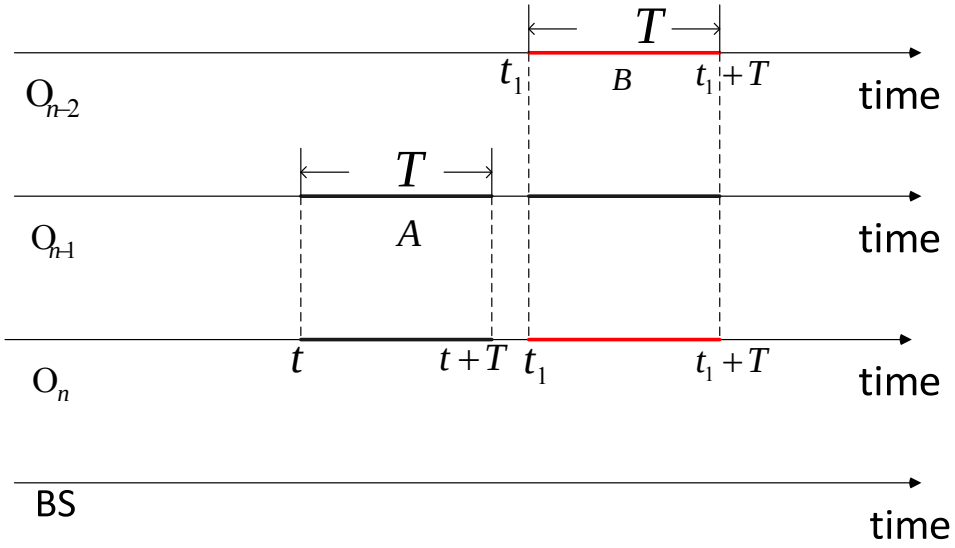

Fig. 2.7 Idle period in terrestrial wireless sensor network

Proof of Theorem 2.7: 1) For $n>2$: During the time period x, the BS needs to receive at least n frames from O_n. Thus, O_n transmits at least n frames (including $n-1$ relayed frames and one of its generated frames). We have $b \geq nT$. Likewise, in order for O_n to receive $(n-1)$ frames from O_{n-1}, O_n needs to listen to at least $(n-1)$ frames, during this time (there is

τ time delay) the BS must be idle. In the proof for terrestrial wireless sensor networks, since the propagation delay is ignored, when O_{n-2} transmits, O_n cannot receive frames from O_{n-1} because O_{n-1} cannot transmit and receive frames at the same time. However, in underwater sensor network in which propagation delay cannot be ignored, when O_{n-2} transmits, O_n still can receive frames from O_{n-1}. This fact is illustrated be the example in Fig. 2.6. As shown in Fig. 2.6, we assume that O_n receives frame A in $(t, t+T)$ and O_{n-2} transmits frame B in (t_1, t_1+T). Since O_{n-2} and O_n are within two-hops, O_n is blocked in (t_1, t_1+T) assuming the propagation delay is the same between both node pairs. For example, the overlap is $(t_1, t+T)$ in Fig. 2.6. In other words, when O_{n-2} transmits in $(t_1, t+T)$, O_n can still receive frames. As illustrated in Fig. 2.7, in terrestrial wireless sensor networks, O_n cannot transmit when either O_{n-1} or O_{n-2} is transmitting. Furthermore, when O_{n-2} transmits B, O_{n-1} cannot transmit A. Thus, the idle period generated by O_{n-2} transmitting B and O_{n-1} transmitting A is $2T$. However, as shown in Fig. 2.6, in underwater sensor networks, the idle period generated by O_{n-2} transmitting B and O_{n-1} transmitting A is t_1+T-t, which is less than $2T$.

Under the constraint of $\tau \le \frac{T}{2}$, when overlapping is maximized, the idle period generated independently by frame B reaches its minimum. To maximize the throughput of O_{n-1}, let O_{n-1} first finish transmitting frame A, then begin receiving of frame B immediately. This analysis is illustrated in Fig. 2.8: O_n receives frame A in $(t, t+T)$, which implies that O_{n-1} transmitted frame A in $(t-\tau, t-\tau+T)$. Let O_{n-2} transmit frame B in $(t+T-2\tau, t+2T-2\tau)$ so that its first bit reaches O_{n-1} in $t+T-\tau$. From Fig. 2.8, it is easy to see that, if $T-2\tau \ge 0$, for $\tau \le \frac{T}{2}$, the

maximum overlapping period is $(t+T-2\tau, t+T)$. Thus, the minimum time during which O_n may not transmit in order to prevent collision with frame B at O_{n-1} is $(t+2T-2\tau)-(t+T)=T-2\tau$. Therefore, the total time in which O_n must be idle, assuming that each frame is sent individually, is $y \geq (n-1)T+(n-2)(T-2\tau)$. Therefore, we have $x=b+y \geq nT+(n-1)T+(n-2)(T-2\tau)=(n-1)(3T-2\tau)+2\tau$.

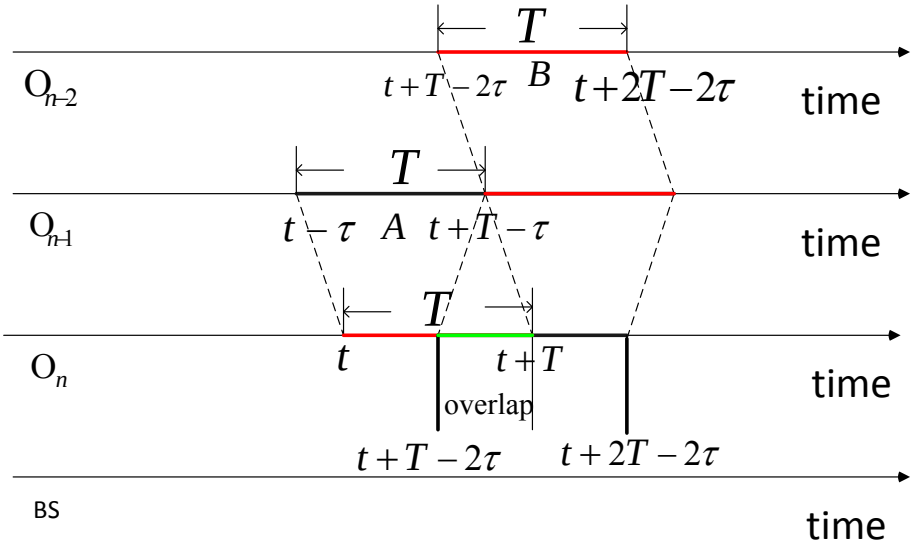

Fig. 2.8 Maximal overlapping ($\tau \leq T/2$)

Since $D(n)=x$, we are able to derive equation (2.13) for the case of $n>2$. During the time period x, the BS may receive more than n frames, but only n frames can be counted in the utilization under the fair-access criterion. Since we must minimize x to achieve the optimal utilization, we have

$U(n) \leq nT/\left[nT+(n-1)T+(n-2)(T-2\tau)\right]=nT/\left[(n-1)(3T-2\tau)+2\tau\right]$ which proves equation (2.13) for the case of $n>2$.

2) For $n=2$: Since we want $G_1=G_2$ during the time period x, O_2 transmits at least two frames (one relayed frame and its own). We have $b \geq 2T$. O_2 needs to listen to at least one frame

from O_1. We have $y \geq T$ and thus $x = b + y \geq 3T$. Therefore, we must minimize x to achieve the optimal utilization, $U(n) = 2T/x \leq 2T/3T = 2/3$, which proves equation (2.13) for this case. Note that the propagation delay can be ignored since it is possible to send the frame from O_1 such that it arrives at O_2 just as O_2 finishes transmitting of the previous frames.

3) For $n = 1$: Obviously, $U(1) \leq 1$. We will prove that the performance bounds $U_{opt}(n)$ are indeed achievable in a special case in the next subsection. #

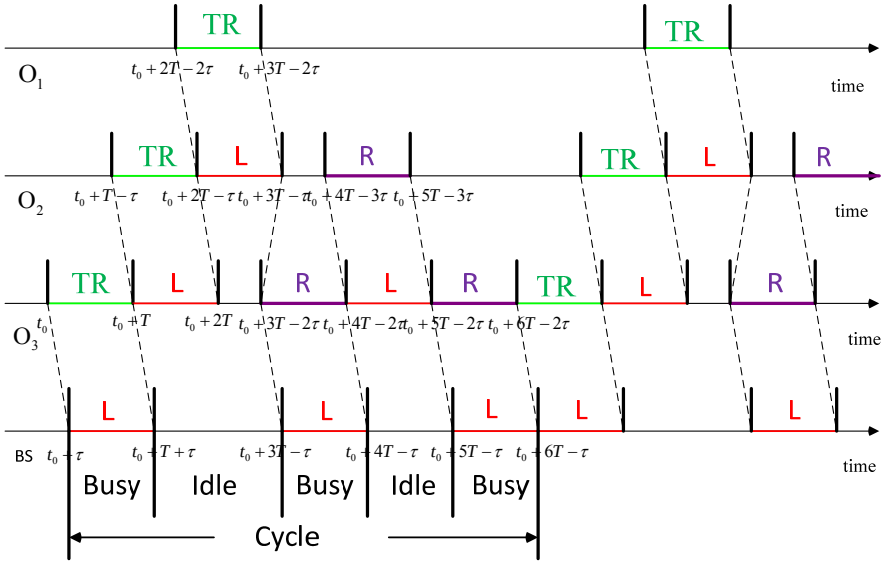

Fig. 2.9 Bottom-up approach for Linear topology (n=3) [Legend: TR: transmit own traffic; R: relay traffic (note: actually relay latest received frame from upstream nodes); L: receiving]

Note that herein the optimal utilization is under the constraint of the fair-access criterion when $\tau \leq T/2$. We first give the algorithm for the optimal fair scheduling. We then show the optimal fair scheduling for the cases of $n = 3,5$ in Figs. 2.9 and 2.10, respectively. Before showing the algorithm, we must provide some notation. Let A_i denote the frame generated by O_i, where $1 \leq i \leq n$.

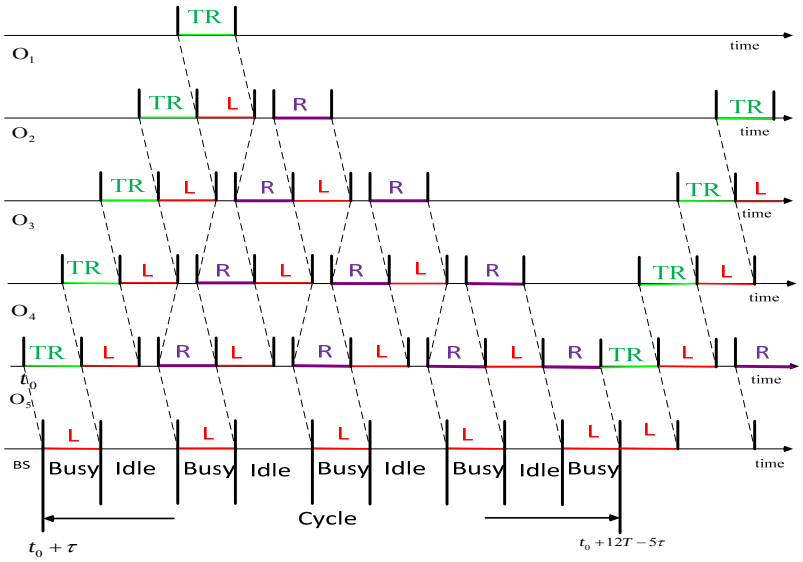

Fig. 2.10 Bottom-up approach for Linear topology (n=5) [Legend: the same]

Algorithm for optimal Fair Scheduling for Linear Topology: First, we define a cycle. Let t_0 denote the time when O_n begins transmission of its own frame, A_n. Thus, the BS receives frame A_n from time $t_0+\tau$. As we mentioned above, x is the cycle time for the network under the fair-access criterion. Thus, we define a cycle as $(t_0+\tau, t_0+\tau+x)$. Therefore, the next cycle is $(t_0+\tau+x, t_0+\tau+2x)$.

Second, for any node O_i, in which $1 \le i \le n$ in the cycle $(t_0+\tau, t_0+\tau+x)$, it has a start time (the time at which O_i starts to transmit its own frame, A_i) and an end time (the time at which O_i just completes A_1's transmission). We denote the start and end times by s_i and d_i, respectively. s_i and d_i are defined as follows:

$$s_i = \begin{cases} t_0 + (n-i)T - (n-i)\tau & 1 \le i < n \\ t_0 & i = n \end{cases}$$

$$d_i = \begin{cases} s_i + T + (i-1)(3T-2\tau) & 1 \le i < n \\ t_0 + x & i = n \end{cases}$$

where $x = 3(n-1)T - 2(n-2)\tau$.

Third, we define (s_i, d_i) as an active period for node O_i, in which $(1 \le i \le n)$ is in the cycle $(t_0 + \tau, t_0 + \tau + x)$. In the period (s_i, d_i), O_i includes a TR (transmit own traffic) period and $i-1$ subcycles. Their definitions are given as follows: $[s_i, s_i + T]$ denotes the TR period during which O_i transmits its own frame A_i; $[s_i + T, d_i]$ is divided into $i-1$ subcycles; we denote a subcycle by $[u_{i,j}, u_{i,j+1}]$, $j = 1,...,i-1$, during which time O_i receives and relays a frame from each upstream node. Thus, we have $\begin{cases} u_{i,1} = s_i + T \\ u_{i,j} = (j-1)(3T - 2\tau) + u_{i,1} \qquad j = 2,...,i-1 \\ u_{i,i} = d_i \end{cases}$;

Finally, for any subcycle $[u_{i,j}, u_{i,j+1}]$, there are three phases. We give them as follows: In phase $[u_{i,j}, u_{i,j} + T]$, O_i receives a frame from O_{i-1}, where $2 \le i \le n$; in phase $[u_{i,j} + T, M]$, O_i is idle (neither receiving a frame nor transmitting a frame), where

$$M = \begin{cases} u_{i,j} + T & i = n \text{ and } j = n-1 \\ u_{i,j} + T + T - 2\tau & \text{others} \end{cases};$$

In phase $[M, u_{i,j+1}]$, where $u_{i,j+1} = M + T$, O_i relays a frame to O_{i+1}, where $2 \le i \le n$. Note, when $i = n$, O_{n+1} represents the base station.

Two examples of this schedule are illustrated in Figs. 2.9 and 2.10. We show the case in which $n = 3$ in Fig. 2.9. The cycle period is $6T - 2\tau$, and the utilization of the BS is $3T/6T - 2\tau$, which is consistent with Theorem 2.7. The theorem also holds for the case in which $n = 5$, as shown in Fig. 2.10, where the cycle period is $12T - 6\tau$ and the utilization of the BS is $5T/12T - 6\tau$. For the case of n nodes, it is easy to verify this (omitted). Thus, the performance bounds are indeed achievable in a special case under the algorithm above.

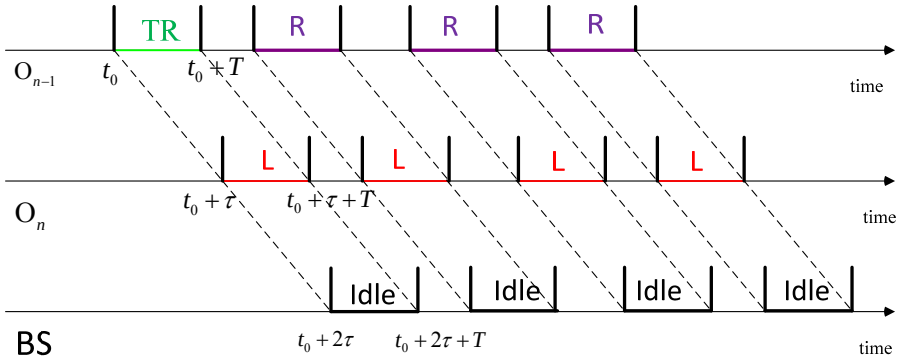

Fig. 2.11 Idle period generated by O_{n-1}'s transmission

Theorem 2.8: For the linear topology, under fair-access, $U(n)$ is upper bounded by $nT/\left[nT+(n-1)T\right]$ for all τ ($\tau > T/2$).

Proof of Theorem 2.8: 1) For $n>2$: During the time period x, the BS needs to receive at least n frames from O_n (including $n-1$ relayed frames and one of its generated frames). Thus, O_n transmits at least n frames. We have $b \geq nT$. In order for O_n to receive $(n-1)$ frames from O_{n-1}, O_n needs to listen for at least $(n-1)$ frames during which time O_n cannot transmit. Thus, there exists $(n-1)T$ corresponding idle periods in the base station. This fact is illustrated in Fig. 2.11. O_{n-1} transmits a frame in (t_0, t_0+T), then O_n receives it in $(t_0+\tau, t_0+\tau+T)$ since there is propagation delay τ. Thus, no frame will arrive base station in $(t_0+2\tau, t_0+2\tau+T)$. Therefore, during the time period x, we have $y \geq (n-1)T$. Therefore, we have the following inequality: $x = b+y \geq nT+(n-1)T = (2n-1)T$. Since we must minimize x to achieve the optimal utilization, we have $U(n) \leq nT/\left[nT+(n-1)T\right] = n/(2n-1)$

2) For $n=2$: Since we want $G_1 = G_2$ during the time period x, O_2 transmits at least two frames (one relayed frame and its own). We have $b \geq 2T$. O_2 needs to listen to at least one frame

from O_1. We have $y \geq T$, and thus $x = b + y \geq 3T$. So, minimizing x yields the optimal utilization, $U(n) = 2T/x \leq 2T/3T = 2/3$, which proves the inequality for this case.

3) For $n = 1$. Obviously, $U(1) \leq 1$.#

Next, we address the impact of end-to-end performance bounds on the traffic load limitation of each sensor. Let ρ denote the traffic load generated by each sensor node. We express the propagation delay, τ, in normalized time units as $\alpha = \tau/T$. For a linear network under the constraint of the criterion, since each node can transmit at most one original frame, which requires a period of T in every $3(n-1)T - 2(n-2)\tau$ time period, we must have $\rho \leq T/x = 1/[3(n-1) - 2(n-2)\alpha]$, where $0 \leq \alpha \leq 1/2$ if $n \geq 2$. Denote m as the fraction of actual data bits in a frame. We have the following theorem:

Theorem 2.9: For the linear topology, under the fair-access criterion, for all τ $(\tau \leq T/2)$, the maximum feasible per node traffic load is $m/[3(n-1) - 2(n-2)\alpha]$ if $n \geq 2$.

Next, we consider the energy consumption aspect $E(n)$ ($\tau \leq T/2$). Let B_T, B_R, B_L, and B_S denote the energy consumption per unit of time for a node to transmit a frame or to receive a frame, when a node is listening, and when a node is sleeping, respectively. It is reasonable to assume that $B_T > B_R \geq B_L > B_S$. Let $E(n)$, $E_T(n)$, $E_R(n)$, $E_L(n)$, and $E_S(n)$ denote the energy consumption, the transmission energy consumption, the reception energy consumption, the listening energy consumption, and the sleeping energy consumption, respectively, for the linear topology under fair-access in a cycle. Let $E_i(n)$ denote node O_i's energy consumption in a cycle.

Theorem 2.10: For the linear topology, under fair-access, $E(n)$ is lower bounded by the minimum energy consumption, $E_{opt}(n)$ when $\tau \le T/2$:

$$E_{opt}(n) = \sum_{i=1}^{n} (B_T iT + B_R(i-1)T + B_L((3n-2i-2)T - 2(n-2)\tau))).$$

Moreover, according to the Algorithm for Optimal Fair Scheduling for Linear Topology in Theorem 2.7, we can let nodes sleep when they neither transmit nor receive frames. Therefore, the more efficient energy consumption $\hat{E}_{opt}(n)$:

$$\hat{E}_{opt}(n) = \sum_{i=1}^{n} (B_T iT + B_R(i-1)T + B_S((3n-2i-2)T - 2(n-2)\tau)))$$

Proof of Theorem 2.10: Let $E(n)$ denote the total energy consumption for the linear topology which includes n nodes. It is easy to see that $E(n) = \sum_{i=1}^{n} E_i(n)$. Since $E_{opt}(n) = \min(E(n))$, $E_{opt}(n) = \min(\sum_{i=1}^{n} E_i(n))$. Since $E_i(n) \ge 0$ for $i = 1,2,...n$, we have $E_{opt}(n) = \sum_{i=1}^{n} \min(E_i(n))$. Therefore, we only need to determine the $\min(E_i(n))$. For any node O_i ($1 \le i \le n$) in a cycle, we have $E_i(n) = B_T T_T + B_R T_R + B_L T_L$, where T_T denotes the period during which O_i transmits frames in a cycle, T_R denotes the period during which O_i receives frames in a cycle, and T_L denotes the period during which O_i listens in a cycle. Thus, it is easy to see that $\min(E_i(n)) = \min(B_T T_T + B_R T_R + B_L T_L) = \min(B_T T_T) + \min(B_R T_R) + \min(B_L T_L)$, where $x = T_T + T_R + T_L$ and $B_T > B_R \ge B_L$. First, we consider the $B_T T_T$, as we know B_T is a positive constant parameter. Therefore, we only need to get the minimum of T_T . Since O_i transmits at least i frames (including $i-1$ relayed frames and one of its generated frames) during a cycle, we have $T_T \ge iT$. Thus, $\min(B_T T_T) = B_T iT$. As mentioned above, O_i relayed at least $i-1$ frames, meaning that O_i receives at least $i-1$ frames. We have $T_R \ge (i-1)T$. Thus we have $\min(B_R T_R) = B_R(i-1)T$.

Likewise, B_L is also a positive constant parameter, therefore, we only need to know the minimum of T_L under the constraint $x = T_T + T_R + T_L$. Therefore, we have $T_L = x - T_T + T_R$. From Theorem 2.7, we have $x = b + y \geq nT + (n-1)T + (n-2)(T - 2\tau)$. Thus we have $T_L \geq (3n - 2i - 2)T - 2(n-2)\tau$. Therefore, we have

$$\min(E_i(n)) = B_T iT + B_R(i-1)T + B_L[(3n - 2i - 2)T - 2(n-2)\tau].$$

Therefore, we have $E_{opt}(n) = \sum_{i=1}^{n} \min(E_i(n)) = \sum_{i=1}^{n} (B_T iT + B_R(i-1)T + B_L((3n-2i-2)T - 2(n-2)\tau))$.

We want to reduce energy consumption further. According to the Algorithm for Optimal Fair Scheduling for Linear Topology in Theorem 2.3, nodes sleep during the period in which they should listen. Thus, we have

$$\hat{E}_{opt}(n) = \sum_{i=1}^{n} \min(E_i(n)) = \sum_{i=1}^{n} (B_T iT + B_R(i-1)T + B_S((3n-2i-2)T - 2(n-2)\tau))) .\#$$

2.5 Performance Evaluation

2.5.1 Performance Evaluation of RF-Based WSNs

In this subsection, we provide some projected performances for WSNs (non-underwater). To account for protocol overhead, the optimal utilizations have been multiplied by α, which is the fraction of actual data bits in a data frame.

Linear Topology: Fig. 2.12(a) shows the optimal utilization versus the number of nodes for different α values for the basic linear topology based on the bounds of Theorem 2.1. The optimal utilization decreases quickly as n increases and approaches the asymptotic lower limit of optimal utilization, as suggested by the theorem. When $n = 5$, the optimal utilization is already near the asymptotic bound, which is indicated by the horizontal, colored lines.

Figs. 2.12(b) and 2.12(c) show the more significant impacts on linear topologies of increasing the network size. The minimum average delay increases linearly with n, as shown in Fig. 2.12(b). The traffic limit per sensor node decreases quickly as n increases, as shown in Fig. 2.12(c), and approaches the asymptotic limit of zero.

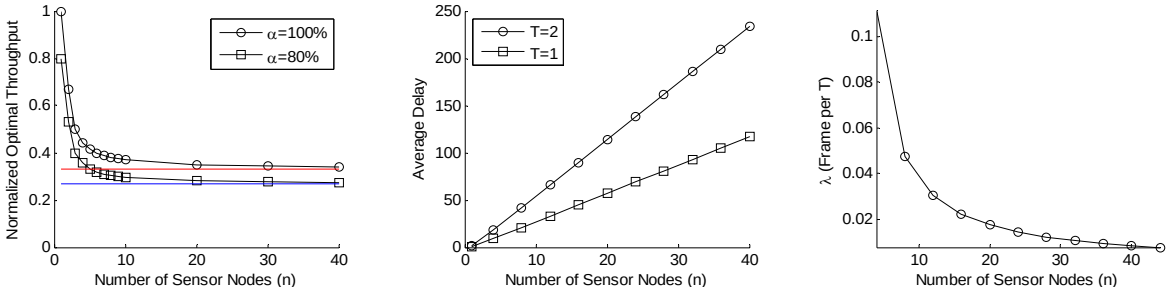

Fig. 2.12 Performance in linear topology (a) Optimal utilization, (b) Delay, and (c) Per node load limit

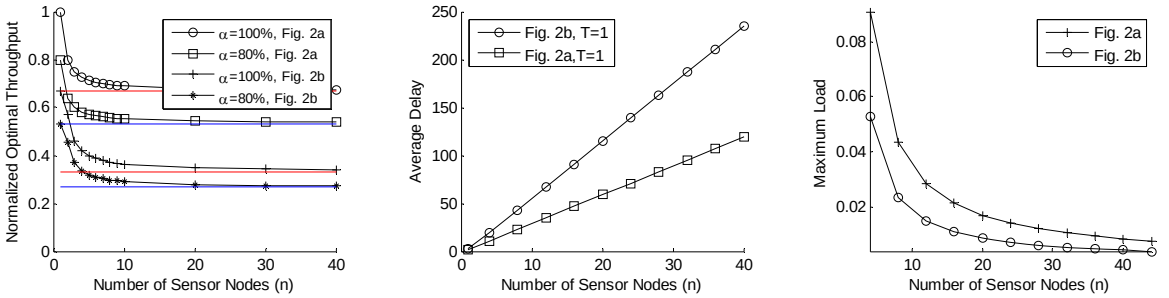

Fig. 2.13 Performance in 2-row grid (a) Optimal utilization, (b) Min Cycle Time, (c) Max per Node Load

Grid Topology: Fig. 2.13(a) shows the optimal utilization vs. n for different α values in the two-row topologies of Fig. 2.2, as derived from Theorems 2.2 and 2.3. Fig. 2.13(a) shows that the topology of Fig. 2.2(a) may achieve much better utilization than the topology of Fig. 2.2(b). The delay and load characteristics of the two-row grid topology are illustrated by Figs. 2.13(b) and 2.13(c).

Linear Topology vs. 2-Row Grid: Fig. 2.14 compares the optimal utilization of the linear topology of Fig. 2.1 with that of the horizontal-first-forwarding 2-row grid of Fig. 2.2(a). It is noteworthy that the optimal utilization of the Fig. 2.2(a) topology is better than that of the one

in Fig. 2.1, due to parallel transmissions of diagonal neighbors. This suggests that a 2-row grid may be preferable to a linear topology for some applications in which a linear topology might have been the first consideration. This issue is left for further study. Note, however, that the vertical-first grid (Fig. 2.2(b)) actually performs worse in terms of network utilization, albeit insignificantly, than the linear topology.

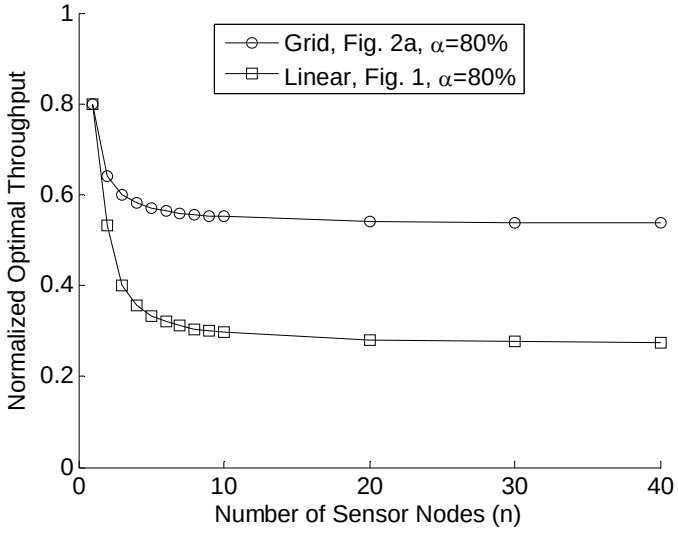

Fig. 2.14 Optimal Utilization (linear versus 2-row grid of Fig. 2.2(a))

2.5.2 Performance Evaluation of Acoustic-Based UASNs

In this subsection, due to limited space, we present some selected results for underwater sensor networks. To account for protocol overhead, the optimal utilizations have been multiplied by m, which is the fraction of actual data bits in a frame. We define the propagation delay factor as $\alpha = \tau/T$.

Fig. 2.15(a) shows the optimal utilization versus the propagation delay factor (α) for different n values (number of nodes) when $m = 1$ based on the bounds of Theorem 2.3. We can

see that for $\alpha = 0.5$, that the throughput achieves maximum in this range of α for different n values. When n goes to infinity, the limit is $1/(3-2\alpha)$.

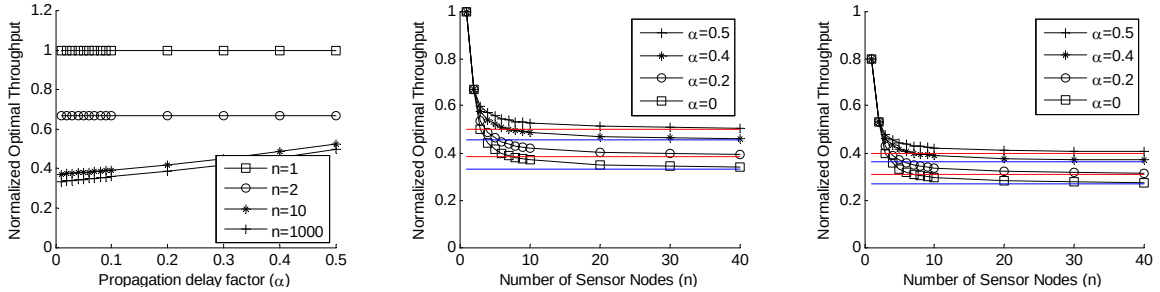

Fig. 2.15 Optimal Utilization

Figs. 2.15(b) and 2.15(c) show the optimal utilization versus the number of nodes when $m=1$ and $m=0.8$, respectively, for different α values based on the bounds of Theorem 2.3. The optimal utilization decreases quickly as n increases and approaches the asymptotic lower limit of optimal utilization, as suggested by the theorem. We can also see for $\alpha = 0.5$, the throughput achieves maximum in this range of α.

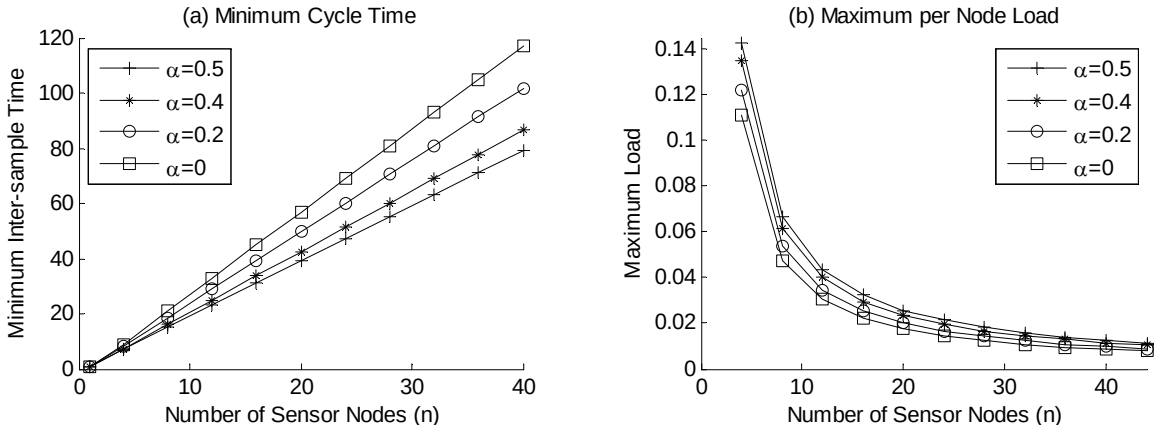

Fig. 2.16 (a) Minimum Cycle Time vs. n (b) Maximum per Node Load vs. n

Fig. 2.16(a) shows that the effective transmission delay increases linearly with n for different α values. Fig. 2.16(b) shows that the traffic limit per sensor node decreases quickly as n increases for different α values, and approaches the asymptotic limit of zero.

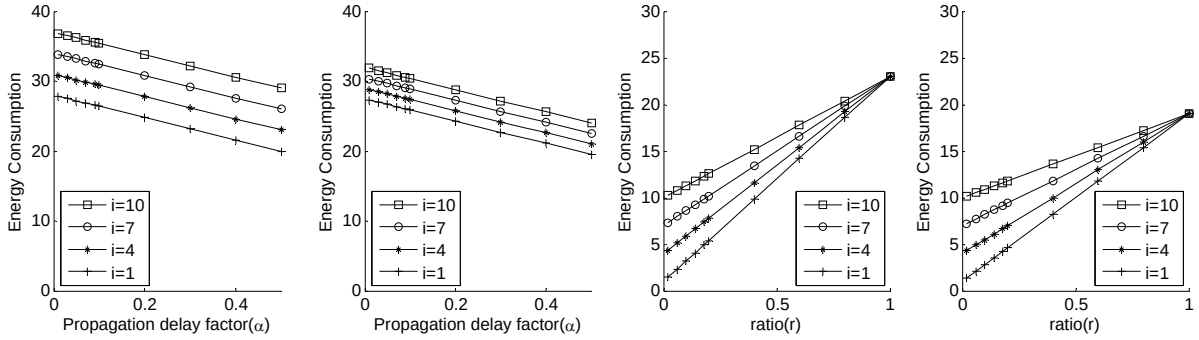

Fig. 2.17 Optimal Energy Consumption

Fig. 2.17(a) shows the optimal energy consumption vs. the propagation delay factor when $n=10$, $B_R=B_L$, and $B_R/B_T=1/2$. We observe that different nodes have equal tendencies to decrease energy consumption as the factor increases and that the downstream nodes consume more energy.

Fig. 2.17(b) shows the optimal energy consumption vs. the propagation delay factor when $n=10$, $B_R=B_L$, and $B_R/B_T=2/3$. We observe that different nodes have equal tendencies to decrease energy consumption as the factor increases and that the downstream nodes consume more energy.

Fig. 2.17(c) shows the optimal energy consumption vs. $r=B_R/B_T$ when $n=10$, $B_R=B_L$ and $\alpha=0.25$. Fig. 2.17(c) shows that energy consumption increases as $r=B_R/B_T$ increases. Also, as the ratio approaches 1, energy consumption of different nodes will be equal.

Fig. 2.17(d) shows the optimal energy consumption vs. $r=B_R/B_T$ when $n=10$, $B_R=B_L$, and $\alpha=0.5$. Fig. 2.17(d) shows that energy consumption increases as $r=B_R/B_T$ increases. Also, as the ratio approaches 1, energy consumption of different nodes will be equal.

2.6 Analysis of Bounds in More Complex Topologies

2.6.1 RF-based Wireless Sensor Network (Non-Underwater)

In this subsection, we show how to obtain the performance bounds of more complex topologies using the analysis mentioned in Theorems 2.1, 2.2, and 2.3. Note that obtained bounds from this analysis in this subsection may not be tight. As for tight bounds, we must have knowledge of entire network topologies and routing patterns such that we can design a scheduling algorithm to achieve them. In our analysis method, no node, including the base station, needs to be aware of the entire network topology. The only knowledge we need in this analysis is given as follows:

- The topology of nodes within three hops of the base station.
- Nodes within three hops of the base station must know how many nodes need them to transfer frames to the base station.

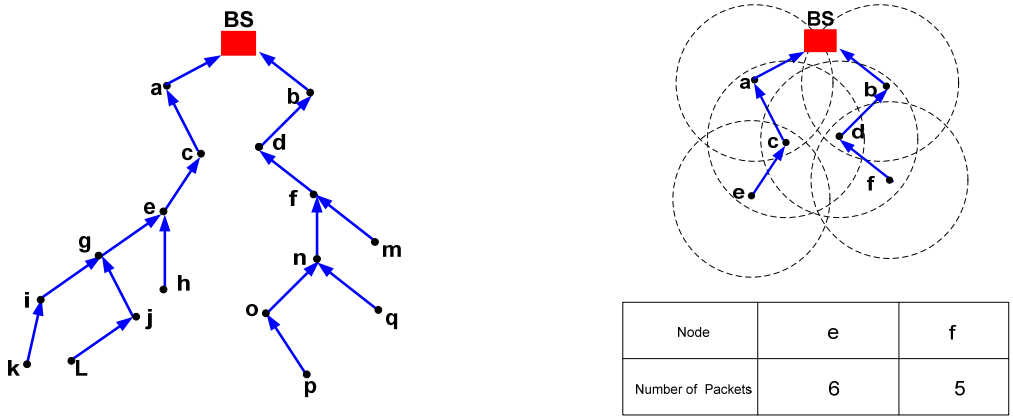

(a) Entire Topology (b) Reduced Topology

Fig. 2.18 Demonstration of Network Topology Simplification

According to the above two rules, a complicated topology can be simplified. For example, to obtain the performance bounds of networks like the one in Fig. 2.18(a), the only

knowledge that we need to know is illustrated in Fig. 2.18(b). From Fig. 2.18(b), the number of nodes which need node e to transfer their frames is 6 and the number of nodes which need node f to transfer their frame is 5. In the following, we apply this analysis method to a $k \times n$ grid network. Data frames are forwarded along parallel rows in this grid network, as illustrated in Fig. 2.19. When k is odd, let $k = 2m+1$, where $m = 0,1,2\ldots$. As illustrated in Fig. 2.19(a), only nodes O_{1n}, O_{2n}, and O_{3n} can transfer data frames to BS directly. Likewise, when k is even, let $k = 2m$, where $m = 1,2\ldots$. As illustrated in Fig. 2.19(b), only nodes O_{1n} and O_{2n} can transfer data frames to the BS directly. We discuss performance upper bounds for this general grid network based on the value of k.

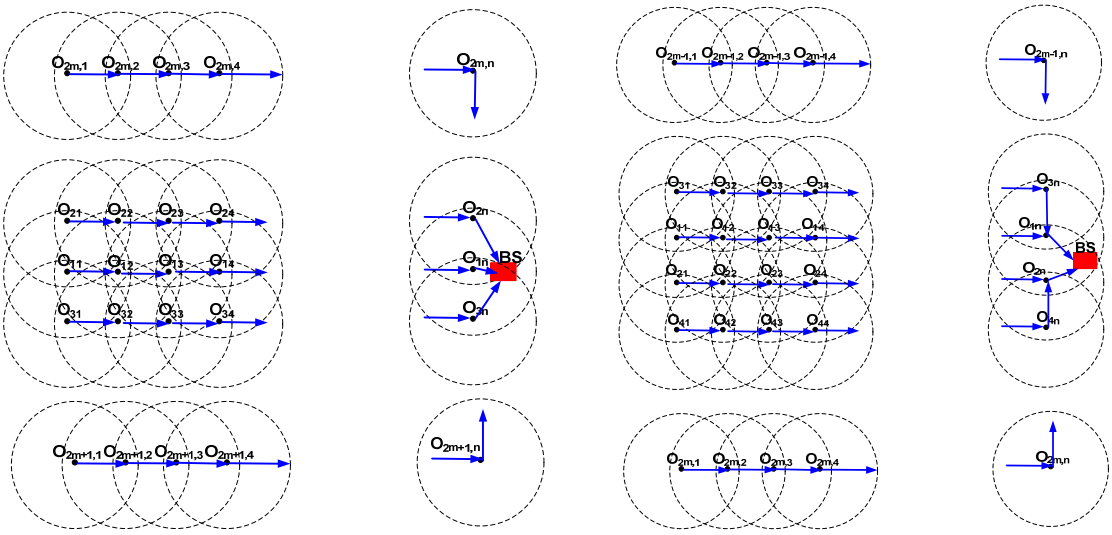

(a) k is odd (b) k is even

Fig. 2.19 General Grid Network

Case 1: $k = 1$**.** When $k = 1$, the general grid network was reduced to the linear topology given in Fig. 2.1. The only knowledge we need to obtain the upper bound on network utilization is given in Fig. 2.20. From Fig. 2.20, during the time period x, $O_{1(n-2)}$ needs to transmit at least $n-2$

frames. The analysis method is given in Theorem 2.1. Thus, the upper bound on network utilization for the case $k=1$ is $U(n) \le n/\left[3(n-1)\right]$.

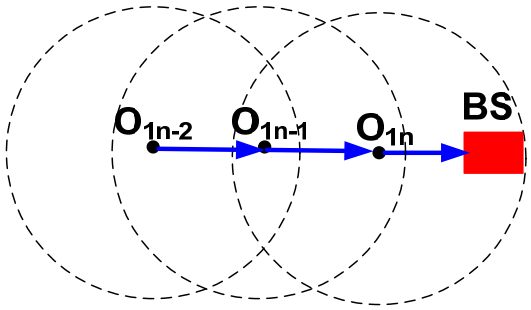

Node	O_{1n-2}
Number of Packets	n-2

Fig. 2.20 $k=1$

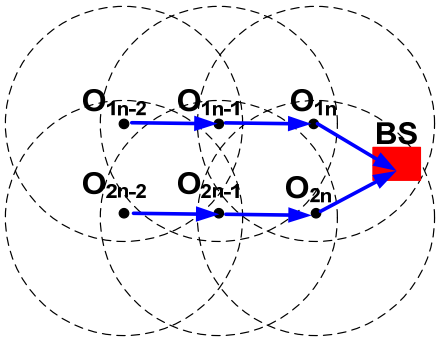

Node	O_{1n-2}	O_{2n-2}
Number of Packets	n-2	n-2

Fig. 2.21 $k=2$

Case 2: $k=2$**.** When $k=2$, the general grid network was reduced to the 2-row grid topology given in Fig. 2.2(a). The knowledge that we need to obtain the upper bound is given in Fig. 2.21. During the time period x, both $O_{1(n-2)}$ and $O_{2(n-2)}$ need to transmit at least $n-2$ frames. Also,

the analysis method to get the upper bound is given in Theorem 2.2. Thus, the upper bound on network utilization for case $k=2$ is $U(2n) \le 2n/(3n-1)$.

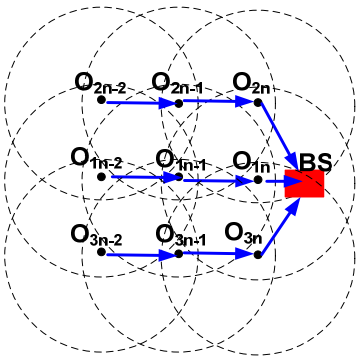

Node	O_{1n-2}	O_{2n-2}	O_{3n-2}
Number of Packets	n-2	n-2	n-2

Fig. 2.22 $k=3$

Case 3: $k=3$**.** For a 3-row grid topology network, the knowledge that we need to obtain the upper bound is given in Fig. 2.22. During the time period x, $O_{1(n-2)}$, $O_{2(n-2)}$, and $O_{3(n-2)}$ need to transmit at least $n-2$ frames. Note that, when $O_{1(n-2)}$ transmits, O_{1n} cannot transmit but either O_{2n} or O_{3n} can. Similarly, when $O_{2(n-2)}$ transmits, O_{2n} cannot transmit but either O_{1n} or O_{3n} can. When $O_{3(n-2)}$ transmits, O_{3n} cannot transmit but either O_{1n} or O_{2n} can. Under the fair-access criterion, O_{1n}, O_{2n}, and O_{3n} each need to transmit at least n frames to the BS. We have $b \ge 3nT$. In order for O_{1n} to receive $n-1$ frames from $O_{1(n-1)}$, O_{1n} needs to listen to at least $n-1$ frames, during which time O_{2n} cannot transmit but it can receive and O_{3n} can either transmit or receive. Similarly, in order for O_{3n} to receive $n-1$ frames from $O_{3(n-1)}$, O_{3n} needs to listen to at least $n-1$ frames during which time O_{2n} cannot transmit but it can receive, and

O_{1n} can either transmit or receive. But in order for O_{2n} to receive $n-1$ frames from $O_{2(n-1)}$, O_{2n} needs to listen to at least $n-1$ frames, during which time neither O_{1n} nor O_{3n} can transmit, which means that the BS must be idle. Thus, $y \geq (n-1)T$. The upper bound on network utilization is $U(3n) \leq 3n/(3n+n-1) = 3n/(4n-1)$. In our paper [79], we proved this upper bound can be achieved by a scheduling algorithm. Thus, this bound is tight.

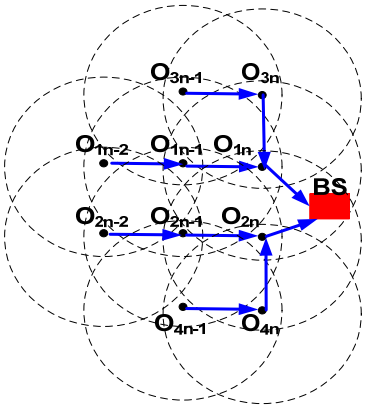

Node	O_{1n-2}	O_{2n-2}	O_{3n-1}	O_{4n-1}
Number of Packets	n-2	n-2	n-1	n-1

Fig. 2.23 $k=4$

Case 4: $k=4$**.** For a 4-row grid topology network, the knowledge that we need to obtain the upper bound is given in Fig. 2.23. During the time period x, under the fair-access criterion, both O_{1n} and O_{2n} need to transmit at least $2n$ frames to the BS. We have $b \geq 4nT$. In order for O_{1n} to receive $n-1$ frames from $O_{1(n-1)}$ and receive n frames from O_{3n}, O_{1n} must listen to at least $2n-1$ frames, during which time O_{2n} cannot transmit (i.e., the BS must be idle). Similarly, O_{2n} also needs to listen to at least $2n-1$ frames, during which time O_{1n} cannot transmit. But note that, when O_{1n} receives frames, O_{2n} can also receive frames. Furthermore, note that when

$O_{3(n-1)}$ transmits, O_{1n} cannot transmit but O_{2n} can. Likewise, when $O_{1(n-2)}$ transmits, O_{1n} cannot transmit but O_{2n} can. Similarly, when $O_{4(n-1)}$ transmits, O_{2n} cannot transmit but O_{1n} can. Likewise, when $O_{2(n-2)}$ transmits, O_{2n} cannot transmit but O_{1n} can. Therefore, the total time in which neither O_{1n} nor O_{2n} can transmit is $y \geq (2n-1)T$. Thus, we have $x = b + y \geq 4nT + (2n-1)T$. The upper bound is $U(4n) \leq 4n/(6n-1)$. We also proved this upper bound can be achieved by a scheduling algorithm in our work [79].

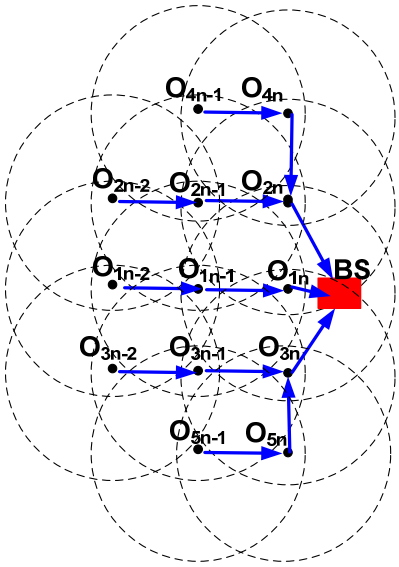

Node	Number of Packets
O_{1n-2}	n-2
O_{2n-2}	n-2
O_{3n-2}	n-2
O_{4n-1}	n-1
O_{5n-1}	n-1

Fig. 2.24 $k = 5$

Case 5: $k = 5$**.** For a 5-row grid topology network, the knowledge that we need to obtain the upper bound is given in Fig. 2.24. Under fair-access criterion, during time period x, O_{1n} needs to transmit at least n frames to the BS. O_{2n} and O_{3n} each need to transmit at least $2n$ frames to the BS. We have $b \geq 5nT$. In order for O_{1n} to receive $n-1$ frames from $O_{1(n-1)}$, O_{1n} must listen to at least $n-1$ frames, during which time both O_{2n} and O_{3n} cannot transmit (i.e., the BS must be idle). Except for node $O_{1(n-1)}$ and for other nodes more than two hops away from the

BS, when they transmit, there always exists a node from O_{1n}, O_{2n}, and O_{3n} which can transmit. For example, when $O_{2(n-1)}$ transmits, O_{1n} and O_{2n} cannot transmit but O_{3n} can. Therefore, the total time when none of O_{1n}, O_{2n}, and O_{3n} can transmit is $y \geq (n-1)T$. Thus, we have $x = b + y \geq 5nT + (n-1)T$. The upper bound is $U(5n) \leq 5n/(6n-1)$.

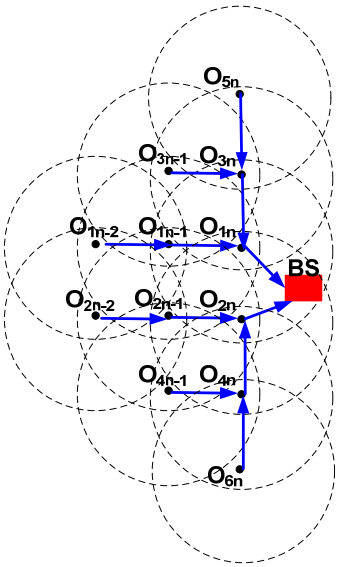

Node	Number of Packets
O_{1n-2}	n-2
O_{2n-2}	n-2
O_{3n-1}	n-1
O_{4n-1}	n-1
O_{5n}	(m-2)*n
O_{6n}	(m-2)*n

Fig. 2.25 k is even and $k \geq 6$

Case 6: $k \geq 6$ and k is even: For the case where k is even and $k \geq 6$, the knowledge that we need to obtain the upper bound is given in Fig. 2.25. In other words, any complicated grid topology with an even number of rows can be simplified to Fig. 2.25. As mentioned above, k can be denoted as $2m$ in this case. During the time period x, under fair-access criterion, both O_{1n} and O_{2n} need to transmit at least mn frames to the BS. We have $b \geq 2mnT$. In order for O_{1n} to receive $n-1$ frames from $O_{1(n-1)}$ and $(m-1)n$ frames from O_{3n}, O_{1n} must listen to at least $mn-1$ frames, during which time O_{2n} cannot transmit (i.e., the BS must be idle). Similarly, O_{2n} also needs to listen to at least $mn-1$ frames, during which time O_{1n} cannot

transmit. But note that O_{1n} and O_{2n} can receive frames at the same time. Furthermore, when nodes which are three hops away from BS transmit, there always exists a node from O_{1n} and O_{2n} which can transmit. For example, when O_{5n} transmits, O_{1n} cannot transmit but O_{2n} can. Therefore, the total time when neither O_{1n} nor O_{2n} can transmit is $y \geq (mn-1)T$. Thus, we have $x = b + y \geq 2mnT + (mn-1)T$. The upper bound is $U(2mn) \leq 2mn/(3mn-1)$.

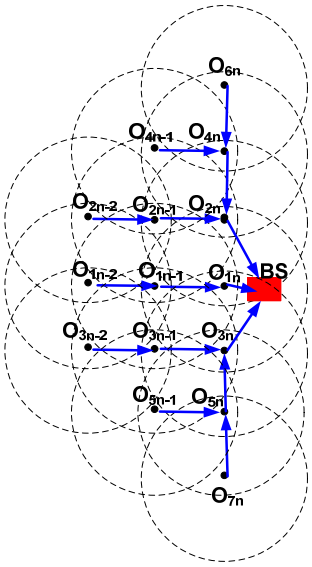

Node	Number of Packets
O_{1n-2}	n-2
O_{2n-2}	n-2
O_{3n-2}	n-2
O_{4n-1}	n-1
O_{5n-1}	n-1
O_{6n}	(m-2)*n
O_{7n}	(m-2)*n

Fig. 2.26 k is odd and $k \geq 7$

Case 7: $k \geq 7$ and k is odd: For the case where k is odd and $k \geq 7$, the knowledge that we need to obtain the upper bound is given in Fig. 2.26. In other words, any complicated grid topology with an odd number of rows can be simplified to Fig. 2.26. As mentioned above, k can be denoted as $2m+1$ in this case. Under fair-access criterion, during time period x, O_{1n} needs to transmit at least n frames to the BS. O_{2n} and O_{3n} each need to transmit at least mn frames to the BS. We have $b \geq (2m+1)nT$. In order for O_{1n} to receive $n-1$ frames from $O_{1(n-1)}$, O_{1n} must listen to at least $n-1$ frames, during which time both O_{2n} and O_{3n} cannot transmit (i.e., the BS

must be idle). Except for node $O_{1(n-1)}$, when other nodes with more than two hops away from BS transmit, there always exists a node from O_{1n}, O_{2n}, and O_{3n} which can transmit. For example, when O_{6n} transmits, O_{2n} cannot transmit but O_{2n} and O_{3n} can. Therefore, the total time when none of O_{1n}, O_{2n}, and O_{3n} can transmit is $y \geq (n-1)T$. Thus, we have $x = b + y \geq (2m+1)nT + (n-1)T$. The upper bound is $U((2m+1)n) \leq (2m+1)n/[(2m+2)n-1]$. Note that upper bounds given in Cases 5, 6, 7 are not necessarily tight.

2.6.2 Acoustic-based Underwater Sensor Network

In this subsection, we discuss the upper bounds on network utilization in multi-line networks. Theorem 2.11 derives the upper bound based on the conclusion of Theorem 2.7.

Theorem 2.11: Let n denote the total number of nodes in the network and M represent the branch with the maximum number of nodes. The number of nodes in branch M is denoted as n_M. The lower bound on the cycle time is $\max((n_M - 1)(3T - 2\tau) + 2\tau, n)$.

Proof of Theorem 2.11: Firstly, under the constraint of fair-access, the base station is required to receive at least one frame from each node in the circle. Thus, n is a lower bound in any network. Furthermore, according to the optimal fair scheduling for linear topology, the minimum cycle time for branch M is $(n_M - 1)(3T - 2\tau)$. Thus, the lower bound on the cycle time is $\max((n_M - 1)(3T - 2\tau) + 2\tau, n)$.#

2.7 Simulation Results

In this section, we provide simulation results on throughput for linear topology and grid topology. Simulations are conducted with discrete event simulation using Java. In our

simulations, the transmission range of each node is just one hop and the interference range is less than two hops. In other words, only neighboring nodes have overlapping transmission ranges. Other characteristics, such as variable propagation delay, frequency dependent path loss and fading noise are not considered in this simulation. Fig. 2.27 shows the normalized utilization vs. the number of nodes for the linear topology. As illustrated in Fig. 2.27, for the optimal fair TDMA scheduling mentioned in Section 2.3, the analytical results exactly match the simulation results. For showing optimal TDMA scheduling indeed has better performance than other scheduling algorithms, a specific TDMA and Aloha are simulated. Here, we briefly specify the TDMA scheduling. In the specific non-optimal TDMA scheduling, a node with hop-count h is assigned time slots of (1) $4i+1$ to send available frames if $h \bmod 4$ is 1, (2) $4i+2$ to send available frames if $h \bmod 4$ is 2, (3) $4i+3$ to send available frames if $h \bmod 4$ is 3, and (4) $4i+4$ to send available frames if $h \bmod 4$ is 0, where $i = 0,1,2,.....$. From Fig. 2.27, we can observe that, although this specific TDMA scheduling is not optimal, it still has better throughput performance than Aloha.

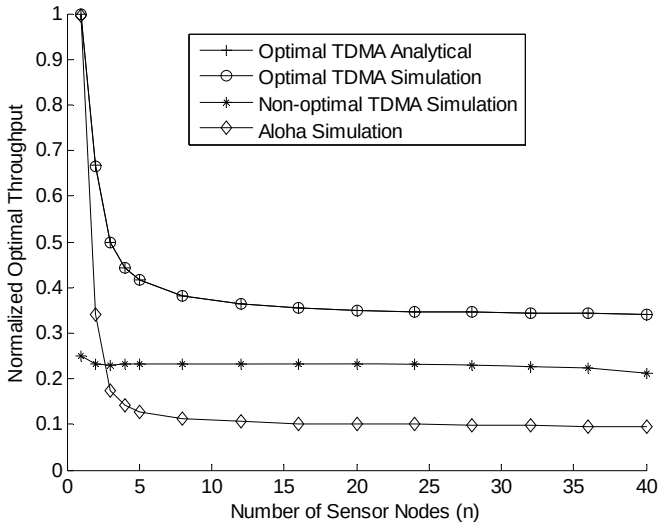

Fig. 2.27 Simulation Results for the Linear Topology

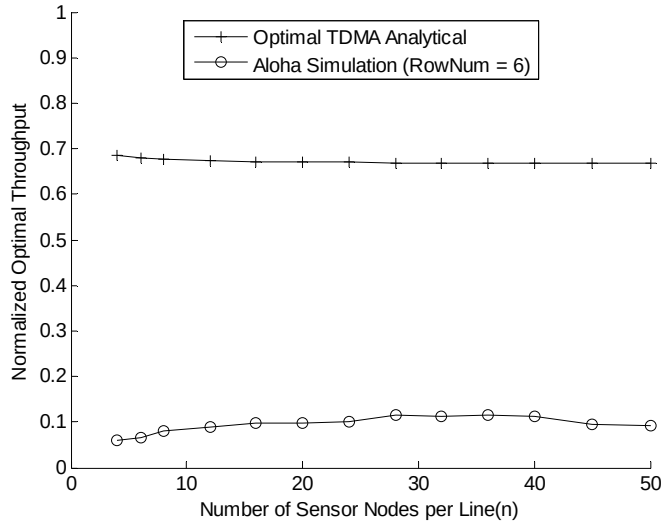

Fig. 2.28 Simulation Results for Grid Topology

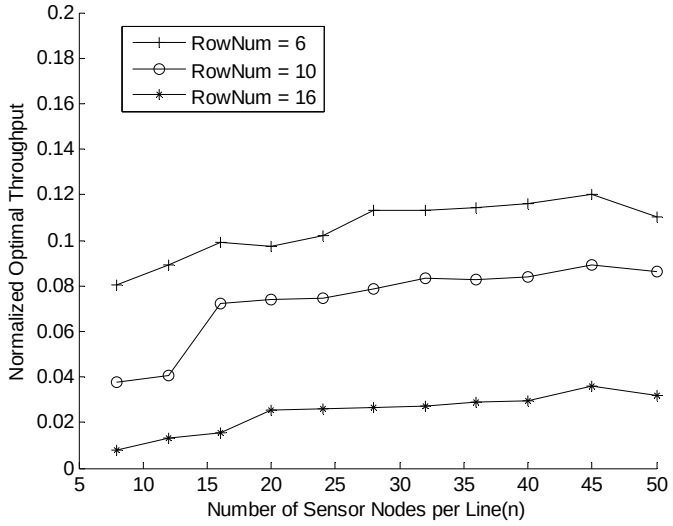

Fig. 2.29 Impact of Row Number on Aloha Simulation

In order to show the upper bound of throughput on general $k \times n$ grid topology, we simulate an Aloha protocol for a specific grid topology network where k is 6. As illustrated in Fig. 2.28, the optimal analytical bound is far better than simulation result of Aloha protocol. Furthermore, we explore the impact of the size of grid network on throughput by simulations. As illustrated in Fig. 2.29, when the size of grid network becomes larger, the throughput becomes

small. That is because the nodes connecting to the BS will stay the same no matter how large the grid network is. Therefore, large network causes more traffic collisions and lead to low throughput.

2.8 Conclusion and Future Work

In this chapter, we explored fundamental limits for sustainable loads, utilization, and delays in specific multi-hop sensor network topologies for both wireless sensor networks and underwater acoustic sensor networks. We derived upper bounds on network utilization and lower bounds for minimum sample time in fixed linear and multi-row grid topologies under the fair-access criterion. This fair-access criterion ensures that the data of all sensors is equally capable of reaching the base station. We proved that under some conditions/assumptions, these bounds are achievable and therefore optimal. From the limitation on the sustainable traffic loads derived, one can determine a lower bound for the sampling interval for such networks. The significance of these limits is that these bounds are independent of the selection of MAC protocols under both single-channel and half-duplex radios. Thus, the performance bounds for specific implementations of such network topologies can be explicitly determined to ensure the proposed networks are capable of satisfying the networks' specified utilization and delay requirements. Further, a self-clocking implementation was described that achieves the utilization bounds.

MAC protocols in WLANs/WPANs such as 802.3 (Ethernet), 802.11 (WiFi), 802.15.1 (Bluetooth), 802.15.3, and 802.15.4 (ZigBee) are contention-based (such as CSMA/CD, CSMA/CA, etc.), contention-free (such as polling), or hybrid. Under a single-channel and a half-duplex radio, our bounds hold for all of these MAC protocols, where a particular optimal TDMA

can achieve the tight bound. For contention-based MAC, the bound could not be achieved due to collisions involved (please refer to the detail of the proofs of tight bounds).

Note that even though we assume acknowledgments are implicit, our bounds are still applied when explicit acknowledgments are used, but they are no longer tight bounds. Obtaining tight bounds for explicit acknowledgements are our future work.

As other future work, we will investigate whether optimal schedules exist for irregular topologies and various routing schemes under the fair-access constraint. For underwater sensor networks, further analysis for $\tau > T/2$ is necessary. Moreover, we will further loosen the assumptions in this paper and explore how to apply our analysis method to other networks with different constraints. For example, instead of assuming that the spacing and propagation delays are fixed and equal, we assume there are always spacing and propagation delays error existing in wireless sensor network. We will also explore whether our analysis method can be extended to other network types where both sides of the base station could have sensor nodes or the communication range could be larger such that two-hop or even more hops neighbors can hear messages.

CHAPTER 3

PERFORMANCE ANALYSIS OF COVERAGE IN SENSOR NETWORKS

The coverage problems have been widely studied in conjunction with energy efficiency and lifetime of WSNs. A sensor node can be in the off-duty cycle or can enter power-save mode to conserve battery power. We refer to a sensor node that is in duty to sense its surroundings as an active sensor node and to a sensor that is off duty or enters power-save mode as an inactive sensor node. In a densely deployed WSN, since multiple sensor nodes may cover a subarea or a target, it may not affect the coverage to deactivate and activate sensor nodes alternatively; however, the lifetime of the WSN will be extended. For this purpose, we first propose a random coverage algorithm (also called k-set randomized scheduling algorithm) for WSNs. Then, we provide an evaluation of this random coverage algorithm on the effects of sensor location distribution via both analytical modeling and computer simulations. Our results show that inaccurate sensor location distribution can lead to non-neglectable error of network coverage estimation. As a result, we propose a distribution-free sensor network modeling approach, in which, we take a small sample of the actual deployment, and then apply Kernel-Density Estimator (KDE), a non-parametric statistical analysis, to capture the distribution of the deployment. In practice, this small sample could be a set of enhanced sensor nodes with GPS receivers, and thus their locations can be known after deployment. Based on the estimated sensor node distribution knowledge, the network coverage metrics can be calculated. At last, the analytical and simulation results show that the distribution-free approach leads to much accurate estimation of network coverage.

The rest of this chapter is organized as follows. Section 3.1 discusses the related work. Section 3.2 defines the network coverage problem we are dealing with: randomized scheduling algorithm and coverage intensity. In this section, we also formulate the coverage intensity using general probability distribution, in other words, no assumption on sensor location distribution is assumed. We propose the distribution-free approach in Section 3.3. We use computer simulations to verify the coverage intensity formulization using general probability distribution in Section 3.4. Section 3.5 studies the impacts of sensor location distribution on network coverage estimation, and shows that inaccurate sensor location distributions can render network coverage estimation worthless. In Section 3.6, we present a concrete example to demonstrate the application and effectiveness of the distribution-free approach. We conclude this chapter in Section 3.7 with a summary of findings and a brief discussion of future work.

3.1 Related Work

A sensor network may contain a large number of simple sensor nodes. Sensor nodes are often powered by batteries, and hence have to operate on limited energy budgets. Furthermore, it is difficult to replace batteries in the sensors deployed in inaccessible or inhospitable environments. Thus, many research efforts have studied the energy conservation of sensor nodes to extend sensor network life time [31]. The network lifetime is defined as the time between the initialization of the network and the first case of battery exhaustion among sensor nodes. Extending the network lifetime has been extensively studied [22-24]. Many protocols keep a subset of sensor nodes vigilant for sensing and communication tasks while putting the others in power-save mode [25]. On the other hand, energy efficiency should not be achieved at the cost of

reduced network coverage and connectivity. Thus, the network coverage and connectivity have also been considered simultaneously in some studies [26-29].

In [30], the authors studied a network with sensor nodes deployed strictly in grids. A great deal of work focuses on sensor networks, in which sensor locations follow a Poisson point process and sensors are uniformly distributed in sensing fields (e.g., [35] and [36]). In [34], barrier coverage problems are studied when sensors are distributed along the line with random offsets due to wind and other environmental factors. In [29], the authors investigate energy efficiency in more general sensor networks where the sensor nodes are deployed randomly. The paper [32] proposes a worst and average case algorithm for coverage calculation from the perspective of computational geometry where no sensor location distribution is required. Nevertheless, little work has been done where no prior knowledge of sensor node location distribution is required.

Sensor nodes can be deployed incrementally. The deployment approach proposed in [44] adds sensor nodes one-at-a-time into the network in the most energy-efficient way identified. It is a greedy algorithm that avoids combinatory complexity while providing possible sub-optimal deployment for minimizing power consumption for communications. In [45], an incremental deployment algorithm deploys nodes one at a time such that network coverage is maximized while full line-of-sight connectivity is maintained. The algorithm utilizes information gathered by previously deployed nodes to determine the deployment location of a node. Both a current and an incremental deployment method are proposed in [46]. Relying on geometric sampling theory, it provides a lower bound of the number of sensors required for coverage and connectivity.

Our approach differs from previous work. This chapter studies the impact of sensor location distributions on network coverage and provides a distribution-free approach in which no assumption of sensor location distribution is required and sensor locations can be in any distribution. To the best of our knowledge, no existing literature applies the distribution-free approach to sensor network coverage problems.

3.2 Coverage Intensity

As indicated in [32] and [33], the concept of WSN coverage (network coverage) has a wide range of interpretations due to a variety of sensors and applications. As a result, many different coverage formulations have been proposed. We provide a network coverage formulation by defining the concept of network coverage intensity and by formulizing the coverage intensity using general probability distribution. In other words, we formulize the coverage intensity without using actual sensor location distribution as a priori. To show the impacts of sensor location distributions, we then study and compare the network coverage intensity of a few sensor location distributions in Section 3.5. To verify the effectiveness of our distribution-free approach, we need to compare the coverage intensity estimation obtained using the distribution-free approach with the estimation obtained when actual distributions are known in Section 3.6. Therefore, we apply the formula of coverage intensity derived using general probability distribution to three specific probability distributions to obtain the corresponding results used in Sections 3.5 and 3.6.

3.2.1 Problem Formulation of Coverage Intensity

Assume that n sensors are randomly deployed to form a wireless sensor network to cover a field, which we refer to as the sensing field. The sensor network runs a randomized scheduling algorithm. The randomized scheduling algorithm is given as follows. Let S denote the set of all the n sensor nodes. Let S be divided into k disjoint subsets S_j $(j = 1,2,...,k)$ with each sensor node being randomly assigned to one of these subsets. At any time, only one subset of sensor nodes is active and the rest are inactive. The objective is to extend the network lifetime and maintain satisfactory coverage. We measure the coverage using coverage intensity.

Network coverage intensity is the ratio of the time when a point in the field of the sensor network is covered by at least one active sensor node to the total time. We model the sensor node deployment field as a two-dimensional Cartesian coordination system. The field ranges from 0 to X and from 0 to Y on the X- and Y-axes, respectively. Assume that the sensing area of a sensor is the area of a circle and the sensing range of sensors is R, the radius of the circle. Let $f(x,y)$ denote the probability density function of sensor node locations. Actual deployment of sensor nodes may be unknown, and $f(x,y)$ can be any distribution. Let $P(g,h)$ denote the probability that a given point, (g,h), is covered by at least one sensor node. We have

$$P(g,h) = \iint_{(x-g)^2+(y-h)^2 \le R^2} f(x,y)dxdy \qquad (3.1)$$

Since n sensors are divided into k disjoint subsets, which take turns waking up and performing sensing tasks while the rest of the subsets are in power-save mode. Then the probability that point (g,h) is covered by an active sensor can be written as

$$C(g,h) = 1-[1-P(g,h)/k]^n \qquad (3.2)$$

Coverage intensity is the detection metric for the whole network. Note that point (g,h) is randomly chosen from the sensing field. Thus, the network coverage intensity for the network is

$$C_n = E(C(g,h)) \tag{3.3}$$

It is worth noting that, in the above discussion, no assumption of sensor location distribution is given, and that the sensor location distribution can be any distribution, even one which has no explicit form.

The above derivation does not consider the edge effect. Since the whole sensing field must have boundaries, the coverage area of a sensor node may not be completely inside the sensing field, which we refer to as the edge effect. The computer simulations in Section 3.4 show that the error rate between the simulation and analytical results is very small and can be neglected when the number of sensors is large.

3.2.2 Uniform Distribution

Assume that sensors are uniformly deployed in the sensing field. Fig. 3.1(a) shows an example deployment. Sensor location (g,h) follows a two-dimensional uniform distribution, namely $f(x,y) = 1/(XY)$. By plugging this into equations (3.1)-(3.3), we can obtain the network coverage intensity of the two dimensional uniform distribution.

$$P^U(g,h) = \iint_{(x-g)^2+(y-h)^2 \le R^2} \frac{1}{XY} dxdy = \frac{\pi R^2}{XY} \tag{3.4}$$

$$C^U(g,h) = 1-[1-\frac{\pi R^2}{kXY}]^n \tag{3.5}$$

$$\begin{aligned} C_n^U &= E(C(g,h)) = \int_0^Y \int_0^X \frac{1}{XY} \left\{ 1-[1-\frac{\pi R^2}{kXY}]^n \right\} dxdy \\ &= 1-[1-\frac{\pi R^2}{kXY}]^n \end{aligned} \tag{3.6}$$

where we use superscript U to indicate that sensor locations follow a two-dimensional uniform distribution.

3.2.3 Two-dimensional Gaussian Distribution

Assume that sensor nodes deployed in the sensing field follow a two-dimensional Gaussian distribution. Fig. 3.1(b) shows an example deployment. The probability density function of the two-dimensional Gaussian distribution is given as

$$f(x,y)=\frac{1}{2\pi\sigma^2}e^{-[(x-X/2)^2+(y-Y/2)^2]/2\sigma^2}$$

Plugging this into (3.1), we have

$$P^G(g,h)=\iint_{(x-g)^2+(y-h)^2\le R^2}\frac{1}{2\pi\sigma^2}e^{-[(x-X/2)^2+(y-Y/2)^2]/2\sigma^2}dxdy$$

where subscript G indicates that sensor locations follow a two-dimensional Gaussian distribution.

Let $x'=x-g$ and $y'=y-h$,

$$P^G(g,h)=\iint_{x'^2+y'^2\le R^2}\frac{1}{2\pi\sigma^2}e^{-[(x'+g-X/2)^2+(y'+h-Y/2)^2]/2\sigma^2}dx'dy'$$

Let $x'=l\sin\theta$, $y'=l\cos\theta$, and $|J|=\left|\frac{\partial(x',y')}{\partial(l,\theta)}\right|=l$,

$$\begin{aligned}&P^G(g,h)\\&=\int_0^R\int_0^{2\pi}\frac{1}{2\pi\sigma^2}e^{-[(l\sin\theta+g-X/2)^2+(l\cos\theta+h-Y/2)^2]/2\sigma^2}\,|J|\,dld\theta\\&=\int_0^R\int_0^{2\pi}\frac{1}{2\pi\sigma^2}e^{-[(l\sin\theta+g-X/2)^2+(l\cos\theta+h-Y/2)^2]/2\sigma^2}ldld\theta\end{aligned}\qquad(3.7)$$

Plug (3.7) into (3.2) and (3.3), and we have,

$$C^G(g,h)=1-[1-P^G(g,h)/k]^n \qquad (3.8)$$

$$C_n^G=E(C^G(g,h)) \qquad (3.9)$$

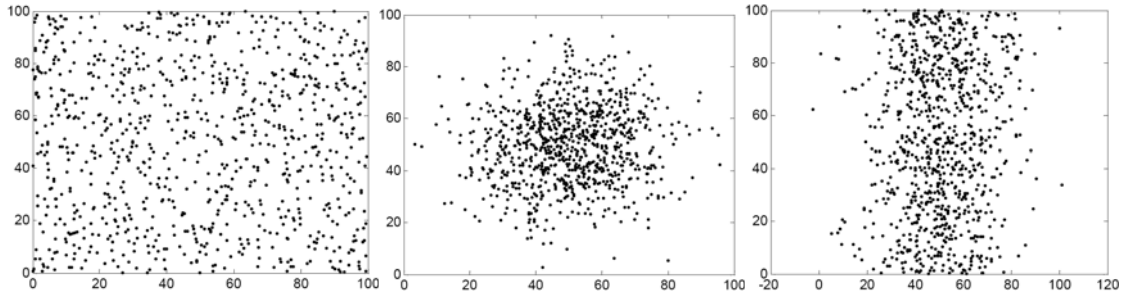

(a) Uniform distribution (b) Gaussian Distribution (c) GU distribution

Fig. 3.1 Sensor node location distributions

3.2.4 GU Distribution

In this subsection, we assume that the known sensor location distribution is the one along the x-axis, where sensor locations follow a Gaussian distribution with a mean of $X/2$, and along the y-axis, where sensor locations follow a uniform distribution with a mean of $Y/2$. Fig. 3.1(c) shows an example deployment. For simplicity, we name this two-dimensional distribution as a GU distribution. As in the above, we need to calculate the probability $P(g,h)$ to obtain coverage intensity under a GU distribution. Thus, we have

$$P^{GU}(g,h) = \iint_{(x-g)^2+(y-h)^2 \le R^2} f(x) f(y) dxdy$$

where $f(x) = \frac{1}{\sqrt{2\pi}\sigma_x} e^{-\frac{(x-X/2)^2}{2\sigma_x^2}}$ and $f(y) = \frac{1}{Y}$. Note that superscript GU indicates that sensor locations follow a GU distribution.

Following steps similar to those in previous subsection, we have

$$P^{GU}(g,h) = \int_0^R \int_0^{2\pi} \frac{1}{\sqrt{2\pi}\sigma_x} e^{-\frac{(l\sin\theta+g-X/2)^2}{2\sigma_x^2}} \frac{1}{Y} l dl d\theta \qquad (3.10)$$

$$C^{GU}(g,h) = 1-[1-P^{GU}(g,h)/k]^n \qquad (3.11)$$

$$C_n^{GU} = E(C^{GU}(g,h)) \quad (3.12)$$

3.3 Distribution-free Approach

In this section, we introduce the distribution-free approach for estimating coverage intensity. The approach uses a non-parametric statistical method [72], [80] It does not require the sensor location distribution to be known. Instead, it requires the locations of a few sensors among the deployed sensors.

There are many studies regarding sensor node localization. Common localization approaches [81-86] rely on a few sensor anchor or beacon nodes whose locations are known in advance, e.g., via GPS signals. Thus, we can have a few sensors whose locations can be accurately determined. Due to random factors in the real world, such as wind, it is impossible for sensor location distributions to be exactly the same as assumed distributions. Since inaccurate knowledge of sensor location distributions can yield misleading or invalid network coverage estimations, we propose a distribution-free approach to estimate the network coverage intensity. The approach is not based on an assumed distribution. Instead, it is based on the locations of a sample of sensor nodes whose locations are known.

In the rest of this section, we first present how we infer sensor location distribution from the locations of a sample of sensor nodes using a non-parametric statistical method, called Kernel-Density Estimation [72], [80]. KDE is one of the mostly used nonparametric techniques. It provides an estimation of arbitrary distribution from empirical data without much prior knowledge. KDE-based methods have been to be robust and effective methods in distributed systems and computer networks [87]. Although other non-parametric statistical methods exist

and are worth investigating, as a step forward, we focus our effort on evaluating the effectiveness of KDE-based method for scheduling and coverage problem in large sensor networks.

3.3.1 Infer Sensor Location Distribution from Locations of Sample Sensor Nodes

Denote the locations of randomly selected sample nodes as (X_i, Y_i), $i = 1,2,...,N$, where N is the sample size. From [80], the probability density at any point (x, y) can be estimated using the locations of the sample of sensor nodes, i.e.,

$$\hat{f}_h(x,y) = \frac{1}{Nh_x h_y} \sum_{i=1}^{N} K\left(\frac{x - X_i}{h_x}, \frac{y - Y_i}{h_y} \right) \tag{3.13}$$

where $K(\square)$ is some kernel and h_x and h_y are smoothing factors or window-width. $K(\square)$ is often taken to be a standard Gaussian function with mean 0 and variance 1, i.e.,

$$K(u,v) = \frac{1}{2\pi} e^{-\frac{1}{2}(u^2+v^2)} \tag{3.14}$$

Plugging (3.14) into (3.13), we get,

$$\begin{aligned} \hat{f}_h(x,y) &= \frac{1}{Nh_x h_y} \sum_{i=1}^{N} K\left(\frac{x - X_i}{h_x}, \frac{y - Y_i}{h_y} \right) \\ &= \frac{1}{Nh_x h_y} \sum_{i=1}^{N} \frac{1}{2\pi} e^{-\frac{1}{2}\left(\frac{(x-X_i)^2}{h_x^2} + \frac{(y-Y_i)^2}{h_y^2} \right)} \end{aligned} \tag{3.15}$$

Note that 1) window-width h_x and h_y indirectly control the variance of the Gaussian function and that 2) probability density functions to be estimated can be multi-modal [72] and by no means have to be Gaussian, even though the kernel is a Gaussian function. Choices of N, h, and $K(\square)$ are the factors determining the efficiency and effectiveness of the estimation of the probability density.

3.3.2 Distribution-free Coverage Intensity Estimation

The approach has four steps: 1) obtaining the locations of the sample sensor nodes; 2) analyzing the locations and obtaining the window-width (h_x and h_y); 3) approximating sensor location distribution using Kernel-density estimation; 4) calculating the coverage intensity based on the Kernel-density estimation.

Though N and $K(\square)$ are also factors related to the efficiency and effectiveness of the approach, they are determined empirically before sensor deployment in this chapter. The above four steps are carried out after sensor deployment without using any assumed sensor location distribution.

The coverage intensity is calculated as follows. Replacing $f(x,y)$ in (3.1) by (3.13), we get

$$\begin{aligned} P^{DF}(g,h) &= \iint_{(x-g)^2+(y-h)^2 \le R^2} \hat{f}_h(x,y)dxdy \\ &= \iint_{(x-g)^2+(y-h)^2 \le R^2} \frac{1}{Nh_xh_y}\sum_{i=1}^{N} K\left(\frac{x-X_i}{h_x},\frac{y-Y_i}{h_y}\right)dxdy \end{aligned} \tag{3.16}$$

where superscript DF indicates we are using the distribution-free approach. Plugging (3.16) into (3.2) and (3.3), we have,

$$C^{DF}(g,h) = 1-[1-P^{DF}(g,h)/k]^n \tag{3.17}$$

$$C_n^{DF} = E(C^{DF}(g,h)) \tag{3.18}$$

3.4 Simulation Verification

In this section, we perform computer simulations to verify the analytical model presented in Section 3.2. We developed our own simulation program in C++. The program is an

implementation of discrete event simulation. The locations of sensors and intrusions are either derived from a given distribution or loaded from a given sensor node configuration. There are three types of events, intrusion events, detection events, and intrusion departure events. An intrusion event is generated randomly. A detection event occurs when the associated intrusion event is detected by at least one sensor node. The departure event is generated whenever the lifetime of the intrusion event expires. In our simulations below, sensor nodes are deployed randomly in the sensing field. The purposes of this section are to demonstrate that 1) the analytical model in Section 3.2 is accurate; and that 2) the edge effect is neglectable. To cope with limited space, we show only the results for GU distributions for the first purpose. For the second purpose, we show only the results for the two-dimensional uniform distributions.

In this section, the standard deviation (σ_x) of Gaussian distribution along the x-axis is 20, the number of deployed sensor nodes (n) is 1000, the size of the whole sensing field is 10000, the sensing area of each sensor is 30, and the number of subsets is 4, unless otherwise stated.

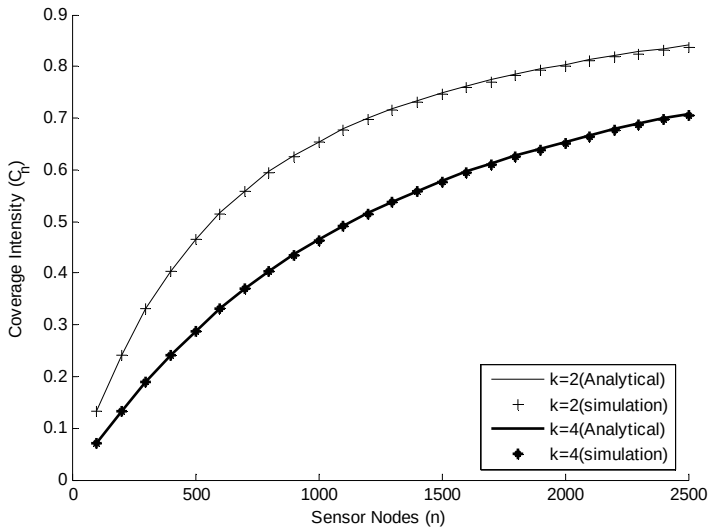

Fig. 3.2 Coverage Intensity vs. Number of Sensor nodes

Fig. 3.2 shows the network coverage intensity vs. the number of sensor nodes with both analytical and simulation results. The figure shows that the analytical results match the simulation results exactly. In addition, the network coverage intensity increases as the number of sensor nodes increases, and the network coverage intensity becomes smaller as the number of disjointed subsets (k) increases.

Fig. 3.3 shows the coverage intensity vs. the number of disjoint subsets (k) with both analysis and simulation. The figure shows that the analytical and simulation results match exactly. Additionally, the network coverage intensity decreases as the number of subsets increases, and the network coverage intensity goes to 0 as the number of disjointed subsets goes to infinity.

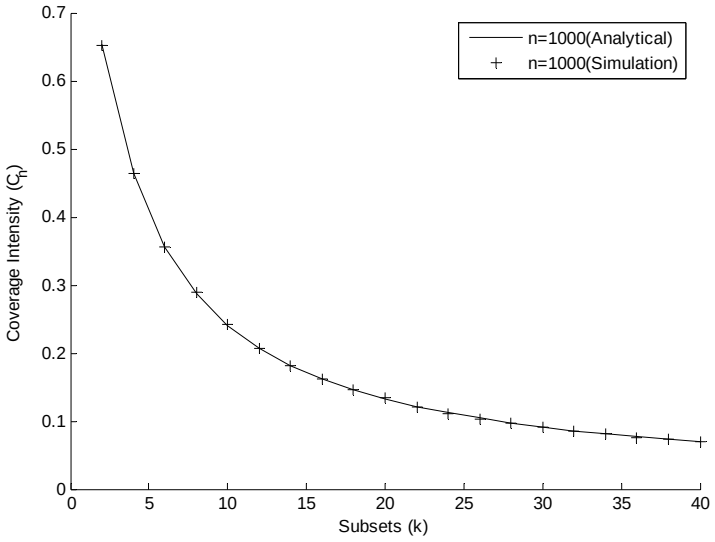

Fig. 3.3 Coverage Intensity vs. Number of Subsets

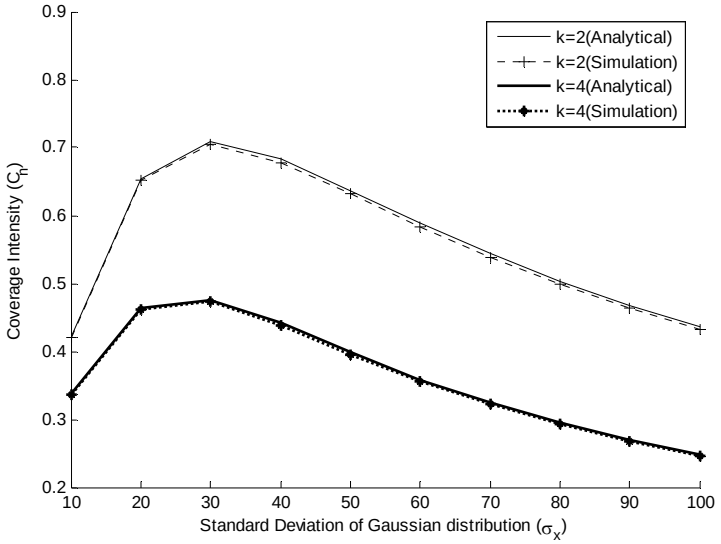

Fig. 3.4 Coverage Intensity vs. Standard Deviation

Fig. 3.4 shows the coverage intensity vs. the standard deviation of Gaussian distribution along the x-axis with both analytical results and simulation results for different numbers of subsets. This figure shows that the analytical results match the simulation results exactly. Furthermore, the network coverage intensity first increases and then decreases as the value of standard deviation increases. A larger k value makes the network coverage intensity smaller. When the value of standard deviation goes to infinity, the network coverage intensity goes to 0. The reason for this trend is that, the larger the standard deviation becomes, the lower the probability that the sensor can be deployed in the designated sensing field becomes.

Fig. 3.5 shows that the error rate between the simulation results and the analytical results is less than 5% when $n = 50$, and much less than 1% when $n = 500$. Error rate is defined as $\left(C_n^a - C_n^s\right) / C_n^s$, where C_n^a and C_n^s denote the coverage intensity obtained from (3.6) and from computer simulations, respectively. It is clear that when the number of sensors is large enough, the error caused by the edge effect can be neglected.

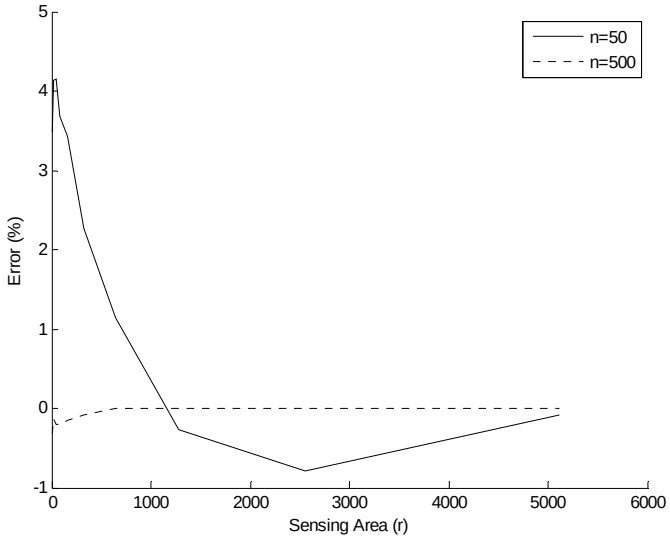

Fig. 3.5 Error of coverage intensity between analytical and simulation results

3.5 Impacts of Sensor Location Distribution on Network Coverage Estimation

In this section, we show the impacts of inaccurate sensor location distribution on network coverage estimation. Intuitively, the discrepancy between actual and estimated network coverage would occur when the knowledge of the sensor location distribution is inaccurate. We intend to demonstrate that the discrepancy is so great that the inaccurate sensor location distributions may in effect render the network coverage estimation worthless and misleading. This section is organized as follows. 1) We compare the calculated coverage intensity when sensor location distributions are uniform and two-dimensional Gaussian respectively. This case can be interpreted to mean that the actual sensor location distribution is a two-dimensional Gaussian distribution; however, we assume the distribution is uniform; or vice versa. 2) Similarly, we next compare the calculated coverage intensity of uniform and GU distributions.

The coverage intensity for uniform distributions is calculated using equation (3.6), that for two-dimensional Gaussian distributions using equation (3.9), and that for GU distributions using equation (3.12). We choose $X = 100$, $Y = 100$, and $R = 3$ unless otherwise stated.

3.5.1 Two-dimensional Gaussian and Uniform Distributions

Figs. 3.6-3.9 show the coverage intensity vs. the number of sensor nodes for both Gaussian and Uniform distributions, when the number of disjoint subsets k and the standard deviation of Gaussian distributions σ vary. The discrepancy of coverage intensity between Gaussian and Uniform distributions when $\sigma = 5$ is greater than that when $\sigma = 15$. Regardless of whether $\sigma = 5$ or 15, the discrepancy of coverage intensity between the two distributions is apparent. Note that when the number of sensors goes to infinity, the coverage intensity of Uniform distribution goes to 1, but the coverage intensity of Gaussian distribution increases much more slowly.

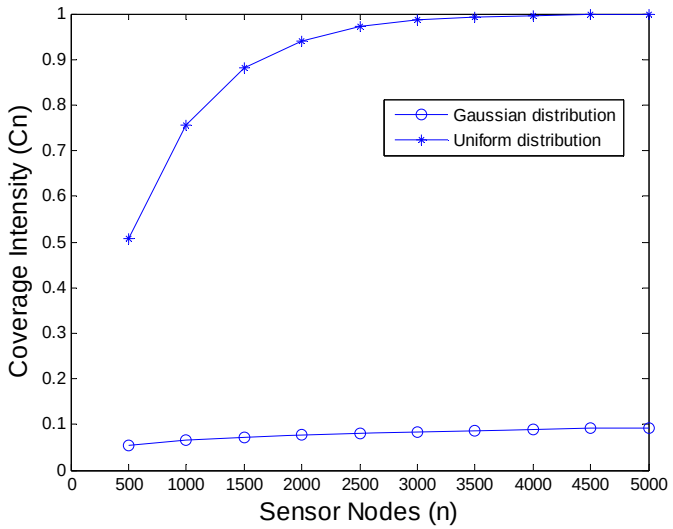

Fig. 3.6 Coverage Intensity vs. Number of Sensor Nodes ($k = 2, \sigma = 5$)

Figs. 3.10-3.11 show the coverage intensity vs. standard deviation of Gaussian distributions. A large discrepancy between uniform and Gaussian distributions can be found when σ is either very small or very large. The reason is that sensors are concentrated at the center of the sensing field when σ is very small and many areas of the field are not covered, and many sensors will be deployed outside of the sensing field when σ is very large.

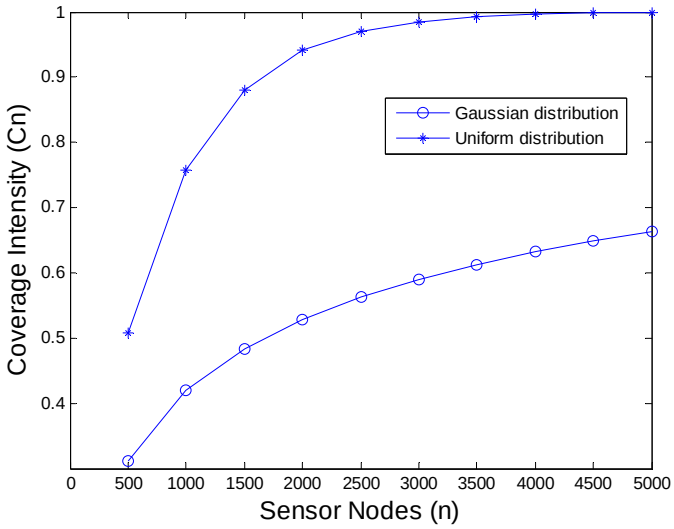

Fig. 3.7 Coverage Intensity vs. Number of Sensor Nodes ($k=2,\sigma=15$)

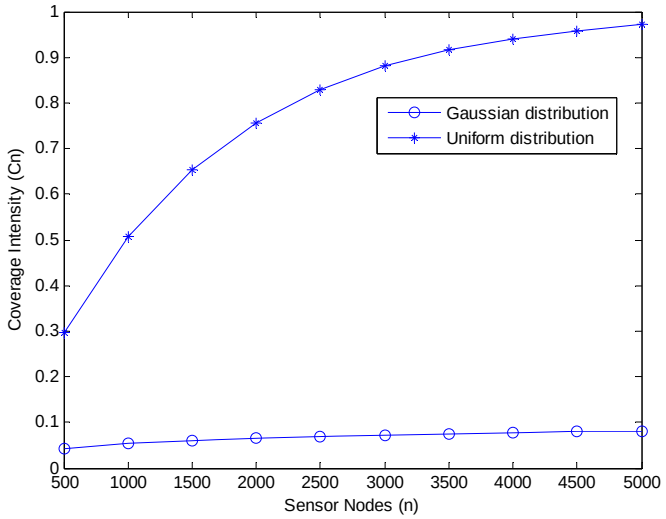

Fig. 3.8 Coverage Intensity vs. Number of Sensor Nodes ($k=4,\sigma=5$)

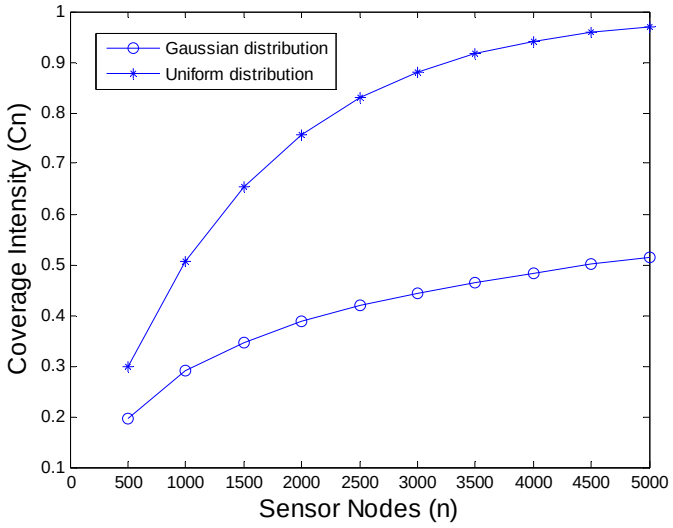

Fig. 3.9 Coverage Intensity vs. Number of Sensor Nodes ($k=4,\sigma=15$)

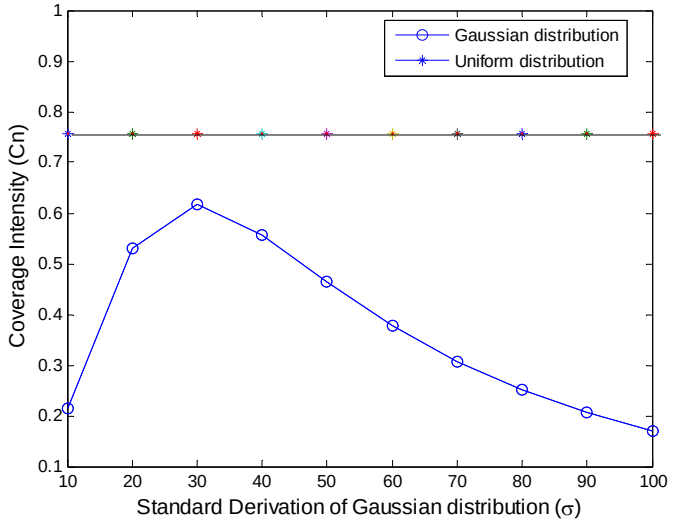

Fig. 3.10 Coverage Intensity vs. Standard Deviation ($n=1000$)

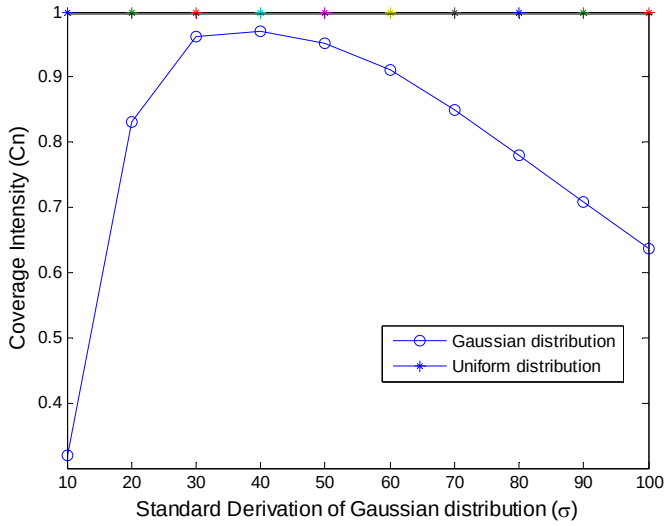

Fig. 3.11 Coverage Intensity vs. Standard Deviation ($n = 5000$)

3.5.2 GU and Uniform Distributions

Figs. 3.12-3.15 show the coverage intensity vs. the number of sensor nodes for both GU and Uniform distributions, when the number of disjoint subsets k and the standard deviation of Gaussian distributions for x-axis σ_x vary. The discrepancy of coverage intensity between GU and Uniform distributions when $\sigma_x = 5$ is greater than that when $\sigma_x = 15$. Regardless of whether in either case, the discrepancy of coverage intensity between two distributions is apparent. Note that, when the number of sensors goes to infinity, the coverage intensity of Uniform distribution goes to 1 but the coverage intensity of GU distribution increases more slowly.

Figs. 3.16-3.17 show the coverage intensity vs. standard deviation of Gaussian distribution. A large discrepancy between uniform and Gaussian distributions can be found when σ_x is either very small or very large. The reason is that sensors are concentrated at the center of the sensing field when σ_x is very small, and many areas of the field are not covered, and many sensors will be deployed outside of the sensing field when σ is very large.

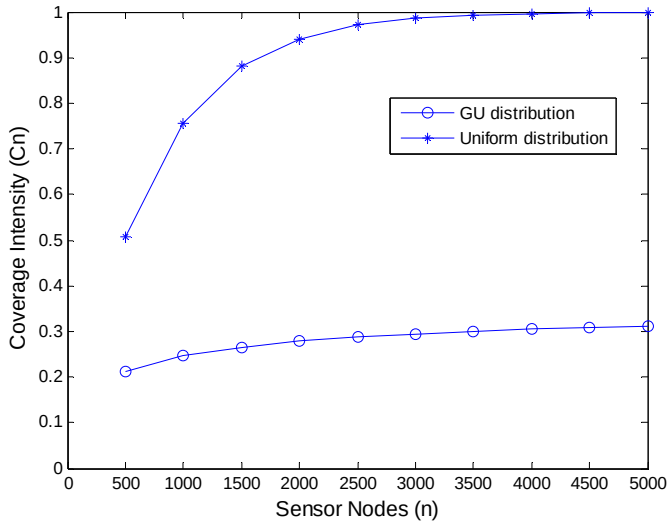

Fig. 3.12 Coverage Intensity vs. Number of Sensor Nodes ($k = 2, \sigma = 5$)

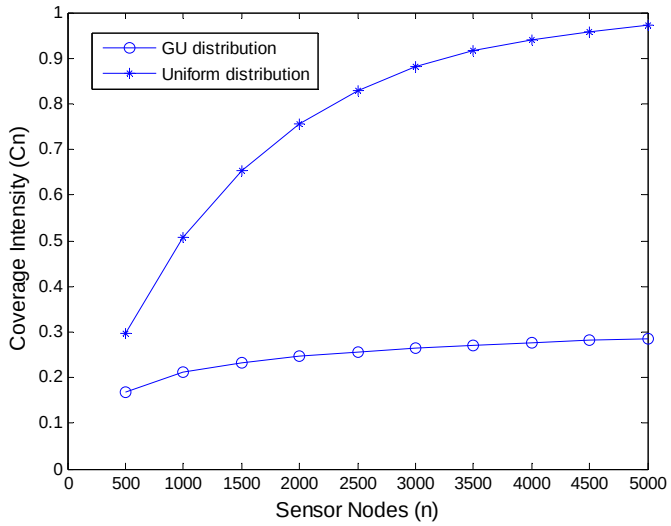

Fig. 3.13 Coverage Intensity vs. Number of Sensor Nodes ($k = 4, \sigma = 5$)

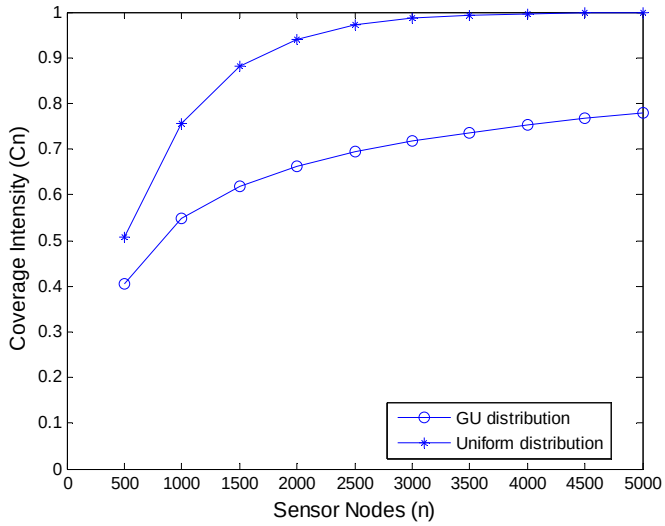

Fig. 3.14 Coverage Intensity vs. Number of Sensor Nodes ($k=2,\sigma=15$)

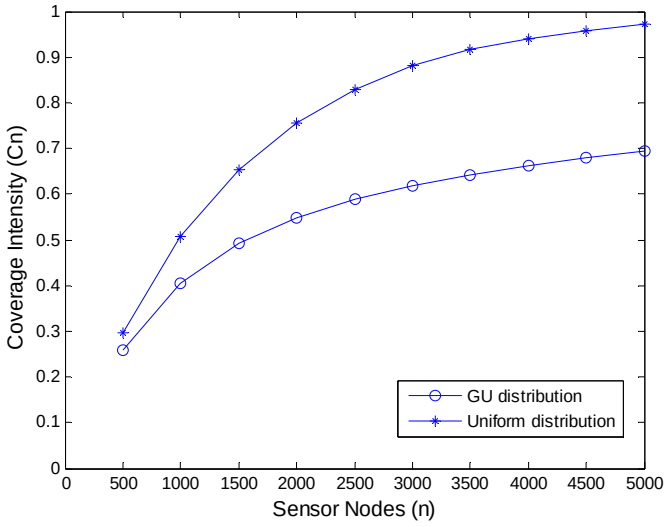

Fig. 3.15 Coverage Intensity vs. Number of Sensor Nodes ($k=4,\sigma=15$)

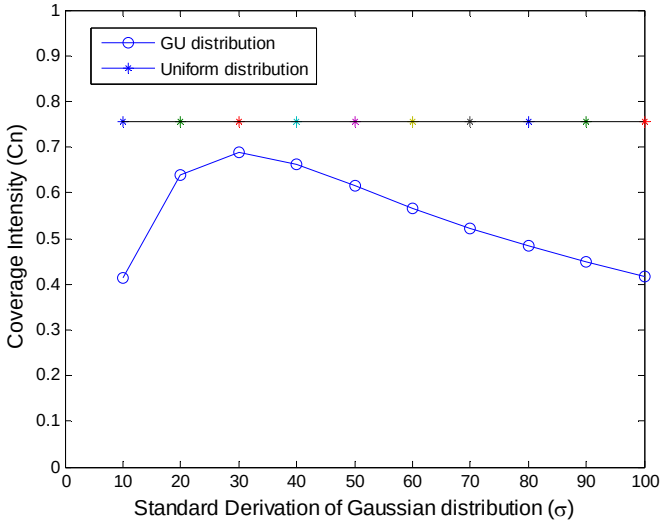

Fig. 3.16 Coverage Intensity vs. Standard Deviation ($n = 1000$)

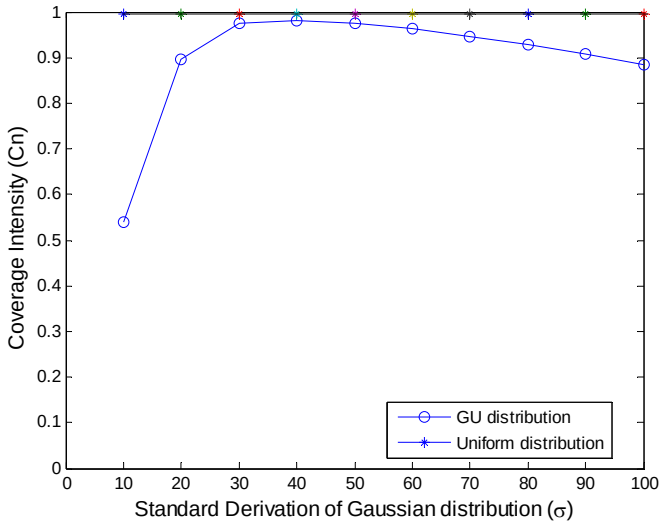

Fig. 3.17 Coverage Intensity vs. Standard Deviation ($n = 4000$)

3.5.3 Deploy-Once and Re-Deploy

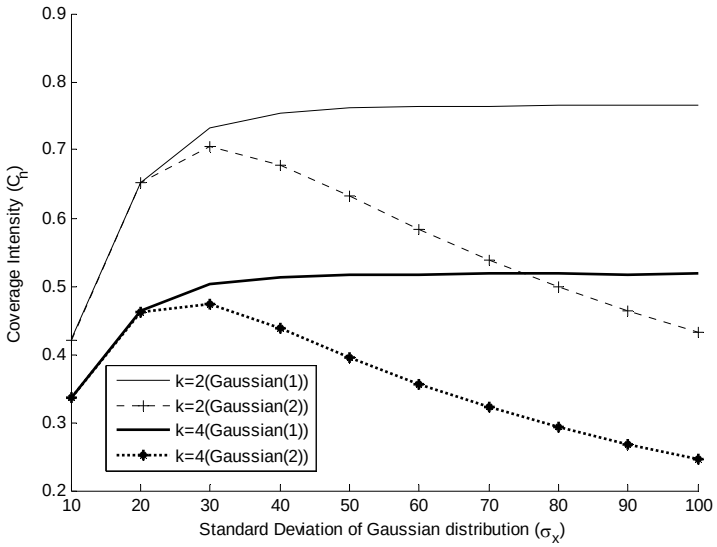

Fig. 3.18 Comparison of two deployment strategies: deploy-once and re-deploy

Fig. 3.18 shows the simulation results of the coverage intensity vs. the standard deviation of Gaussian distribution along the x-axis under two different deployment assumptions. The first assumes that the sensor deployment follows a GU distribution. Under this assumption, the sensor nodes can be deployed either within the intended sensing field or outside of the field. In the second assumption, after deploying a set of sensor nodes, we collect those sensor nodes which are outside the intended sensing field and redeploy them. We repeat this procedure until all sensor nodes are deployed in the designated sensing field. As illustrated in the figure, the network intensity is larger under the second assumption. This figure also shows that the discrepancy of coverage intensity caused by different assumptions can be large.

From the above three cases, we can conclude that the discrepancy of network coverage generated by inaccurate probability distributions is very large and cannot be neglected

3.6 Example and Evaluation of Distribution-Free Approach

In this section, we demonstrate how to apply the distribution-free approach to estimate network coverage intensity. As discussed in Section 3.3, three factors affect the effectiveness and efficiency of the approach. The three factors are kernel $K(\square)$, sample size N, and windows-widths h_x and h_y. Literature has shown that Gaussian function is a good choice for estimating the probability density of continuous random variables using the Kernel-density estimation method [16]. Note that probability density functions to be estimated can be multi-modal and by no means have to be Gaussian, though the kernel is a Gaussian function. Nevertheless, we have to determine sample size and windows-widths beforehand. In subsection 3.6.1, we present some discussion on the sample size and the window-width. In subsection 3.6.2, we present a complete example of the distribution-free approach and compare the result obtained from the distribution-free approach with that obtained from actual distribution.

3.6.1 Sample Size

A larger number of sample sensor nodes leads to better estimation of network coverage. A large sample can be obtained by deploying large numbers of anchor or beacon sensor nodes, or by determining accurate locations of a large number of sensor nodes, which is difficult to do. However, when too few sample sensor nodes are chosen, the network coverage estimation can be inaccurate. In this paper, we use a simple method to determine the sample size. The main idea is to choose a sample size so that the difference of the sample mean and the population mean is within a threshold with a large probability or confidence. The method requires many field experiments and proceeds as follows,

1) Deploy N sensors in a sensing field via a desirable vehicle, e.g., an aircraft or a rocket. Obtain the locations of all the sensors. The sensors are treated as a population, and we

calculate the mean and the variance of the locations of the sensors. Denote the population mean and the population variance as $\bar{Y}$ and S^2 respectively.

2) Randomly select a small number of sensors. The sensors constitute a sample. Obtain their locations. Calculate the mean and the variance of the locations. Denote the sample mean and the sample variance as $\bar{y}$ and s^2, respectively.

3) Calculate the error between the sample mean and the population mean, and denote it as $r = \left(\bar{y} - \bar{Y}\right) \Big/ \bar{Y}$.

4) As suggested in [12], the proper sample size is estimated as $n = \left(\frac{u_{\alpha/2} S}{r\bar{Y}}\right)^2 \Bigg/ \left[1 + \frac{1}{N}\left(\frac{u_{\alpha/2} S}{r\bar{Y}}\right)^2\right]$, where $u_{\alpha/2}$ is the value of the vertical boundary for the area of $\alpha/2$ in the right tail of the standard normal distribution.

5) Repeat the above steps a few times to reach a consensus.

The work of deciding sample size is implemented in a test field where we can easily collect the data of sensor locations. In reality, the sensor network is usually deployed in a hostile field or a rough area where it is hard to collect the locations of many sensors. However, based on the result of sample size obtained from our experiment in the test field, we can choose a small group of sensors as samples before the real deployment and equip these sample sensors as beacons which have the functions to know their coordinates after deployment from satellite information [15]. After deployment in reality, we can estimate the distribution of sensor deployment based on sample sensor locations which will introduce in the following section.

3.6.2 Window-Width

For simplicity, let $h_x = h_y = h$ in this subsection. In the following, we will show the impact of window-width (h) for the coverage intensity estimation in three different cases, 1) two-dimensional Gaussian distribution, 2) two-dimensional Uniform distribution, and 3) GU (X-Gaussian Y-Uniform) distribution.

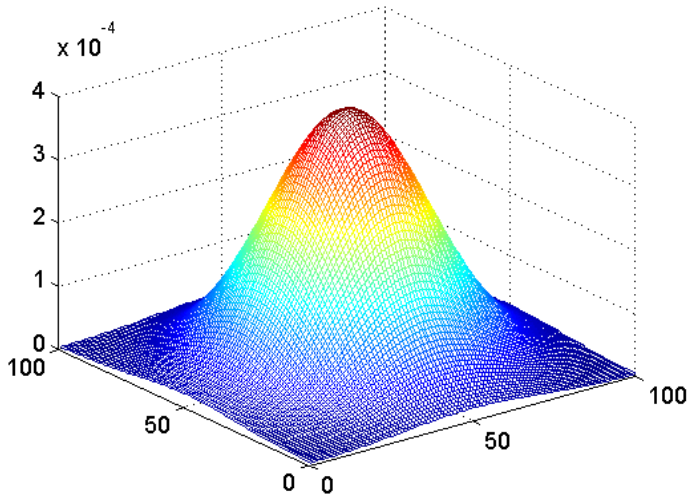

Fig. 3.19 Two-dimensional Gaussian distribution

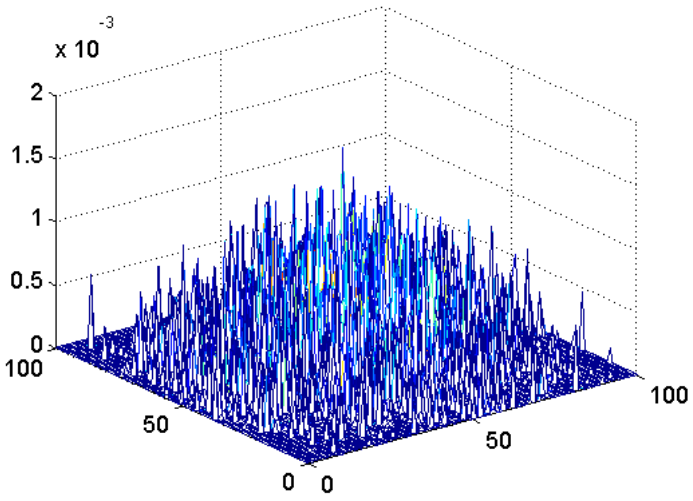

Fig. 3.20 Estimation (window-width (h) =1)

Fig. 3.19 shows the probability density function of two-dimensional Gaussian distribution on the whole sensing field. Fig. 3.20 shows the estimated distribution when window-width (h) is chosen as 1. From the figure, we can see many interferences. From Fig. 3.22, where the window-width (h) is chosen as 25, we can see that the estimation is too flat because we ignore too much random interference in locality. Finally, from Fig. 3.21, where the window-width (h) is chosen as 10, we see that the approximated estimation is the best.

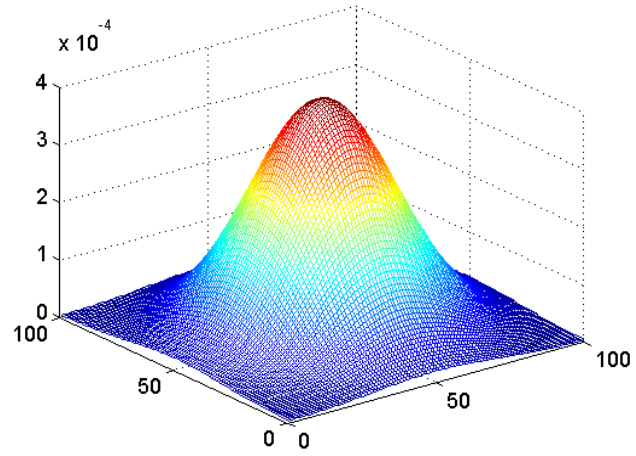

Fig. 3.21 Estimation (window-width (h) =10)

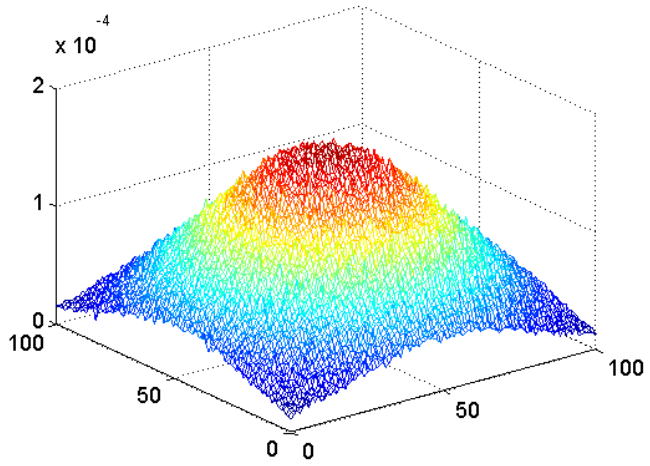

Fig. 3.22 Estimation (window-width (h) =25)

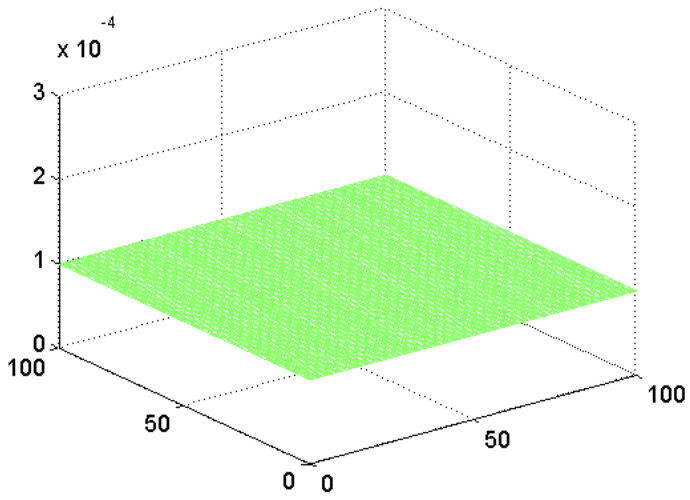

Fig. 3.23 Two-dimensional uniform distribution

Fig. 3.23 shows two-dimensional uniform distribution on the whole sensing field. Fig. 3.24 shows the estimated density function when window-width (h) is chosen as 1. From the figure, we can see many interferences. From Fig. 3.26, where the window-width (h) is chosen as 3.25, we can see that the estimation is too curved because we ignore too much random interference in locality. Finally, from Fig. 3.25, where the window-width (h) is chosen as 10, we see that the approximated estimation is the best.

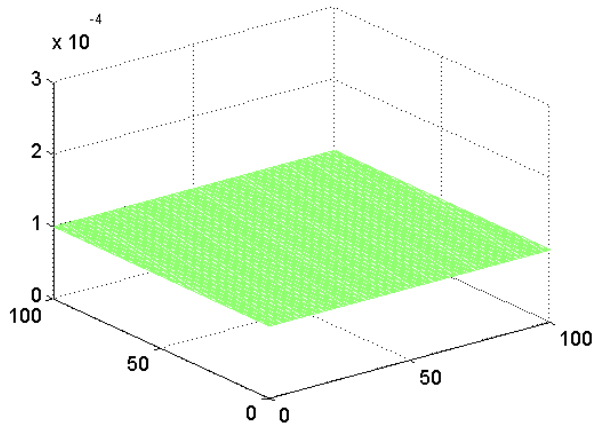

Fig. 3.24 Estimation (window-width (h) =1)

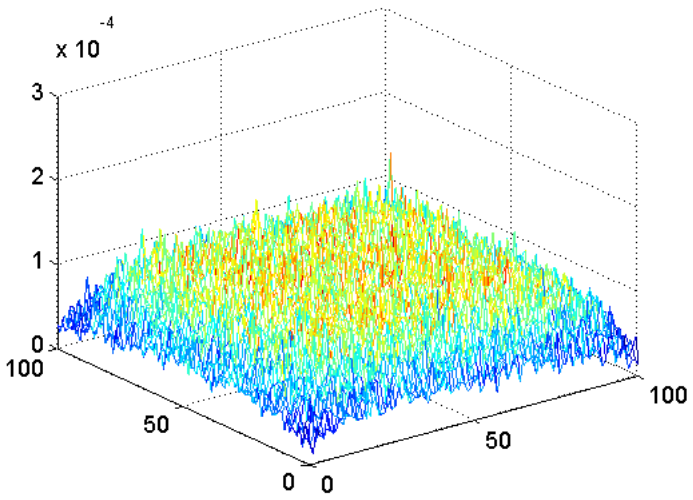

Fig. 3.25 Estimation (window-width (h) =10)

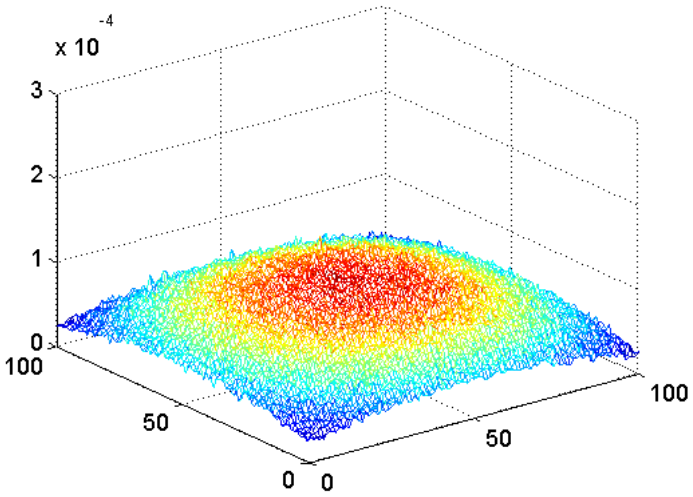

Fig. 3.26 Estimation (window-width (h) =25)

Fig. 3.27 shows GU distribution on the whole sensing field. Fig. 3.28 shows the estimated distribution when window-width (h) is chosen as 1. From the figure, we can see much interference. From Fig. 3.30, where the window-width (h) is chosen as 25, we can see that the curve face is too flat because we ignore too much random interference in locality. Finally, from

Fig. 3.29, where the window-width (h) is chosen as 10, we see that the approximated estimation is the best.

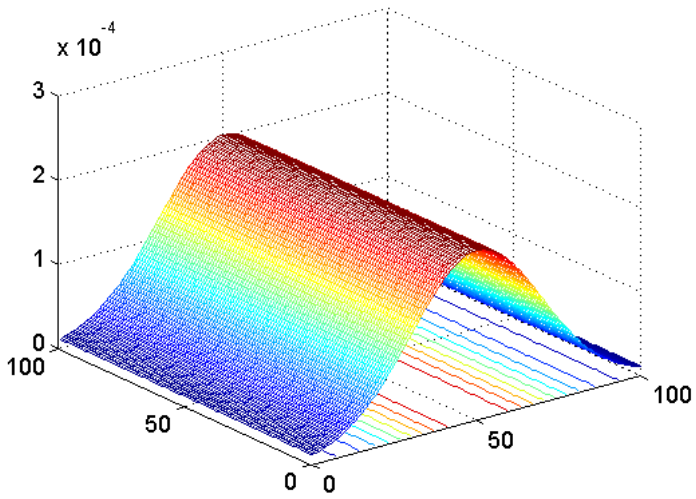

Fig. 3.27 x-Gaussian, y-uniform distribution

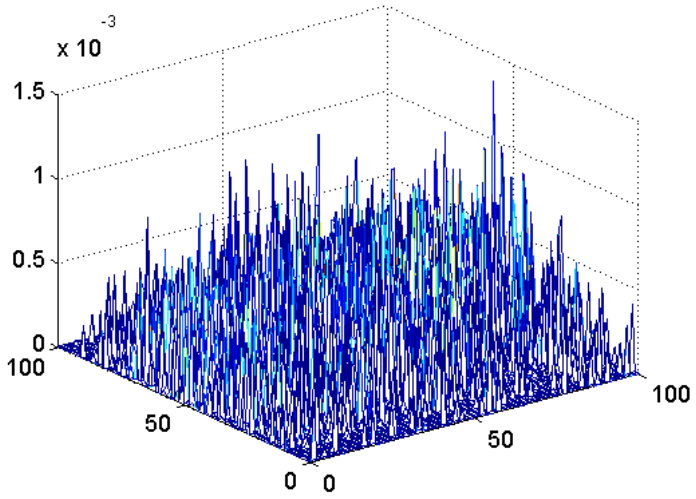

Fig. 3.28 Estimation (window-width (h)=1)

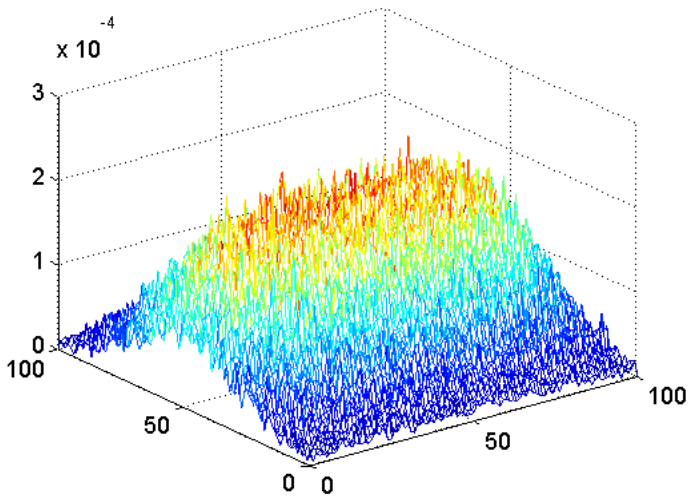

Fig. 3.29 Estimation (window-width (h) =10)

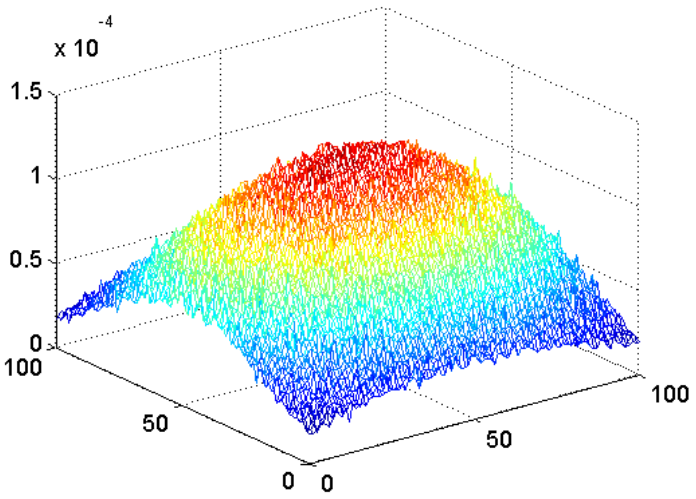

Fig. 3.30 Estimation (window-width (h) =25)

3.6.3 Example of Distribution-Free Approach

Step 1: Obtain locations of sample sensors

First, before deployment, according to the number of sensor nodes deployed in the sensor network, we decide how many samples we need to provide based on the results obtained from

the sample size section. Then we randomly choose the number of sample nodes and set them as anchor nodes. Second, after random deployment, the sample sensors' location coordinates can be obtained via a sensor localization protocol. Here, the locations of the sample sensors are (X_i, Y_i), $i = 1, 2, ..., N$, where N is the sample size. Table 3.1 shows an example of the locations of the sample sensors. In the example, the whole deployment area is $X \times Y = 100m \times 100m$, the sensing area of each sensor is 30 m^2, the number of sample sensor nodes is $N = 50$, and the standard deviation of GU distribution along the x-axis is 5.

Table 3.1 Locations of Sample Sensors

Sample		Sample	
(X_1, Y_1)	44.95, 19.34	(X_{14}, Y_{14})	48.83, 70.27
(X_2, Y_2)	53.07, 68.22	(X_{27}, Y_{27})	50.59, 54.66
(X_3, Y_3)	52.54, 30.28	(X_{28}, Y_{28})	51.57, 44.49
(X_4, Y_4)	58.46, 54.17	(X_{29}, Y_{29})	57.22, 69.45
(X_5, Y_5)	52.96, 15.09	(X_{30}, Y_{30})	48.25, 62.13
(X_6, Y_6)	46.78, 69.79	(X_{31}, Y_{31})	53.17, 79.48
(X_7, Y_7)	51.90, 37.84	(X_{32}, Y_{32})	53.99, 95.68
(X_8, Y_8)	44.95, 86.00	(X_{33}, Y_{33})	54.70, 52.26
(X_9, Y_9)	49.90, 85.37	(X_{34}, Y_{34})	45.04, 88.01
(X_{10}, Y_{10})	49.76, 59.36	(X_{35}, Y_{35})	51.06, 17.29
(X_{11}, Y_{11})	50.00, 49.66	(X_{36}, Y_{36})	51.19, 97.97
(X_{12}, Y_{12})	48.41, 89.98	(X_{37}, Y_{37})	44.96, 27.14
(X_{13}, Y_{13})	55.48, 82.16	(X_{38}, Y_{38})	46.29, 25.23
(X_{14}, Y_{14})	40.63, 64.49	(X_{39}, Y_{39})	55.41, 87.57
(X_{15}, Y_{15})	52.14, 81.80	(X_{40}, Y_{40})	49.34, 73.73
(X_{16}, Y_{16})	54.48, 66.02	(X_{41}, Y_{41})	51.95, 13.65
(X_{17}, Y_{17})	53.65, 34.20	(X_{42}, Y_{42})	50.44, 1.17
(X_{18}, Y_{18})	52.89, 28.97	(X_{43}, Y_{43})	46.82, 89.39
(X_{19}, Y_{19})	50.20, 34.12	(X_{44}, Y_{44})	47.20, 19.91
(X_{20}, Y_{20})	53.38, 53.40	(X_{45}, Y_{45})	52.22, 29.87
(X_{21}, Y_{21})	52.84, 72.71	(X_{46}, Y_{46})	45.25, 66.14
(X_{22}, Y_{22})	48.72, 30.93	(X_{47}, Y_{47})	53.91, 28.44
(X_{23}, Y_{23})	48.11, 83.85	(X_{48}, Y_{48})	52.84, 46.92
(X_{24}, Y_{24})	48.52, 56.81	(X_{49}, Y_{49})	45.89, 6.48
(X_{25}, Y_{25})	42.62, 37.04	(X_{50}, Y_{50})	48.67, 98.83

Step 2: Window-Width (h)

In Kernel Density Estimation, the window-width plays an important role. Many numerical methods have been developed to find h, and they mostly minimize the so-called Mean Integrated Squared Error [72]. In our experiment, we use a fast and accurate bivariate kernel density estimator as in [72] to obtain the window-width values (h_x and h_y). For example, based

on the sample sensor location data in Fig. 3.19, the bivariate window-width we obtained is $(h_x, h_y) = (3.88, 16.71)$.

Step 3: Distribution Estimation

Based on the sample location coordinates from step 1 and the bivariate window-width from step 2, the density function can be calculated using equation (3.15) since we use Gaussian function as the kernel.

The sensor location distribution in the real world (GU distribution) is given in Fig. 3.31(a), and the estimation based on the locations of sample sensors as shown in Table 3.1 is given in Fig. 3.31(b). Through comparing these two distribution figures, we can see that the estimated distribution is quite close to the actual distribution. Note that a better estimation can be achieved by increasing the size of the sample of sensor nodes.

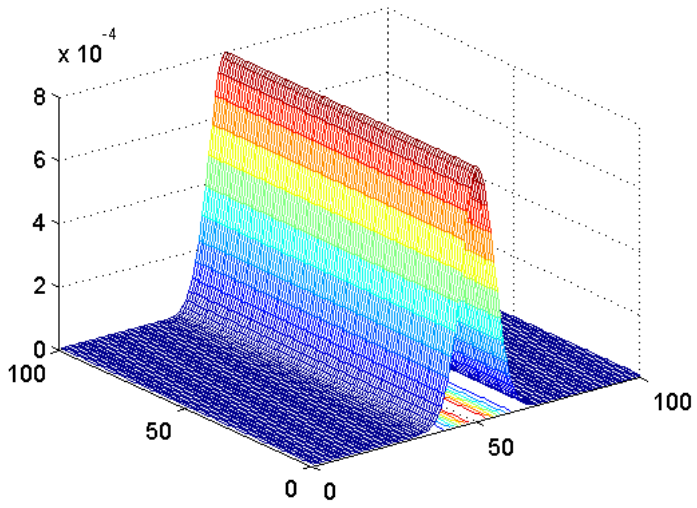

(a) GU distribution (standard deviation=5)

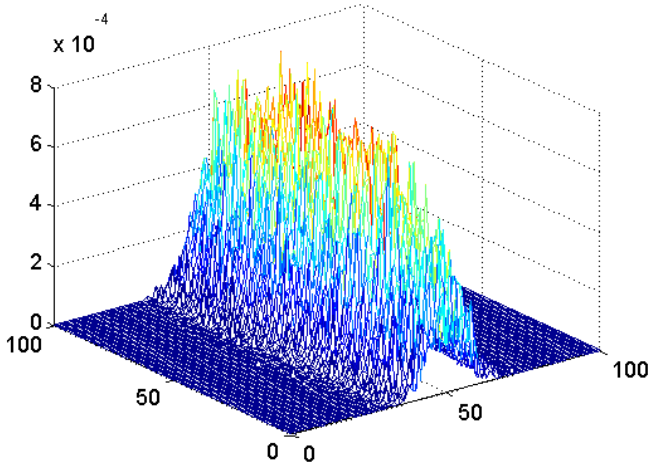

(b) Distribution Estimation

Fig. 3.31 Estimation Evaluation

Step 4: System performance evaluation

In this step, we can use the distribution estimation result to study the network performance metrics of interest. In our experiment, the coverage intensity is the studied network metric. Based on (3.16)-(3.18), the estimated coverage intensity can be obtained. Fig. 3.32 shows the estimation results.

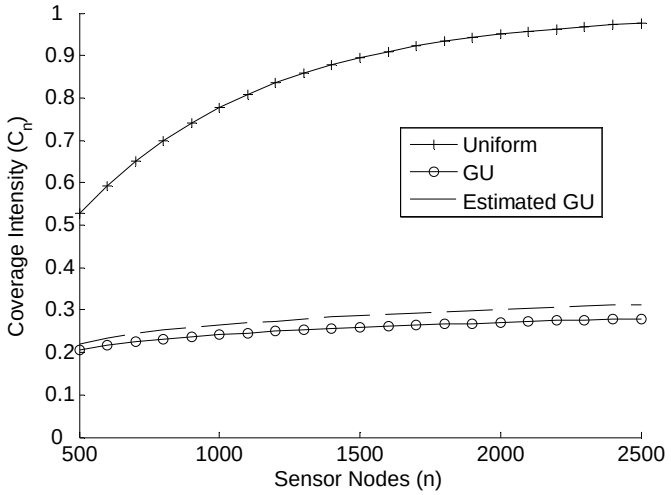

Fig. 3.32 Estimation performance (size of sample=50)

Fig. 3.32 shows the network coverage intensity vs. the number of sensor nodes for Uniform distribution, GU distribution, and the Estimated GU distribution, where the standard deviation of Gaussian distribution along the x-axis is 5 and the number of disjointed subsets is 2. In the experiment, the size of the whole sensing field is 10000 and the sensing area of each sensor is 30. In Fig. 3.32, in the sensor network, the number of whole deployed sensors varies from 500 to 2500; but we only use 50 sample sensors to estimate the distribution through the kernel density estimation method.

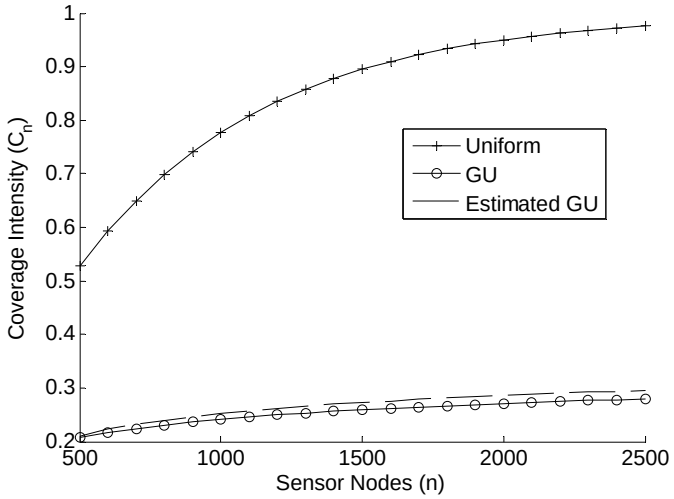

Fig. 3.33 Estimation performance (size of sample=100)

By increasing the size of the sample, we can improve our estimation accuracy, as illustrated in Fig. 3.33; the estimation of coverage intensity using 100 sensor nodes is better than the performance estimation shown in Fig. 3.32, where 50 sensor nodes are used.

3.7 Conclusion

Network coverage is an important problem of WSNs. Previous works are largely based on assumed probability density functions that govern the distribution of sensor nodes in the sensing field. However, the actual distribution of sensor nodes may be very different from the

assumed one. Our analytical and simulation study shows that, when a different assumption is used, the introduced error in the network coverage metrics is very large and cannot be neglected.

In this chapter, we first reformulated the network coverage intensity using general probability distribution. In other words, we did not assume that the sensor location distributions were known. We verified the formulization using computer simulations, which showed that the analytical results and computer simulations matched exactly.

Most importantly, we proposed a distribution-free approach for estimating network coverage intensity. In our proposed method, no assumption on sensor location distribution was required. Instead, we take a small sample of the actual deployment, and carry out a statistical analysis to capture the distribution function of the deployment. In practice, this small sample could be a set of enhanced sensor nodes with GPS receivers, and thus their locations can be known. Furthermore, we used the Kernel Density Estimator to estimate the deployment distribution. Based on the obtained knowledge, the network coverage metrics can be calculated.

The results show that a small sample of sensor nodes yields fairly good estimates of the distribution used. In particular, compared to the case in which a different assumption (the uniform distribution) than actual sensor location distribution (GU distribution) is used, the distribution-free approach yields far better results.

CHAPTER 4

ERROR ANALYSIS AND KERNEL DENSITY APPROACH OF SCHEDULING SLEEPING NODES IN WIRELESS SENSOR NETWORKS

In this chapter, we investigate system performance metrics including energy consumption and network lifetime in WSNs. In chapter 3, we proposed a distribution-free approach for estimating network coverage intensity. In this chapter, we show this distribution-free methodology can be generalized and extended to study many other sensor network metrics including network lifetime. Furthermore, previous studies normally assume that battery energy levels of sensor nodes are the same. However, in a real network, battery quality is different and the battery energy in each sensor node is a random variable. We provide a mathematical approximation and a standard deviation study for energy consumption, as well as a more deep study for network lifetime under random battery energy. We adopt network energy consumption model in [47] as an example to verify our ideas.

The rest of this chapter is organized as follows. In Section 4.1, we review some background. In Section 4.2, we provide an error analysis with different distributions via mathematical analysis. A standard derivation study and a network lifetime study are presented in Section 4.3. In Section 4.4, we use the distribution free method to estimate the energy consumption and present some numerical results. Finally, we conclude this paper in Section 4.5.

4.1 Background

This section summarizes a Randomized Scheduling (RS) scheme [47], in which nodes are randomly selected to sleep in high density cluster-based sensor networks. In other words, each sensor node is selected by the cluster head with the probability β under following assumptions. 1) Each sensor node belongs to the same cluster throughout its lifetime. 2) Nodes are randomly distributed as a two-dimensional Poisson point process with density ρ. In other words, the probability of finding n nodes in a region of area A is equal to $(\rho A)^n \exp(-\rho A)/n!$. Furthermore, these n nodes in the area A are uniformly distributed. 3) The maximum transmission range of the cluster head is denoted by R and there are n sensor nodes in the cluster. The cluster covers a circular geographic area of πR^2 with the cluster head at the center. The cluster head plans to allow, on average, $n \cdot \beta$ ($\beta < 1$) nodes to sleep in each cycle.

The energy consumption rate is defined as the energy consumed per second when the sensor is active and is generally a positive, convex function of the distance between the sensor node and the head of cluster $E_{active}(x) = C(x) + K$, where K is a positive constant and $C(x)$ is a nonnegative convex function. In [47] the authors used a power function as

$$E_{active}(x) = \lambda \cdot k_1 \cdot [\max(x_{\min}, x)]^{\gamma} + k_2 \tag{4.1}$$

where λ denotes the average packet transmission rate per second of each sensor node, x is the distance between the sensor node and the cluster head, k_1 is the constant corresponding to energy consumption due to transmission of each packet, k_2 is the idle/receive energy consumption per second, $x_{\min}$ is the minimum allowable transmission range corresponding to the minimum allowable transmission energy, and $\gamma \geq 2$ is the path loss exponent. From [47], the expected energy consumption of each node during a second in the RS scheme is computed as

$$E = \int_0^R (1-\beta) \cdot f(x) \cdot E_{active}(x) \cdot dx \tag{4.2}$$

where $f(x)$ is the probability density function of the distance, x, between a sensor and the cluster head. Because it is assumed that sensor nodes are uniformly distributed in the circular coverage area of the cluster, based on [47], $f(x)$ is

$$f(x) = \frac{\partial F}{\partial x} = \frac{\partial[\Pr(X \le x)]}{\partial x} = \frac{\partial}{\partial x}\left[\frac{\pi x^2}{\pi R^2}\right] = \frac{2x}{R^2} \tag{4.3}$$

where $0 \le x \le R$. According to the assumption that the number of sensor nodes is distributed according to a two-dimensional Poisson point process with expected density ρ, from [47], the average E over all possible numbers of nodes in a cluster:

$$E^{(overall)} = \sum_{n=0}^{\infty} nE \frac{(\rho\pi R^2)^n}{n!} \cdot e^{-\rho\pi R^2} = E \cdot \rho\pi R^2 . \tag{4.4}$$

Based on [47], the network lifetime $T(\beta_d)$ is defined as the time when a fraction of sensor nodes, β_d, run out of energy. Let Ψ be the total battery energy each sensor node carries when the sensor network is initialized. In the RS scheme, the time when β_d fraction of nodes run out of battery is the time when sensor nodes with $x \ge x_d$ all run out of battery, from [47] x_d satisfies:

$$\beta_d = \int_{x_d}^R f(x)dx = \frac{R^2 - [x_d]^2}{R^2} . \tag{4.5}$$

The network lifetime of the RS scheme is

$$T(\beta_d) = \frac{\Psi}{E(x_d)} = \frac{\Psi}{(1-\beta)\{\lambda \cdot k_1 \cdot [\max(x_{\min}, x_d)]^{\gamma} + k_2\}} \tag{4.6}$$

4.2 Discrepancy Analysis

System performance evaluations are always based on certain set of assumptions. However, those assumptions may not be held exactly in real world systems. For example, in the RS scheme [47], all the conclusions for the scheme are based on the assumption that sensor nodes are independently and uniformly distributed in each cluster. In fact, deployment of sensor nodes is impacted by many factors such as weather, terrain and so on. Thus, locations of sensor nodes do not necessarily follow a uniform distribution, or other distributions which researchers may choose. In this section, we will present the error analysis when the assumptions are different. For simplicity, we give some notations. Let $\tilde{E}^{(overall)}$ and $\tilde{T}(\beta_d)$ denote the overall expected energy consumption and the network lifetime in a cluster derived from real-world sensor node distribution data, respectively. Thus, their discrepancy can be given by

$$E_{error} = | E^{(overall)} - \tilde{E}^{(overall)} | \tag{4.7}$$

$$T_{error} = | T(\beta_d) - \tilde{T}(\beta_d) | \tag{4.8}$$

In order to show the discrepancy in system performance generated by assumptions, based on [47], we first assume that sensor nodes are still randomly distributed as a two-dimensional Poisson point process with density ρ. That is, the probability of finding n nodes in a region of area A is equal to $(\rho A)^n \exp(-\rho A)/n!$. However, n nodes in the area A follow a two-dimensional Gaussian distribution. We assume that the deployment region of sensor nodes in a cluster is modeled in a two-dimensional Cartesian coordination system and cluster head located at point (0, 0). Then, we present the performance derived from this new assumption. Finally, the performance from two assumptions is compared by several figures. In the following, we give the performance error analysis.

4.2.1 Energy consumption

According (4.1) and (4.2), the expected energy consumption of each node during a second is

$$\tilde{E} = \int_0^R (1-\beta) \cdot \tilde{f}(x) \cdot E_{active}(x) \cdot dx \qquad (4.9)$$

where $\tilde{f}(x)$ is the probability density function (PDF) of the distance, X, between a sensor and the cluster head. It is clear that X is a random variable and $\Pr(X \le x)$ denotes the probability that the distance between a sensor and the cluster head is less than or equal to x. Since nodes follow the two-dimensional Gaussian distribution in each cluster, we have

$$\tilde{F}(x) = \Pr(X \le x) = \frac{1}{2\pi\sigma^2} \iint_{i^2+j^2 \le x^2} e^{-\frac{i^2+j^2}{2\sigma^2}} didj \qquad (4.10)$$

Let $i = r\sin\theta$ and $j = r\cos\theta$, where $0 \le r \le x$ and $0 \le \theta \le 2\pi$. Thus we have

$$\tilde{F}(x) = \Pr(X \le x) = \frac{1}{2\pi\sigma^2} \int_0^{2\pi} \int_0^x e^{-\frac{r^2}{2\sigma^2}} |J| drd\theta \qquad (4.11)$$

where $|J| = \begin{vmatrix} \frac{\partial i}{\partial r} & \frac{\partial i}{\partial \theta} \\ \frac{\partial j}{\partial r} & \frac{\partial j}{\partial \theta} \end{vmatrix} = r$.

Thus, we have

$$\tilde{f}(x) = \frac{\partial \tilde{F}(x)}{\partial x} = \frac{\partial[\Pr(X \le x)]}{\partial x} = e^{-\frac{x^2}{2\sigma^2}} \cdot \frac{x}{\sigma^2}. \qquad (4.12)$$

Therefore, for the expected energy consumption of each node during a second, we have

$$\tilde{E} = \lambda k_1 (1-\beta)[x_{\min}^{\gamma}(1 - e^{-\frac{x_{\min}^2}{2\sigma^2}}) + \int_{x_{\min}}^R e^{-\frac{x^2}{2\sigma^2}} \frac{x^{\gamma+1}}{\sigma^2} dx] + k_2(1-\beta)(1 - e^{-\frac{R^2}{2\sigma^2}}) \qquad (4.13)$$

From (4.4) we have

$$\tilde{E}^{(overall)} = \tilde{E} \cdot \rho\pi R^2 \qquad (4.14)$$

To show the error analysis, we need choose the same parameters in [47] for the sensor network. Thus, based on [47], in the sensor network, we assume that there are $n = 500$ sensor nodes in each cluster, $k_1 = 10^{-6} J/(frame \cdot m^2)$, $k_2 = 0.1J/\sec$, $x_{\min} = 5m$, and $\lambda = 100\, frame/\sec$. The maximum transmission range of the cluster head is $R = 100$.

Figs. 4.1(a)-(c) show the energy consumption vs. fraction of sensor nodes allowed to sleep β for both Gaussian distribution and Uniform distribution where the standard derivation of Gaussian distribution is 50 or 30, namely $\sigma = 50$ or $\sigma = 30$, respectively. As illustrated in the figures, the energy consumption decreases when β increases for both Gaussian distribution and Uniform distribution. When $\beta = 0$, the energy consumption achieves the maximum value. Also, it is easy to see that when the fraction of sensor nodes allowed to sleep goes into 1, the energy consumption goes to 0 for both distributions. When β increases, each sensor node in the cluster has higher probability to be selected to sleep, and thus, the energy consumption decreases. When $\beta = 1$, that means that all sensor nodes are elected to sleep, and thus the energy consumption is 0. From Figs. 4.1(a)-(c), we observe that when path loss exponent increases, the energy consumption for both distributions increases quickly. When β increases, the discrepancy between two distributions decreases until reaching zero. Because when β increases, each sensor node in the cluster has higher probability to be selected to sleep, and thus, the energy consumption decreases. When $\beta = 1$, that means all sensor nodes are elected to sleep, and thus for both distribution the energy consumption is 0.

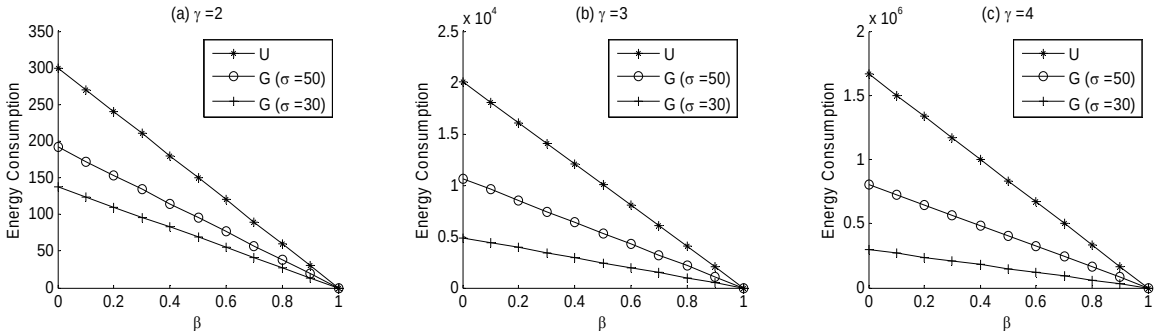

Fig. 4.1 Energy Consumption Comparison (β=Fraction of Sensor Nodes Allowed to Sleep; U=Uniform Distribution; G=Gaussian Distribution)

Comparing Figs. 4.1(a)-(c), we find that under the same parameters, when path loss exponent increases, the discrepancy becomes larger. As illustrated in Fig. 4.1, when the standard derivation of Gaussian distribution is 30, the discrepancy is larger than when the standard derivation of Gaussian distribution is 50. This fact shows that the deployment of sensor nodes in paper [47] is more similar with the Gaussian distribution with $\sigma = 50$ than Gaussian distribution with $\sigma = 30$. Fig. 4.1 also shows that the discrepancy of energy consumption is pretty large under different assumptions of deployment distributions of sensor nodes.

4.2.2 Approximation

As mentioned above, we can obtain the expected energy consumption of each node during a second by equation (4.13). When the coverage radius of the cluster R is large and the minimum transmission range $x_{\min}$ is small, we can get an approximation expression of expected energy consumption of each node during a second. Firstly, when R is large and $x_{\min}$ is small, we have

$$\int_{x_{\min}}^{R} e^{-\frac{x^2}{2\sigma^2}} \cdot \frac{x^{\gamma+1}}{\sigma^2} dx \approx \int_{0}^{\infty} e^{-\frac{x^2}{2\sigma^2}} \cdot \frac{x^{\gamma+1}}{\sigma^2} dx \qquad (4.15)$$

Then, we do some mathematic transformations for (4.15) as follow:

$$\int_0^\infty e^{-\frac{x^2}{2\sigma^2}} \frac{x^{\gamma+1}}{\sigma^2} dx = \frac{1}{2\sigma^2}\int_0^\infty e^{-\frac{x^2}{2\sigma^2}} (x^2)^{\frac{\gamma}{2}} dx^2 = \frac{1}{2\sigma^2}\int_0^\infty e^{-\frac{y}{2\sigma^2}} (y)^{\frac{\gamma}{2}} dy$$

$$= \frac{1}{2\sigma^2}(2\sigma^2)^{\frac{\gamma+2}{2}}\Gamma(\frac{\gamma+2}{2})\int_0^\infty \frac{(\frac{1}{2\sigma^2})^{\frac{\gamma+2}{2}}}{\Gamma(\frac{\gamma+2}{2})}(y)^{\frac{\gamma+2}{2}-1} e^{-\frac{1}{2\sigma^2}y} dy$$

Note that the probability density function of gamma distribution is,

$$f(x) = \begin{cases} \frac{\beta^\alpha}{\Gamma(\alpha)} \cdot x^{\alpha-1} \cdot e^{-\beta x} & x \geq 0 \\ 0 & x < 0 \end{cases}$$

where the gamma function is defined as $\Gamma(z) = \int_0^\infty e^{-z} x^{z-1} dx$. Thus, we have

$$\int_0^\infty e^{-\frac{x^2}{2\sigma^2}} \frac{x^{\gamma+1}}{\sigma^2} dx = \frac{1}{2\sigma^2}(2\sigma^2)^{\frac{\gamma+2}{2}}\Gamma(\frac{\gamma}{2}+1) = 2^{\frac{\gamma}{2}-1}\sigma^\gamma \gamma\Gamma(\gamma/2).$$

Thus, the equation (4.13) can be approximated by a close form expression:

$$\tilde{E} \approx (1-\beta)\left(k_1 \lambda 2^{\gamma/2-1}\sigma^\gamma \gamma\Gamma(\gamma/2) + k_2\right) \qquad (4.16)$$

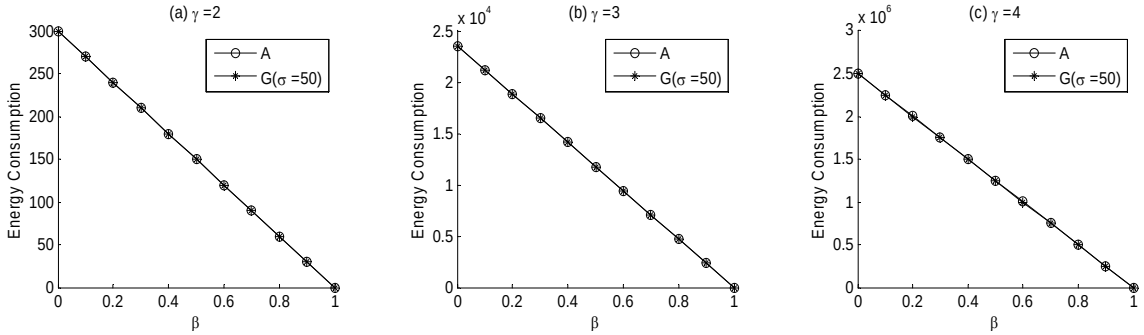

Fig. 4.2 Approximation of Energy Consumption (β=Fraction of Sensor Nodes Allowed to Sleep; A=Approximation; G=Gaussian distribution)

Figs. 4.2(a)-(c) show the approximation of energy consumption where the coverage radius of the cluster R is 250 and the minimum transmission range $x_{\min}$ is 5. As illustrated in the figures, the approximation is effective and accurate for large R. Thus, when the coverage

radius R is greater than 250, we can estimate the energy consumption by (4.16) instead of (4.13). This simplifies the calculation to avoid integration.

4.2.3 Network Lifetime

From [47], the network lifetime parameter is β_d which represent the fraction of sensor nodes running out of energy. Based on (4.5), we have $\beta_d = \int_{x_d}^{R} \tilde{f}(x)dx$, where $\tilde{f}(x) = e^{-\frac{x^2}{2\sigma^2}} \cdot \frac{x}{\sigma^2}$.

Thus, $\beta_d = \exp(-[x_d]^2/2\sigma^2) - \exp(-R^2/2\sigma^2)$, leading to $x_d = \sqrt{-2\sigma^2 \cdot \ln(\beta_d + \exp(-R^2/2\sigma^2))}$.

Based on (4.6), we have $\tilde{T}(\beta_d) = \frac{\Psi}{\tilde{E}(x_d)} = \frac{\Psi}{(1-\beta)\{\lambda \cdot k_1 \cdot [\max(x_{\min}, x_d)]^{\gamma} + k_2\}}$.

Figs. 4.3(a)-(c) show the network lifetime vs. fraction of sensor nodes allowed to sleep β for both Uniform distribution and Gaussian distribution where the standard derivation of Gaussian distribution is 50, namely $\sigma = 50$ and the battery energy is $\Psi = 10^3 J$. In addition, we assume that when a fraction of sensor nodes, $\beta_d = 0.5$, run out of energy, the network will be on longer working. As illustrated in the figures, the network lifetime increases when β increases for both Gaussian distribution and Uniform distribution. Because when β increases, each sensor node has higher probability to be selected to sleep, the energy consumption rate of each sensor node decreases which means the network lifetime increases. When $\beta = 0$, each sensor node works all the time and its energy consumption rate is the largest, and thus, the network lifetime achieves the minimum value. Also, it is easy to see that when the fraction of sensors allowed to sleep goes into 1, the network lifetime goes high for both distributions. From Figs. 4.3(a)-(c), we can see that when path loss exponent increases, the network lifetime for both distributions decreases quickly. When β increases, the discrepancy between two distributions increases

quickly. Comparing Figs. 4.3(a)-(c), we find that under the same parameters, when the path loss exponent increases, the discrepancy becomes smaller.

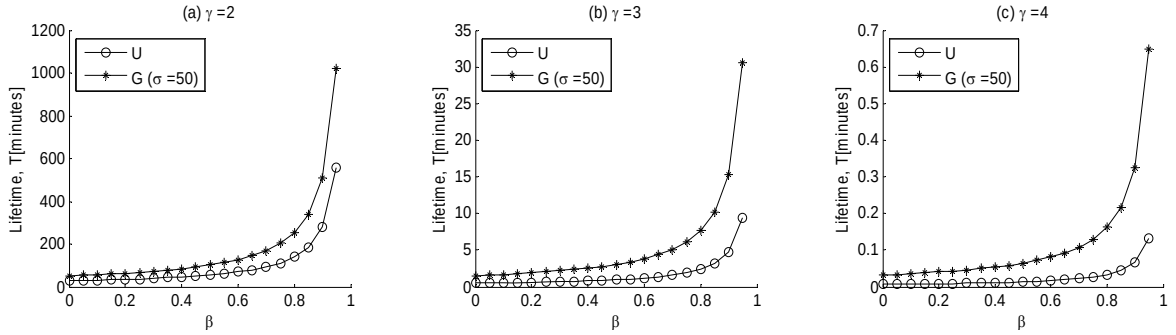

Fig. 4.3 Network Lifetime Comparison (β=Fraction of Sensor Nodes Allowed to Sleep; U=Uniform distribution; G=Gaussian distribution)

In Fig. 4.3, we can observe the discrepancy of network lifetime between two distributions is not large. That is because that comparing with the battery energy $\Psi = 10^3 J$, the energy consumption rate of each sensor node is too large. For example, from Fig. 4.1(c), the order of magnitude of energy consumption rate is 10^6, and thus, the order of magnitude of network lifetime is $\Psi/10^6 = 10^{-3}$. Thus, even if the discrepancy of energy consumption rates between two distributions is large, the discrepancy of network lifetime between two distributions can be small. However, if we set a proper value for battery energy, we can still see the significant discrepancy in network lifetime between two distributions.

4.3 Studies of Standard Deviation of Energy Levels and Network Lifetime

4.3.1 Standard Deviation

When we discuss the system performance, we usually consider the expected value of system performance. For example, in [47] or in the previous sections of this chapter, when referring to energy consumption rate, we actually computed the expected value of energy

consumption rate of one sensor node in a cluster. The energy consumption of each node during a second is random variable which is denoted as $E(X)$. In RS scheme, the energy consumption $E(X)$ can be expressed as

$$E(X) = (1-\beta)E_{active}(X) = (1-\beta)(\lambda \cdot k_1 \cdot [\max(x_{\min}, X)]^{\gamma} + k_2)$$

where X is random variable which denotes the distance between a sensor and the cluster head. Thus, the standard deviation of energy consumption rate can be computed as $Var(E) = \int_0^R [E(x) - E]^2 f(x)dx$, where $f(x)$ is the probability density function of X, and $E = \int_0^R (1-\beta) f(x) E_{active}(x)dx$, as given in (4.2), i.e.,

$$Var(E) = \int_0^R ((1-\beta)E_{active}(x))^2 f(x)dx - (\int_0^R (1-\beta) f(x) E_{active}(x)dx)^2 . \quad (4.17)$$

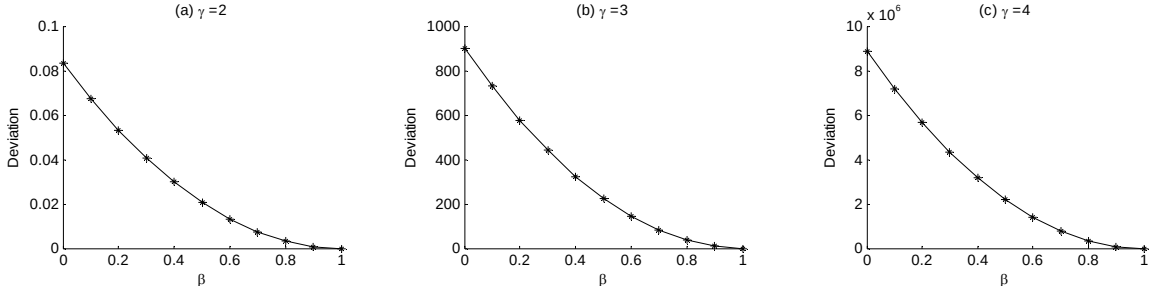

Fig. 4.4 Deviation of energy consumption (β=Fraction of Sensor Nodes Allowed to Sleep)

Thus, we can compute the standard derivation of energy consumption whether the deployment distribution is Uniform distribution or Gaussian distribution. Based on the results of standard derivation, we can further estimate the energy consumption of the network.

Fig. 4.4 shows the deviation of energy consumption versus fraction of sensor nodes allowed to sleep β when the deployment of sensor nodes is a uniform distribution. The variance of the energy consumption rate decreases when β increases for all path loss parameters. When the path loss parameter increases, the variance sharply increases.

4.3.2 Study of Network Lifetime under Random Battery Energy

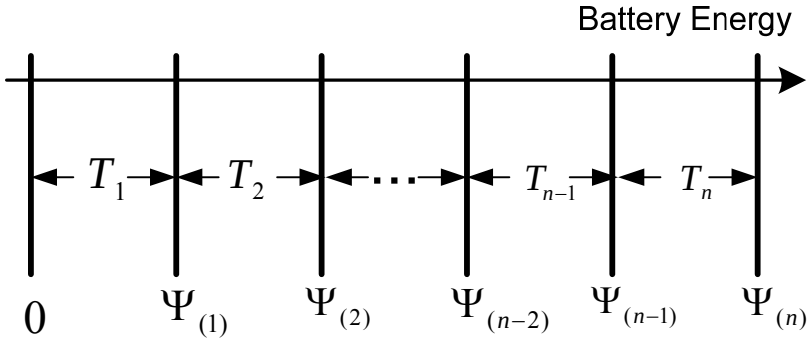

Fig. 4.5 Order Statistics of Battery Energy

In [47], when referring to network lifetime, it actually implied an assumption that the battery energy which each sensor node carries when the sensor network is initialized is the same. But in real world, we know that the quality of battery is different and the energy that each battery contains is random. In this subsection, we will reconsider the network lifetime where the impact of random battery energy is included. We still assume that n sensor nodes are deployed in each cluster. Thus the total battery energy of n sensor nodes can be denoted as $\Psi_1, \Psi_2, \cdots\cdots \Psi_n$, where $\Psi_i, (i = 1, 2....., n)$ are random variables. The order statistics $\Psi_{(1)}, \Psi_{(2)}, \cdots\cdots \Psi_{(n)}$ are defined by sorting the realizations of $\Psi_1, \Psi_2, \cdots\cdots \Psi_n$ in an increasing order. Let $f(x)$ and $F(x)$ be the probability density function and the cumulative distribution function of $\Psi_i, i = 1, 2....., n$, respectively. According [76], the probability density of the kth statistic can be given as follows.

$$
\begin{aligned}
f_{\Psi_{(k)}}(x) &= \tfrac{d}{dx} F_{\Psi_{(k)}}(x) = \tfrac{d}{dx} P(\Psi_{(k)} \le x) \\
&= \tfrac{d}{dx} P(\text{ at least k batteries whose energy } \le x) \\
&= \tfrac{d}{dx} \sum_{j=k}^{n} \binom{n}{j} P(\Psi_1 \le x)^j (1 - P(\Psi_1 \le x))^{n-j} \\
&= \tfrac{d}{dx} \sum_{j=k}^{n} \binom{n}{j} F(x)^j (1 - F(x))^{n-j} \\
&= \frac{n!}{(k-1)!(n-k)!} F(x)^{k-1} (1 - F(x))^{n-k} f(x)
\end{aligned}
$$

Based on [47], the network lifetime $T(\beta_d)$ is defined as the time when a fraction of sensor nodes, β_d , run out of energy. Thus, in this method, the time when β_d fraction of nodes run out of battery is the time when the sensor who carries $\Psi_{(k)}$ when the sensor network is initialized run out of battery, where $k = \lfloor n\beta_d \rfloor$. Here, we assume that the each sensor in the cluster has same energy consumption rate E. Thus, the expected lifetime of the node which carries $\Psi_{(k)}$ energy is given as follows;

$$
T(\beta_d) = \int_0^{\infty} x f_{\Psi_{(k)}}(x) \Big/ E \cdot dx \qquad (4.18)
$$

where E is given by (4.2).

In this subsection, we assume that the initial battery energy levels of sensor nodes follow an exponential distribution. In other words, $\Psi_1, \Psi_2, \cdots\cdots \Psi_n$ are independent, and identically distributed random variables following an exponential distribution with mean value Ψ. An important property of an exponential distribution is that it is memoryless: $P\{X > s+t \mid X > t\} = P\{X > s\}, s,t \ge 0$. Based on this property, we can transform the general expected lifetime equation (4.18) to a simple form.

As illustrated in Fig. 4.5, $T_i = \Psi_{(i)} - \Psi_{(i-1)}$, where $\Psi_{(1)}, \Psi_{(2)}, \cdots\cdots \Psi_{(n)}$ are the order statistics of $\Psi_1, \Psi_2, \cdots\cdots \Psi_n$. Because the memoryless property of exponential distribution, we have following facts [S15]: the random variable T_i follows the exponential distribution $Exp((n-i+1)/\Psi)$, where $i = 1, 2.....,n$. Thus, the expected value of T_i is $\Psi/(n-i+1)$. Based on the equation that $\Psi_{(i)} = \sum_{j=1}^{i} T_j$, the expected value of $\Psi_{(i)}$ is given by $\sum_{j=1}^{i} \frac{\Psi}{(n-j+1)}$. Thus, the expected lifetime of the network is given by

$$T(\beta_d) = \left(\sum_{j=1}^{k} \frac{\Psi}{(n-j+1)} \right) \Big/ E, \tag{4.19}$$

where $k = \lfloor n\beta_d \rfloor$.

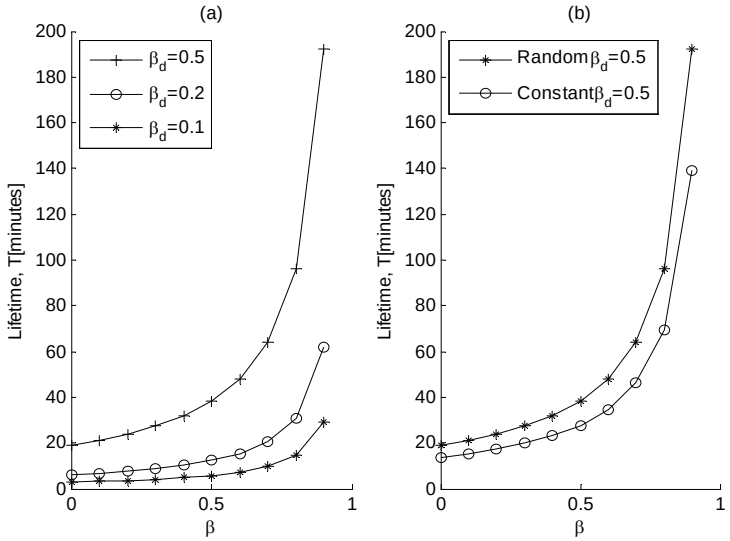

Fig. 4.6 Network Lifetime

Fig. 4.6(a) shows the network lifetime versus β (fraction of sensor nodes allowed to sleep) for a uniform distribution. We adopt the same parameters of network model in section 4.2.3. The lifetime of network improves as β increases for all the values of the parameter β_d due to the energy saving by increasing the portion of sleep sensor nodes.

Fig. 4.6(b) compares two network lifetime cases: one is under the assumption that every sensor in the network carries same battery energy, and the other is under the assumption that every sensor in the network carries random battery energy which follows an exponential distribution. As illustrated in Fig. 4.6(b), when sensor nodes carry random battery energy, the network lifetime is longer than the case that sensors carry the same energy. Also, the network lifetime with random battery energy can better reflect the network lifetime in the real world.

4.4 Kernel Density Estimation of Energy Consumption

In this section, we apply kernel density estimation introduced in Chapter 3 to estimate the energy consumption of WSNs. As stated in Chapter 3, Kernel density estimation belongs to a class of estimation called non-parametric density estimator. In comparison with parametric estimators, where the estimator has assumed a known distribution function and the parameters of this function (e.g., mean and variance) are the only information that we need to explore, non-parametric estimation has no assumed known distribution function and depends upon all the data points to reach an estimate. Likely, the estimation function of two-dimension is expressed as

$$\hat{f}_n(x,y) = \frac{1}{nh_1h_2}\sum_{i=1}^{n} K\left(\frac{x-X_{i1}}{h_1}, \frac{y-X_{i2}}{h_2}\right)$$

where $K(\bullet)$ is kernel density function and h is called window-width; $X_1,...,X_n$ are random samples from observations and $X_i = (X_{i1}, X_{i2})^T$.

Now, we focus on a cluster to give the performance analysis of energy consumption. When a cluster head is found, a coordinate frame is established where the location of cluster head is $(0,0)$. Thus, each location in this cluster can be given by math coordinate. Firstly, we collect n_0 sensor samples from same cluster, and their coordinates are denoted by

$(X_1,Y_1),(X_2,Y_2),...(X_{n_0},Y_{n_0})$. Then, the estimated probability density function of deployment of sensor nodes in a cluster is give by

$$\hat{f}_{n_0}(k,l)=\frac{1}{n_0 h_1 h_2}\sum_{i=1}^{n_0}K\left(\frac{k-X_i}{h_1},\frac{l-Y_i}{h_2}\right) \tag{4.20}$$

where the kernel density function is chosen as two-dimensional Gaussian density function, namely $K(u,v)=\frac{1}{2\pi}e^{-\frac{1}{2}(u^2+v^2)}$, because Gaussian kernel function is the mostly used and powerful kernel function in K.D.E method. Thus, we have

$$\hat{f}_{n_0}(k,l)=\frac{1}{2\pi n_0 h_1 h_2}\sum_{i=1}^{n_0}\exp\left(-\frac{(k-X_i)^2}{2h_1^2}-\frac{(l-Y_i)^2}{2h_2^2}\right) \tag{4.21}$$

Next, we need to derive the probability density function $\hat{f}(x)$ of the distance x between a sensor and the cluster head under the estimated sensor distribution. Based on (4.10), the probability distribution function of the distance x between a sensor and the cluster head is

$$\begin{aligned}\widehat{F}(x)&=\Pr(\widehat{X}\le x)=\iint_{k^2+l^2\le x^2}\hat{f}_{n_0}(k,l)dkdl\\&=\iint_{k^2+l^2\le x^2}\frac{1}{2\pi n_0 h_1 h_2}\sum_{i=1}^{n_0}\exp\left(-\frac{(k-X_i)^2}{2h_1^2}-\frac{(l-Y_i)^2}{2h_2^2}\right)dkdl\\&=\frac{1}{2\pi n h_1 h_2}\sum_{i=1}^{n_0}\iint_{k^2+l^2\le x^2}\exp\left(-\frac{(k-X_i)^2}{2h_1^2}-\frac{(l-Y_i)^2}{2h_2^2}\right)dkdl\end{aligned}$$

We still take use of integral transformation to solve our problem. Let $i=r\sin\theta$ and $j=r\cos\theta$, where $0\le r\le x$ and $0\le\theta\le 2\pi$, thus we have

$$\begin{aligned}&\tilde{F}(x)=\Pr(\widehat{X}\le x)\\&=\frac{1}{2\pi n_0 h_1 h_2}\sum_{i=1}^{n_0}\int_0^{2\pi}\int_0^{x}\exp\left(-\frac{(r\sin\theta-X_i)^2}{2h_1^2}-\frac{(r\cos\theta-Y_i)^2}{2h_2^2}\right)|J|drd\theta\end{aligned}$$

where $|J| = \begin{vmatrix} \frac{\partial i}{\partial r} & \frac{\partial i}{\partial \theta} \\ \frac{\partial j}{\partial r} & \frac{\partial j}{\partial \theta} \end{vmatrix} = r$.

Thus, the probability density function $\hat{f}(x)$ is given by

$$\begin{aligned} \tilde{f}(x) &= \frac{\partial \tilde{F}(x)}{\partial x} = \frac{\partial[\Pr(\bar{X} \le x)]}{\partial x} \\ &= \frac{1}{2\pi n_0 h_1 h_2} \sum_{i=1}^{n_0} \int_0^{2\pi} \exp\left(-\frac{(x\sin\theta - X_i)^2}{2h_1^2} - \frac{(x\cos\theta - Y_i)^2}{2h_2^2} \right) \cdot x d\theta \quad (4.22) \\ &= \frac{1}{2\pi n_0 h_1 h_2} \sum_{i=1}^{n_0} \int_0^{2\pi} \exp\left(\begin{array}{l} -\frac{(x\sin\theta)^2 - 2x(X_i\sin\theta) + X_i^2}{2h_1^2} \\ -\frac{(x\cos\theta)^2 - 2x(Y_i\cos\theta) + Y_i^2}{2h_2^2} \end{array} \right) \cdot x d\theta \end{aligned}$$

Based on (4.2), the expected energy consumption of each node during a second derived from K.D.E is

$$\begin{aligned} \hat{E} &= \int_0^R (1-\beta) \cdot \hat{f}(x) \cdot E_{active}(x) \cdot dx = \int_0^R (1-\beta) \cdot \tilde{f}(x) \cdot (\lambda k_1 [\max(x_{\min}, x)]^\gamma + k_2) dx \\ &= \frac{(1-\beta)(\lambda k_1 x_{\min}{}^\gamma + k_2)}{2\pi n_0 h_1 h_2} \sum_{i=1}^{n_0} \int_0^{x_{\min}} \int_0^{2\pi} \exp\left(\begin{array}{l} -\frac{(x\sin\theta)^2 - 2x(X_i\sin\theta) + X_i^2}{2h_1^2} \\ -\frac{(x\cos\theta)^2 - 2x(Y_i\cos\theta) + Y_i^2}{2h_2^2} \end{array} \right) \cdot x d\theta dx \\ &+ \frac{(1-\beta)\lambda k_1}{2\pi n_0 h_1 h_2} \sum_{i=1}^{n_0} \int_{x_{\min}}^R \int_0^{2\pi} \exp\left(\begin{array}{l} -\frac{(x\sin\theta)^2 - 2x(X_i\sin\theta) + X_i^2}{2h_1^2} \\ -\frac{(x\cos\theta)^2 - 2x(Y_i\cos\theta) + Y_i^2}{2h_2^2} \end{array} \right) \cdot x^{\gamma+1} d\theta dx \quad (4.23) \\ &+ \frac{(1-\beta)k_2}{2\pi n_0 h_1 h_2} \sum_{i=1}^{n_0} \int_{x_{\min}}^R \int_0^{2\pi} \exp\left(\begin{array}{l} -\frac{(x\sin\theta)^2 - 2x(X_i\sin\theta) + X_i^2}{2h_1^2} \\ -\frac{(x\cos\theta)^2 - 2x(Y_i\cos\theta) + Y_i^2}{2h_2^2} \end{array} \right) \cdot x d\theta dx \end{aligned}$$

After giving the mathematical formula of energy consumption, we can follow those steps introduced in Chapter 3 to obtain proper sample size and window-width. Here, for testing our method, we assume that after deployment, the sensor locations follow two-dimensional Gaussian

distribution in real world, rather than the uniform distribution which the author assumed in [47]. Thus, according to Gaussian distribution, sample location data can randomly be generated. Then, the estimation distribution can be obtained based on sample data. Finally, by comparing the energy consumption derived from assumed distribution (uniform), real-world (Gaussian), and estimation distribution, we show that our approach is more efficient for reflecting the real system performance in the real world.

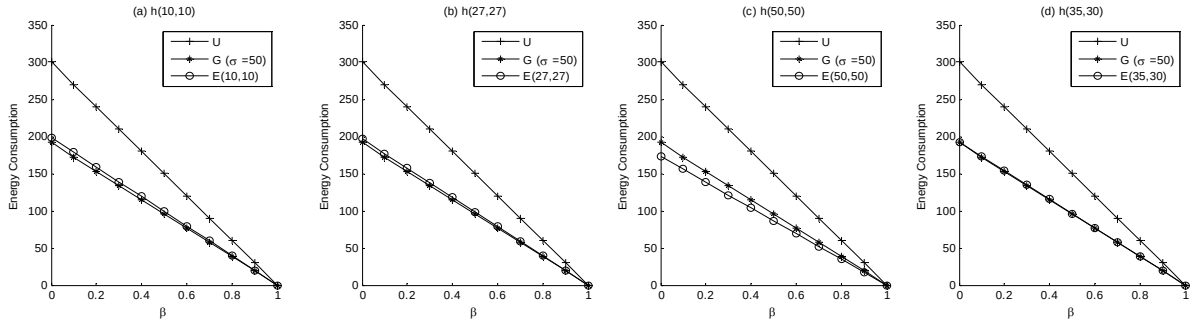

Fig. 4.7 Performance Estimations: (a) window-width (h) =(27,27), (b) window-width (h) =(10.10), (c) window-width (h) =(50,50), (d) window-width (h) = (35,30)

In our experiment, the expected energy consumption can be studied based on equation (4.23). Figs. 4.7(a)-(d) show the energy consumption versus fraction of sensor nodes allowed to sleep for uniform, Gaussian and the estimated Gaussian distributions, where window-width (h) are (27,27), (10,10) (50,50) and (35,30) respectively. In the experiment, we use the same parameters in Figs. 4.1(a)-(c) for the sensor network and we collect $n_0 = 50$ location information of sensor nodes from a cluster. From Figs. 4.7(a)-(d), we can see that when $h = (35,30)$ the estimated performance is best, because this window-width (h) is generated by the fast and accurate state-of-the-art bivariate kernel density estimator approach. From Figs. 4.7(a)-(c), we can observe that although the election of window-width is not very good, but the estimated performance is still better than the performance from an inaccurate distribution assumption

(uniform distribution). Thus, we can take use of K.D.E method to estimate the system performance in real world and reduce the error caused by an incorrect assumption

4.5 Conclusion

In this chapter, we show that distribution-free methodology can be generalized and extended to study many others sensor network metrics including network lifetime. Furthermore, we provide a mathematical approximation and a standard deviation study for energy consumption, as well as a more deep study for network lifetime.

CHAPTER 5

MONITORING SPACE SEGMENTATION IN DESIGNING WIRELESS BINARY PYROELECTRIC SENSORS

In this chapter, we focus on the segmentation of source space (monitoring space) in a specific sensor system topology. We first study the maximum number of signatures in a sensor system where the monitoring space is a disk and modulators are placed along the circle of the disk as shown in Fig. 5.1. We prove that the maximum number of signatures in such sensor network with n sensors is 2^n and that it can be achieved by n modulators under a defined procedure and an assumption. Through the procedure, assumption, and proof, we know how to realize the maximum number of signatures. Then, we release the constraint on the number of modulators and prove that the maximum number of signatures (i.e., 2^n) in n sensors system can be achieved when there is no constraint on the number of modulators. Through these theorems, we show how reference structure is used to segment the monitoring space.

5.1 Related Work

Since the term "reference structure" was first proposed in computational imaging systems [53-54], we first give a brief introduction of its origin in imaging systems. Before the advent of computational imaging systems, most imaging systems were optical imaging systems, which usually implemented a one-to-one mapping between the source space and the measurement space. Thus, such optical imaging systems are regarded as isomorphic imaging systems. To improve resolution and depth of field, a better isomorphism is the primary concern of the design of an optical system. Such isomorphism imaging systems have dominated the field of two-

dimensional imaging for a long time. However, in the field of multidimensional imaging, the isomorphic model cannot be physically achieved. With the advent of advanced digital processors and focal planes, computational imaging systems have emerged. These computational imaging systems implement non-isomorphic mapping between the source space and the measurement space [60-61]. Since non-isomorphic imaging systems primarily measure the linear combinations of source data, they are called multiplex imaging systems. Because of the capability of multidimensional imaging [62-63], computational imaging systems are becoming more and more popular. Conventional tomographic systems reconstruct a three-dimensional source by capturing several projected images of the source and obtaining depth information by scanning the source [64]. Then, scan-free multidimensional imaging was achieved through computational imaging system by using reference structure tomography. Coded aperture imaging was the original source of reference structure tomography. In coded aperture imaging systems, the mapping between source points and a sensor array is modulated by a 2D mask [65-66]. However, coded aperture systems only can implement a limited class of mappings [67]. By using 3D reference structure rather than 2D modulation, reference structure tomography implements a more general class of mappings [54]. Thus, better geometric reference structures will lead more efficient reconstruction of multidimensional objects. In addition to reconstructing imaging in imaging system [53, 54, 55, 68], reference structure is applied to source analysis, including object tracking and identification [48, 50, 56, 57, 58]. The function of reference structure is to segment the object space [55]. Based on this characteristic, a class of sensor systems with reference structure was exploited to enable a data-efficient and computation-efficient source analysis, including object tracing and identification.

Compared to traditional video camera based tracking systems, the sensor systems with reference structures enhance the data efficiency and computation efficiency of object tracking. For example, the most common tracking applications have focused on vehicles and humans. Such tracking can be implemented using one or more video cameras, and a variety of algorithms have been implemented [69-70]. At the huge cost of system deployment, management and data processing, video systems are capable of advanced tracking. Video systems will typically sense billions of pixels in order to obtain just a few target characteristics. In some low-precision applications, this is unnecessary. A sensor system with reference structure can fulfill low-precision applications with benefits of data-efficiency and computation-efficiency [56-58].

From these applications, the significance of segmenting source space by geometric reference structure is presented. The source space is segmented into cells, each of which has its own signature. The number, structure, and distribution of these cells are of profound interest to the design and data analysis of a sensor system.

According to our knowledge, only one work [59] has been written to explore the number of distinct signatures. In [59], P.K. Agarwal et al. consider a radiation sensor system, in which optical modulators placed between the sensors and the objects modulate the visibility of an object to a sensor. The object space is segmented into signature cells. Based on a one dimensional object space model in which sensors and modulators are placed in separate parallel lines, the authors in [59] give an almost tight lower bound on the maximum number of distinct signatures. However, as pointed out in [59], the problem of optimal reference structure remains completely open.

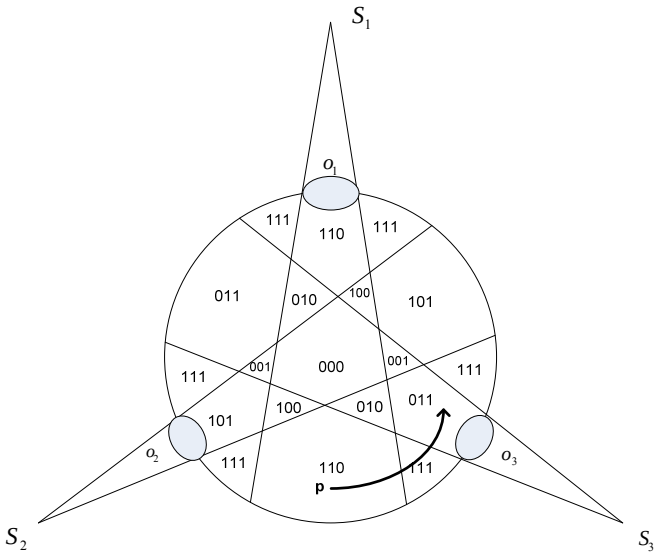

Fig. 5.1 Segmentation of the monitoring space by 3 pyroelectric sensors and 3 modulators (i.e., reference structure)

5.2 Problem Formulation

Sensor System Definition: Consider a sensor system consisting of pyroelectric binary sensors and modulators. Modulators, known as reference structure, are those physical materials that can manipulate the fields of view of sensors. The sensor system is built in two-dimensional space. Let $S \subset R^2$ denote the monitoring space in which source objects, also known as intrusions, may appear. Let $M \subset R^2$ denote the subspace in which the modulators are placed. Assume that sensors can be placed anywhere except the interior of the monitoring space. Consequently, sensor placement space can be denoted as $R^2 - S$. Let $\{s_1, s_2, ..., s_n\}$ denote n sensors distributed in the sensor placement space and $\{o_1, o_2, ..., o_m\}$ denote m modulators distributed in the modulator space. For example, as illustrated in Fig. 5.1, the monitoring space is a disk which can be divided into many identified regions by adjusting the locations of sensors and modulators.

Signature Definition: Based on [59], we give the definition of the signature used to identify the regions. For any point p in the monitoring space, if it is visible to a sensor, the sensor will mark point p as 1. Otherwise, the sensor will mark the point as 0. We denote the value of the point p marked by sensor s_i as $f_i(p)$. In other words, we have

$$f_i(p)=\begin{cases}1 & p \text{ is visible for } s_i \\ 0 & p \text{ is invisible for } s_i\end{cases}.$$

Let $f(p)$ denote a binary sequence which has n digits that is a concatenation of n digits of $f_i(p), i=1,...,n$, as follows:

$$f(p)=f_n(p)f_{n-1}(p)\cdots f_1(p), \qquad (5.1)$$

where $f_i(p)$ is the value of the i-th digit. $f(p)$ is defined as the signature of source point p. Based on [59], we define $f(p)$ as the signature of the regions which p is in. As described above, reference structure segments the monitoring space into regions with signatures. All regions in the monitoring space with the same signature are defined as a signature cell. In other words, the points in each signature cell have the same signature. For example, Fig. 5.1 shows that the monitoring space is marked into several signature cells by three sensors and three modulators. Let $N(n,m,S)=\{f(p)\,|\,p\in S\}$ denote the set of signatures realized by a system with n sensors and m modulators. Let $|N(n,m,S)|$ denote the number of distinct signatures realized by a system with n sensors and m modulators.

As illustrated in Fig. 5.1, for point p in the monitoring space, we can observe that p is visible to sensors s_2, s_3, and not to sensor s_1. Consequently, $f_1(p)=0$, $f_2(p)=1$, $f_3(p)=1$. From (5.1), the signature of p is 110, i.e., $f(p)=110$. Also, we can observe that the modulators segment the monitoring space into 19 regions with signatures, and these regions form 8 signature

cells because some regions are in the same cell, i.e. having same signature. The set of signatures $N(3,3,S)$ in Fig. 5.1 is

$$\{000,001,010,100,011,101,110,111\}$$

Therefore, $|N(3,3,S)|=8$. From Fig. 5.1, we can see the benefits of reference structure. A traditional sensor node can detect the intrusion emerging in the monitoring space but cannot locate the intrusion. Furthermore, a traditional sensor node cannot detect the movement of the intrusion in the monitoring space. However, after adding modulators to the sensor system, the monitoring space is segmented into several signature cells and is helpful in locating the intrusion. As illustrated in Fig. 5.1, when an intrusion appears at point p, the system can locate the sensor in a signature cell with signature 110. By combining this fact with prior knowledge, we can predict the intrusion location. Moreover, we can detect the movement of the intrusion in the monitoring space. As shown in Fig. 5.1, the intrusion moves from point p through signature cells with signatures 110, 111, 011. Accordingly, we have the ability to predict the possible activity space of the intrusion. With more prior knowledge of the intrusion, we can monitor its movement more precisely.

5.3 Maximum Number of Signatures

In this section, we determine the maximum number of signatures for a specific sensor system where the monitoring space is a disk, and modulators are placed along the circle of the disk as shown in Fig. 5.1. Obviously, for such a sensor system with n sensors, the upper bound of signatures is 2^n. First, we study the case in which the number of sensors and the number of modulators are the same, namely $n=m$. In this case, we prove that the maximum number of signatures in our sensor system with n sensors is 2^n under a defined procedure and an

assumption. Through this procedure, assumption, and the proof, we provide a way to realize the maximum number of signatures. Then, we release the constraint on the number of modulators and prove that the number 2^n can be achieved without the procedure and the assumption.

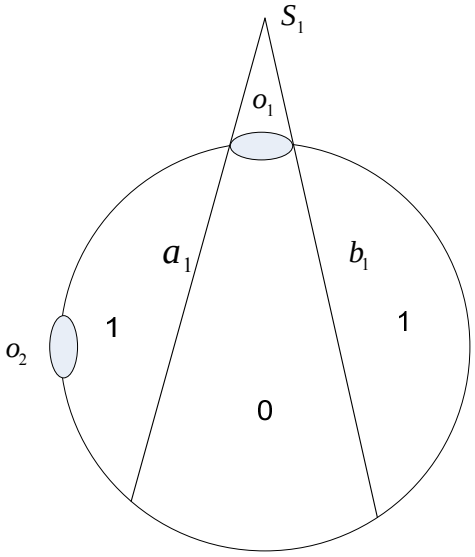

Fig. 5.2 single pair of sensor and modulator

5.3.1 Same Number of Sensors and Modulators

In this subsection, we give Theorem 5.1 to show that the upper bound of signatures in our sensor system with n sensors is 2^n and that it can be achieved under a constraint. To express this theorem and its assumption clearly, we first introduce some terms and analysis. Mathematical induction is adopted in our analysis where sensors are adding one by one into the above sensor system model.

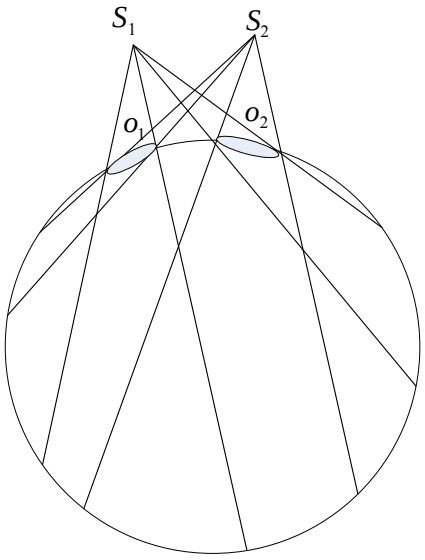

Fig. 5.3 multiple pairs of sensors and modulators

A modulator can block the visibility of a sensor from the monitoring space. As illustrated in Fig. 5.2, modulator o_1 blocked the sensor s_1 such that the space between lines a_1 and b_1 was not visible for s_1. Thus, each sensor and modulator pair can generate two lines. When a modulator blocks the sensor, they can be called a pair. As illustrated in Fig. 5.2, s_1 and o_1 can be called a pair. However, s_1 and o_2 cannot be called a pair because modulator o_2 does not block sensor s_1. As the number of sensors and modulators grows, one sensor can pair with multiple modulators. As illustrated in Fig. 5.3, s_1 and s_2 can pair with both modulators o_1 and o_2. Consequently, four lines are generated by sensor s_1 with modulators o_1 and o_2 in Fig. 5.3. Now, we introduce a recursive procedure and an assumption for Theorem 5.1. The following statement describes the procedure: In our sensor system model, there already exist $n-1$ sensors and $n-1$ modulators. The monitoring space is divided into many signature cells. The set of these signatures can be denoted as $N(n-1,n-1,S)$. Note that the number of signature cells is equal to $|N(n-1,n-1,S)|$. Then, sensor s_n and modulator o_n are added to the sensor system. As shown

above, sensor s_n may pair with several modulators. Here, we assume that m_0 modulators can pair with sensor s_n. Thus, we can imagine $2m_0$ lines ejected by s_n. Let $l_1, l_2, ..., l_{2m_0}$ denote these lines. Each line can intersect one or more signature cells which are identified by their signatures. Let C_{l_i} denote the set of signature cells that are intersected by line l_i. Each signature cell is identified by a signature. Thus, let N_{l_i} denote the signature set generated by C_{l_i}. If and only if $|\bigcup_{i=1}^{2m_0} N_{l_i}| = \max|N(n-1,n-1,S)|$ for each n, the maximum number of signatures 2^n can be achieved. Thus, Theorem 5.1 is given as follows:

Theorem 5.1: In our sensor system, we add one sensor and one modulator each time. Furthermore, we assume that sensors and modulators are added in a way such that $|\bigcup_{i=1}^{2m_0} N_{l_i}| = \max|N(n-1,n-1,S)|$ for each n. In such a sensor system with n sensors and n modulators, the number of signatures is 2^n.

Proof: Mathematical induction is used in this proof. To begin, we consider $n=1$ and $n=2$. For $n=1$, as illustrated in Fig. 5.2, the set of signatures $N(1,1,S)$ is $\{0,1\}$. Thus, $|N(1,1,S)| = \max|N(1,1,S)| = 2$, i.e. the number of signatures is $2^1 = 2$. In Fig. 5.2, there exists two signature cells with signatures 1 or 0. As shown in Fig. 5.4, sensor s_2 and modulator o_2 are added into the system. As shown above, sensor s_2 can only pair with modulator o_2. Thus, we can imagine two lines generated by sensor s_2, as illustrated in Fig. 5.4. They are denoted as a_2 and b_2, respectively. Let N_{a_2} denote the signature set that is composed of signatures whose signature cells are intersected by line a_2. As illustrated in Fig. 5.4, a_2 intersects two signature cells with signatures 1 and 0. Thus, $N_{a_2} = \{0,1\}$. Likewise, for line b_2, we have $N_{b_2} = \{0,1\}$.

Since $|N_{a_2} \bigcup N_{b_2}| = \max|N(1,1,S)| = |\{0,1\}|$, the assumption is satisfied for $n=2$. If Theorem 11 is correct, the number of signatures should be $2^2 = 4$. From Fig. 5.4, the signature set is $\{01,01,10,11\}$, which verifies our conclusion. When line a_2 intersects a signature cell with signature 0, one side of a_2 in this signature cell is visible to sensor s_2, and the signature of this new signature cell is 10. The other side of a_2 is not visible to sensor s_2, and the signature of the new signature cell is 00, as illustrated in Fig. 5.4. Now, we prove that Theorem 5.1 is correct for $n=1$ and $n=2$.

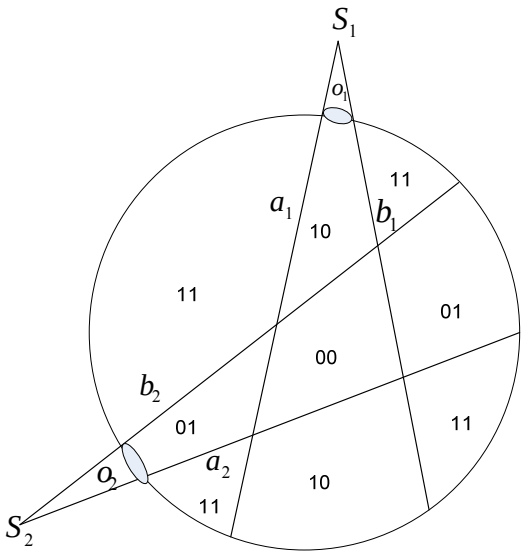

Fig. 5.4 Maximized segmentation for two sensors and two modulators

Assume that in a sensor system with $n-1$ sensors and $n-1$ modulators, the number of signatures is 2^{n-1}. As we know, $N(n-1,n-1,S) = \{f_{n-1}(p) f_{n-2}(p) \cdots f_1(p) \big| p \in S\}$ denotes the set of signatures realized by a system with $n-1$ sensors and $n-1$ modulators. Thus, we have

$$|N(n-1,n-1,S)| = \max|N(n-1,n-1,S)| = 2^{n-1}$$

We will then prove that the theorem is correct for a sensor system with n sensors and n modulators. Consider any signature $f_{n-1}(p_0) f_{n-2}(p_0) \cdots f_1(p_0)$ in the signature set

$N(n-1,n-1,S)$ where $p_0 \in S$, there must exist a signature cell S_{p_0} with signature $f_{n-1}(p_0) f_{n-2}(p_0) \cdots f_1(p_0)$. According to the procedure and assumption $|\bigcup_{i=1}^{2m_0} N_{l_i}| = \max |N(n-1,n-1,S)|$, we know that signature cell S_{p_0} is intersected by at least one line l_n generated by sensor s_n. As shown above, one side of l_n in the signature cell is visible to sensor s_n and the other side is not. Thus, the visible side's signature is $1 f_{n-1}(p_0) f_{n-2}(p_0) \cdots f_1(p_0)$, and the nonvisible side's signature is $0 f_{n-1}(p_0) f_{n-2}(p_0) \cdots f_1(p_0)$. For any signature in $N(n-1,n-1,S)$, we have a similar conclusion. Thus, after adding sensor s_n and modulator o_n, the signature set $N(n,n,S)$ is

$$\{1 f_{n-1}(p) f_{n-2}(p) \cdots f_1(p), 0 f_{n-1}(p) f_{n-2}(p) \cdots f_1(p) \big| p \in S\}$$

As we know,

$$N(n-1,n-1,S) = \{ f_{n-1}(p) f_{n-2}(p) \cdots f_1(p) \big| p \in S\}$$

$$|N(n-1,n-1,S)| = 2^{n-1}.$$

Thus, we have $|N(n,n,S)| = 2^{n-1} \times 2 = 2^n$. Theorem 5.1 is proved.#

5.3.2 Non-constraint of the Number of Modulators

In Theorem 5.1, we provide an intuition of how to find the maximum number of signatures. In this section, we release the constraint on the number of modulators and prove that the assumption in Theorem 5.1 can always be satisfied in this case. Consequently, we can prove that 2^n signatures can be achieved in a sensor system with n sensors.

Theorem 5.2: If in our sensor system with n sensors we can have any number of modulators, 2^n signatures can be achieved.

Proof: As shown in Theorem 5.1, when the sensor number is $n=1$ or $n=2$, the maximum number of signatures 2^n can be achieved by n modulators. Assume that $n=k$, is the first time that we cannot achieve 2^k signatures using just k modulators. Let $N(k-1,k-1,S)$ denote the set of signatures realized by a system with $k-1$ sensors and $k-1$ modulators. Thus,

$$|N(k-1,k-1,S)|=\max|N(k-1,k-1,S)|=2^{k-1}$$

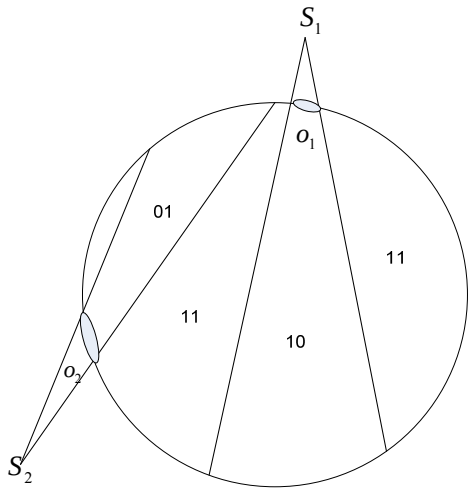

Fig. 5.5 Non-maximum number of signatures in a sensor network with two sensors and two modulators

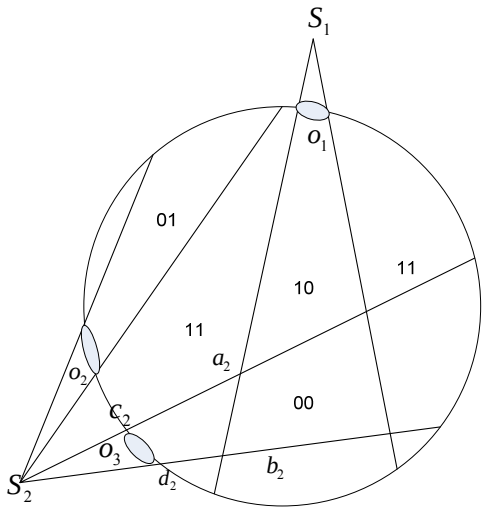

Fig. 5.6 Maximum number of signatures in sensor network with two sensors and three modulators

After adding sensor s_k and modulator o_k, the upper bound of signatures 2^k cannot be achieved. From Theorem 5.1, there must exist at least one signature $f(p_1) \in N(k-1,k-1,S)$, and the signature cell with signature $f(p_1)$ is not intersected by any line generated by sensor s_k. We can solve this problem by adding more modulators. We yield two lines a_k and b_k from sensor s_k and make these two lines intersect the signature cell with signature $f(p_1)$. As stated above, the monitoring space is a disk, and modulators are placed along the circle of the disk. Thus, a_k and b_k intersect this circle at two points which are denoted as c_k and d_k, respectively. Then, we placed a new modulator between c_k and d_k. We show this procedure through a simple example. As illustrated in Fig. 5.5, before adding sensor s_2 and modulator o_2, we have $N(1,1,S) = \{0,1\}$. After adding sensor s_2 and modulator o_2, two lines generated by sensor s_2 only intersect signature cells with signature 1. Thus, the signature set is $\{01,10,11\}$ and the maximum number of signatures $2^2 = 4$ cannot be achieved. To maximize the number of signatures, lines generated by sensor s_2 should cut through all existing signatures in $N(1,1,S)$. By adding a new modulator, we can guarantee this. As illustrated in Fig. 5.6, we yield lines a_2 and b_2 from sensor s_2, which both intersect the signature cell with signature 0. We denote the points generated by the intersections of lines a_2 and b_2 with the circle as c_2 and d_2. Then we add a new modulator o_3 between c_2 and d_2. Thus, we can get the signature set $\{00,01,10,11\}$. Theorem 5.2 is therefore proved.

5.4 Simulation

5.4.1 Simulation Setting

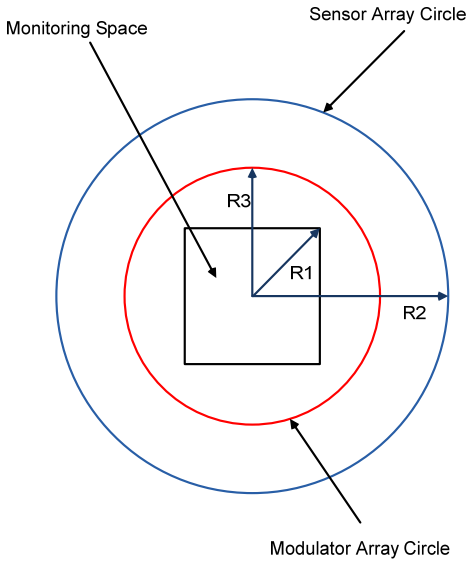

Fig. 5.7 Sensor System Setting in Simulation

As illustrated in Fig. 5.7, we consider a scenario where monitoring space is a square field whose length of a side is $\sqrt{2}R_1$. The sensors are deployed along a circle with radius R_2 with equal angle distance. Likewise, the occlusions are deployed along a circle with radius R_3 with equal angle distance. As shown in Fig. 5.8, the modulator is assumed to be in round shape with radius R_4. Moreover, each sensor has a view limit with angle α, where $\alpha = 2\arcsin(R_1/R_2)$.

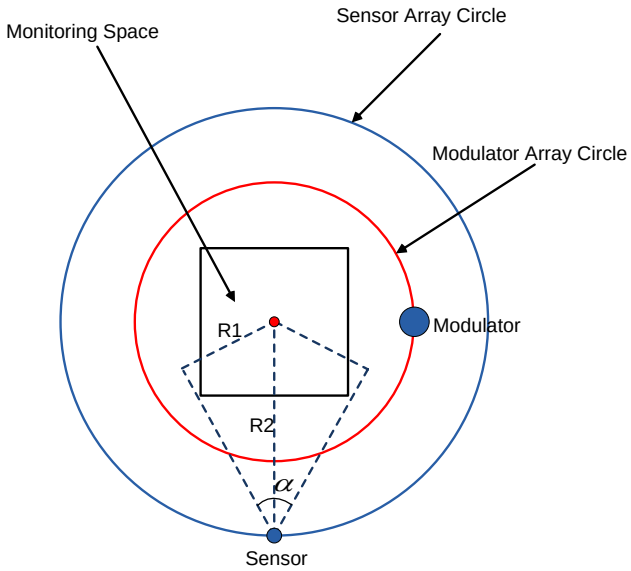

Fig. 5.8 Demonstration of Sensor View Limit

The monitoring space is inside of the modulator circle. The goal of this simulation is to provide preliminary results on the deployment of the sensor nodes and the modulators such that the field of interest could have the best quality of segmentation. Commonly, there are three metrics that are used to measure the quality of segmentation.

- Variance of size of all signature cells. The variance is smaller; the quality of segmentation is better.
- Number of signature cells. The number of signature cells is more; the quality of segmentation is better.
- Maximum difference between the sizes of signature cells. The maximum difference is smaller; the quality of segmentation is better.

5.4.2 Simulation Preliminary Results

In this subsection, we conduct some results based on the simulation setting described above. Notice that the size of modulator and sensor nodes is not proportional to the setting in result figures. In other words, the segmentation might appear to be tilted. The default geometric relationship in our simulation is $R_2 = 2R_1$, $R_3 = 7R_1/6$, $R_4 = R_1/28$. Several factors that may impact the quality of segmentation are considered throughout the simulation. We show the impact of the number of sensors and modulators on the quality of segmentation. From Fig. 5.9-5.11, it is easy to see more sensors and modulators will lead to more signature cells, thus the quality of segmentation is better.

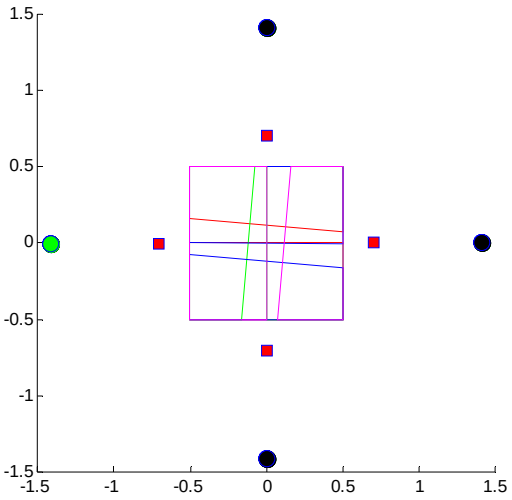

Fig. 5.9 segmentation when the number of sensors and modulators is 4

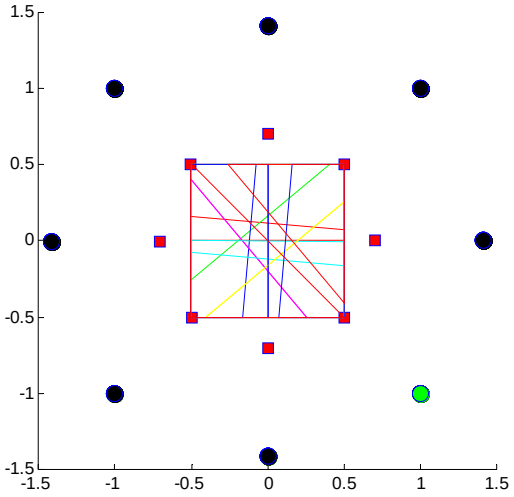

Fig. 5.10 segmentation when the number of sensors and modulators is 8

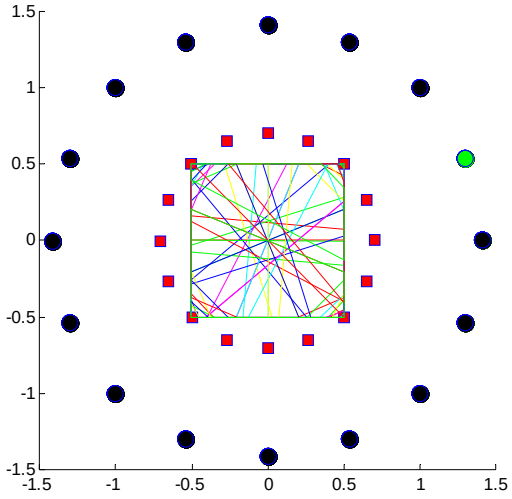

Fig. 5.11 segmentation when the number of sensors and modulators is 16

Then, we show the impact of relative position between sensors and modulators on the quality of segmentation. From Fig. 5.12-5.14, we may notice that when the relative position between sensors and modulators becomes large, the maximum difference between the sizes of signature cells also becomes large. From this viewpoint, the quality of segmentation becomes worse.

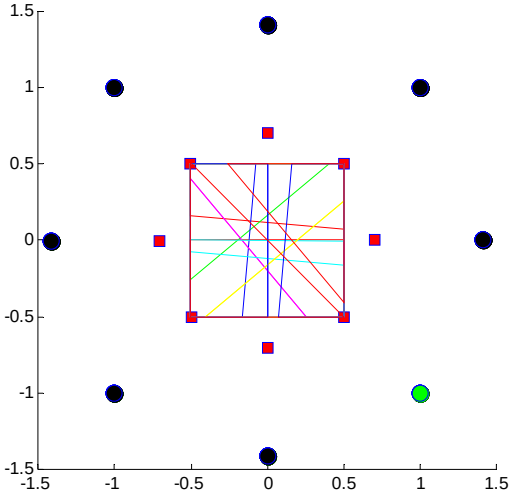

Fig. 5.12 relative position between sensor and modulator is 0°

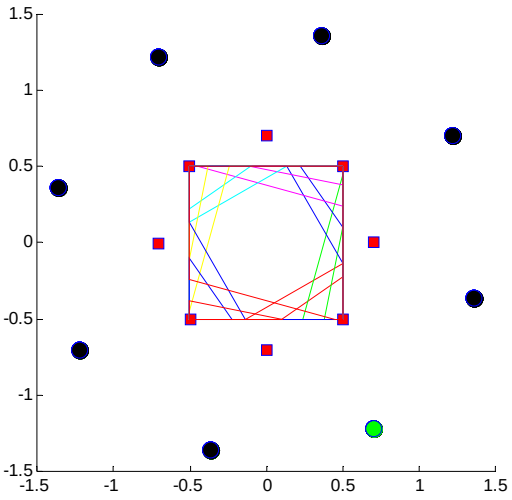

Fig. 5.13 relative position between sensor and modulator is 15°

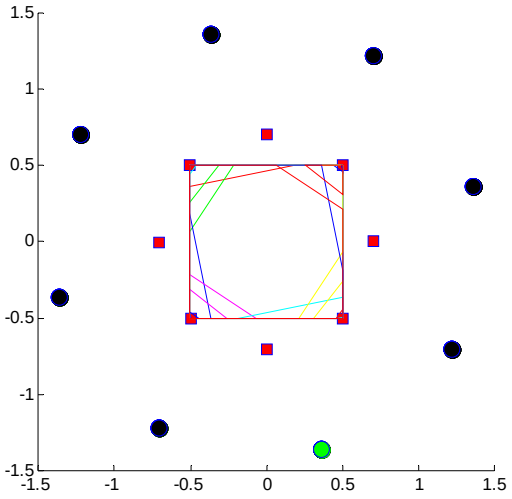

Fig. 5.14 relative position between sensor and modulator is 30°

5.5 Conclusion

In this chapter, we present a method that may be used in order to take advantage of reference structure to optimize the design of a wireless pyroelectric binary sensor system. Since the number of signature cells is important to the design and data analysis of a sensor system, we explore these features in this chapter. Firstly, we show that the maximum number (i.e., 2^n) of

signatures can be achieved by using n binary sensors and n modulators under some conditions. Furthermore, we prove that the maximum number of signatures 2^n can be achieved in a sensor network with n binary sensors without the constraint of the number of modulators. At last, we conduct some simulation results.

CHAPTER 6

CONCLUSIONS

The research presented in this dissertation has addressed several important issues in wireless sensor network design and performance analysis, including performance limits of medium access control protocols, enhancing sensor awareness, network coverage and network lifetime.

The dissertation explored fundamental limits for sustainable loads, utilization, and delays in specific multi-hop sensor network topologies for both wireless sensor networks and underwater acoustic sensor networks. The significance of these limits is that these bounds are independent of the selection of MAC protocols under both single-channel and half-duplex radios. As future work, we will investigate whether optimal schedules exist for irregular topologies and various routing schemes under the fair-access constraint. For underwater sensor networks, when propagation delay is larger than half of the frame transmission time, further analysis is necessary.

The dissertation also studies network service including network coverage and lifetime. Previous works are largely based on assumed probability density functions that govern the distribution of sensor nodes in the sensing field. However, the actual distribution of sensor nodes may be very different from the assumed one which will introduce performance analysis error. Thus, we proposed a distribution-free approach which will yield far better performance estimation.

Finally, the research presents a method which uses reference structure to optimize the design of a wireless pyroelectric binary sensor system. Since the number of signature cells is important to the design and data analysis of a sensor system, we explore the maximum number of signatures in a specific sensor system topology. The size and shape distribution of signature cells also play an important role in tracking and identification applications. We will study these characteristics of signature cells in future work.

REFERENCES

[1] B. Benson, G. Chang, D. Manov, B. Graham, and R. Kastner, "Design of a Low-cost Acoustic Modem for Moored Oceanographic Applications," Proc. of WUWNet'06, Sep. 25, 2006, Los Angeles, California, USA.

[2] R. Ramaswami and K.K. Parhi, “Distributed Scheduling of Broadcasts in a radio network,” Proc. of IEEE INFOCOM 1989.

[3] S. Ramanathan, “A unified framework and algorithm for channel assignment in wireless network,” Wireless Networks, Volume5, Number 2, 1999, pp. 81-94.

[4] F. Hu, Y. Malkawi, S. Kumar, and Y. Xiao, “Vertical and Horizontal Synchronization Services with Outlier Detection in Underwater Sensor Networks," Wireless Communications and Mobile Computing (WCMC) Journal, John Wiley & Sons, Vol. 8, No. 9, Nov. 2008, pp. 1165 - 1181, DOI: 10.1002/wcm.559.

[5] F. Hu, P. Tilghman, Y. Malkawi, and Y. Xiao, “A prototype underwater acoustic sensor network platform with topology-aware MAC scheme,” International Journal of Sensor Networks, Vol. 2, Nos.5/6, pp. 386 - 398, 2007.

[6] Y. Zhang, Y. Xiao, M. Chen, P. Bahri, and M. Kamboj, "Medium Access Control layer for underwater sensor networks," Underwater Acoustic Sensor Networks, Auerbach Publications, Taylor & Francis Group, ISBN-10: 1420067117, ISBN-13: 978-1420067118, 2009.

[7] Y. Huang, W. Liang, H.-B. Yu, and Y. Xiao, "Target tracking based on a distributed particle filter in underwater sensor networks,” Wireless Communications and Mobile Computing (WCMC), Special issue on Underwater Sensor Networks: Architectures and Protocols, John Wiley & Sons, Vol. 8, No. 8, pp. 1011 - 1022, Oct. 2008. DOI: 10.1002/wcm.656.

[8] L. Liu, Y. Xiao, and J. Zhang, "Effect of Node Movement to Time Synchronization of Underwater Wireless Sensor Network," Proceedings of IEEE 2009 International Conference on Communications (IEEE ICC 2009).

[9] S. Gandham, Y. Zhang, and Q. Huang, “Distributed Minimal Time Convergecast Scheduling in Wireless Sensor Networks,” Proceedings of the 26th IEEE International Conference on Distributed Computing Systems (ICDCS), 2006.

[10] J. Wang, H. Choi and E. A. Hughes, “Scheduling on Sensor Hybrid Network,” In IEEE ICCCN, 2005.

[11] S.C. Ergen and P. Varaiya, “TDMA scheduling algorithms for wireless sensor networks,” Wireless Networks, vol. 16, 2010, pp. 985–997.

[12] S.C. Ergen and P. Varaiya, “Power efficient and delay aware medium access protocol for sensor networks,” IEEE Trans. on Mobile Computing, vol.5, issue.7, pp.920-930, 2007.

[13] C. Florens, M. Franceschetti, and R.J. McEliece, “Lower bounds on data collection time in sensory networks,” IEEE Journal on selected Areas in Communications, vol. 22, 2004.

[14] C. Florens and R. McEliece, “Packets distribution algorithms for sensor networks,” IEEE Societies INFOCOM 2003.

[15] G. G. Xie and J. Gibson, “A Networking Protocol for Underwater Acoustic Networks,” In Technical Report TR-CS-00-02, Department of Computer Science, Naval Postgraduate School, December 2000.

[16] D. Pompili, T. Melodia, and I.F. Akyildiz, “A Distributed CDMA Medium Access Control for Underwater Acoustic Sensor Networks,” In Proc. of Mediterranean Ad Hoc Networking Workshop (Med-Hoc-Net), Corfu, Greece (2007).

[17] L.F.M. Vieira, J. Kong, U. Lee, and M. Gerla, “Analysis of ALOHA protocols for underwater acoustic sensor networks,” The First ACM International Workshop on Underwater Networks (2006).

[18] N. Chirdchoo, W.S. Soh, and K.C. Chua, “ALOHA-based MAC Protocols with Collision Avoidance for Underwater Acoustic Networks,” The 26th IEEE International Conference on Computer Communications, IEEE, Los Alamitos (2007).

[19] M. Molins, and M. Stojanovic, “Slotted FAMA: a MAC Protocol for Underwater Acoustic Networks,” In OCEANS. Proc. of MTS/IEEE Conference and Exhibition for Ocean Engineering, Science and Technology, Boston, MA (September 2006).

[20] A.A Syed, W. Ye, and J. Heidemann, “T-Lohi: A New Class of MAC Protocols for Underwater Acoustic Sensor Networks,” In Technical Report ISI-TR-638, USC/Information Sciences Institute (April 2007).

[21] F. Salva-Garau, and M. Stojanovic, “Multi-cluster Protocol for Ad Hoc Mobile Underwater Acoustic Networks,” In Proc. of MTS/IEEE OCEANS, San Francisco, CA (September 2003).

[22] A. Sankar and Z. Liu, “Maximum Lifetime Routing in Wireless Ad Hoc Networks,” In Proc. of IEEE INFOCOM, 2004, pp. 1089-1097.

[23] J. H. Chang and L. Tassiulas, “Maximum Lifetime Routing in Wireless Sensor Networks,” IEEE/ACM Transactions on Networking, vol.12, no.4, pp.609-619, 2004.

[24] R. Madan, Z. Q. Luo, and S. Lall, "A Distributed Algorithm with Linear Convergence for Maximum Lifetime Routing in Wireless Sensor Networks," In Proc. of the Allerton Conference on Communication, Control and Computing, 2005.

[25] Z. Abrams, A. Goel, and S. Plotkin, "Set k-cover Algorithms for Energy Efficient Monitoring in Wireless Sensor Networks," In Proc. of IPSN 2004.

[26] C. Liu, K. Wu, Y. Xiao, and B. Sun, "Random Coverage with Guaranteed Connectivity: Joint Scheduling for Wireless Sensor Networks," IEEE Transactions on Parallel and Distributed Systems, Vol. 17, No. 6, June 2006, pp. 562-575.

[27] H. Gupta, S. Das, and Q. Gu, "Connected Sensor Cover: Self-organization of Sensor Networks for Efficient Query Execution," Proc. of Mobihoc 03.

[28] X. Wang, G. Xing, Y. Zhang, C. Lu, R, Pless, and C. Gill, "Integrated Coverage and Connectivity Configuration in Wireless Sensor Networks," Proc. of Sensys 2003.

[29] H. Zhang and J. Hou, "Maintaining Coverage and Connectivity in Large Sensor Networks," Proc. of WTASA 2004.

[30] S. Shakkottai, R. Srikant, and N. Shroff, "Unreliable Sensor Grids: Coverage, Connectivity and Diameter," Proc. of INFOCOM 2003.

[31] L. Wang and Y. Xiao, "A Survey of Energy-Efficient Scheduling Mechanisms in Sensor Networks," Mobile Networks and Applications (MONET), Vol. 11, No. 5, 2006, pp. 723-740.

[32] S. Meguerdichian, F. Koushanfar, M. Potkonjak, and M.B. Srivastava, "Coverage Problem in Wireless Ad-hoc Sensor Networks," Proc. of INFOCOM 2001.

[33] M. Cardei and J. Wu, "Coverage in Wireless Sensor Networks," Handbook of Sensor Networks, M. Ilyas and I. Magboub (eds.), CRC Press, 2004.

[34] A. Saipulla, C. Westphal, B. Liu, and J. Wang, "Barrier Coverage of Line-Based Deployed Wireless Sensor Networks," Proc. of IEEE INFOCOM'09, pp. 127-135, April 2009.

[35] S. Bandyopadhyay and E. Coyle, "An Energy Efficient Hierarchical Clustering Algorithm for Wireless Sensor Networks," Proc. of IEEE INFOCOM'03. pp. 1713 – 1723, April 2003.

[36] P.-J. Wan, and C.-W. Yi, "Coverage by Randomly Deployed Wireless Sensor Networks," IEEE Transactions on Information Theory, Vol. 52, No. 6, pp. 2658-2669, June 2006.

[37] M. Welsh, "Sensor Networks for the Sciences," Communications of the ACM, Vol. 53, No. 11, pp. 36 – 39, November 2010.

[38] B. Hull, V. Bychkovsky, K. Chen, M. Goraczko, A. Miu, E. Shih, Y. Zhang, H. Balakrishnan, and S. Madden, "CarTel: A Distributed Mobile Sensor Computing System," Proceedings of the 4th International Conference on Embedded Networked Sensor Systems (SenSys'06), pp. 125 - 138, 2006.

[39] V. Dyo, S. A. Ellwood, D. W. Macdonald, A. Markham, C. Mascolo, B. Pasztor, S. Scellato, N. Trigoni, R. Wohlers, and K. Yousef, "Evolution and Sustainability of a Wildlife Monitoring Sensor Network," Proceedings of the 8th ACM Conference on Embedded Networked Sensor Systems (SenSys '10). pp. 127- 140, 2010.

[40] I. F. Akyildiz, W. Su, Y. Sankarasubramaniam, and E. Cayirci, "Wireless Sensor Networks: a Survey," Computer Networks, Vol. 38, No. 4, pp. 393 - 422, 2002.

[41] J. Yick, B. Mukherjee, and D. Ghosal, "Wireless Sensor Network Survey," Computer Networks, Vol. 52, No. 12, pp. 2292 – 2330, 2008.

[42] S. Slijepcevic and M. Potkonjak, "Power Efficient Organization of Wireless Sensor Networks," Proc. of IEEE International Conference on Communications, vol 2, pp 472-476, Helsinki, Finland, June 2001.

[43] S. Kumar, T. H. Lai, and A. Arora, "Barrier coverage with wireless sensors," Proceedings of the 11th Annual International Conference on Mobile Computing and Networking (MobiCom '05), pp. 284 – 298, 2005.

[44] W. Li and C. G. Cassandras, "A Minimum-Power Wireless Sensor Network Self-Deployment Scheme," Proceedings of 2005 IEEE Wireless Communications and Networking Conference, 2005.

[45] A. Howard, M. J. Mataric, and G. S. Sukhatme, "An Incremental Self-Deployment Algorithm for Mobile Sensor Network," Autonomous Robots, Vol. 13, pp. 113 – 126, 2002.

[46] V. K. Isler and K. S. Daniilidis, "Sampling based Sensor-Network Deployment," Proceedings of 2004 IEEE/RSJ International Conference on Intelligent Robots and Systems, 2004.

[47] J. Deng, Y.S. Han, W.B. Heinzelman and P.K. Varshney, "Scheduling Sleeping Nodes in High Density Cluster-based Sensor Networks," Mobile Network and Applications, Vol. 10, 2005, pp. 825–835.

[48] J. S. Fang, Q. Hao, D. J. Brady, M. Shankar, B. D. Guenther, N. P. Pitsianis, and K. Y. Hsu, "Path-dependent human identification using a pyroelectric infrared sensor and Fresnel lens arrays," Optics Express, vol. 14 no. 2 , 2006, pp. 609 – 624.

[49] J. Liu, M. Chu, and J. E. Reich, "Multi-target tracking in distributed sensor networks," IEEE Signal Processing Mag., vol. 24, no. 3, May 2007, pp. 36–46.

[50] J. S. Fang, Q. Hao, D. J. Brady, B. D. Guenther and K.Y. Hsu, "Real-time human identification using a pyroelectric infrared detector array and hidden Markov models," Opt. Express , vol. 14 no. 15, 2006, pp. 6643-6658.

[51] M. Shankar, J. Burchett, S. D. Feller, B. Jones, R. Swagart, B. D. Guenther, and D. J. Brady, "Biometric tracking with coded pyroelectric sensor clusters," Proceedings of SPIE - The International Society for Optical Engineering, vol. 5796, 2005, pp. 174 – 185.

[52] B. Jung and G. S. Sukhatme, "Multi-target tracking using a mobile sensor network," In proceedings of the IEEE international conference on Robotics and Automation, Washington, DC, 2002, pp. 1050–1055.

[53] P. Potuluri, M. Xu and D. J. Brady, "Imaging with random 3D reference structures", Opt. Express, vol 11, 2003, pp. 2134-2141.

[54] D. J. Brady, N. P. Pitsianis, and X. Sun, "Reference structure tomography," Opt. Soc. Am. A, vol.21, no. 7, July 2004, pp.16-18.

[55] P. Potuluri and D. J. Brady, "3D spatial segmentation using reference structures," Optics in Computing, OSA topical meeting, Washington, DC, May 2003.

[56] Q. Hao, D. J. Brady, B. D. Guenther, J. B. Burchett, M. Shankar and S. Feller, "Human tracking with wireless distributed pyroelectric sensors," IEEE Sensors Journal, vol. 6 no. 6, 2006, pp. 1683 – 1695.

[57] M. Shankar, J. B. Burchett, Q. Hao, B. D. Guenther and D. J. Brady, "Human-tracking systems using pyroelectric infrared detectors," Optical Engineering, vol. 45 no. 10, 2006, 106401,pp. 1-10.

[58] Q. Hao, F. Hu, and Y. Xiao, "Multiple Human Tracking and Identification with Wireless Distributed Pyroelectric Sensor Systems," IEEE Systems Journal, vol. 3, no. 4, Dec. 2009, pp. 428-439.

[59] P. K. Agarwal, D. J. Brady and J. Matousek, "Segmenting object space by geometric reference structures," ACM Trans. Sensor Networks, vol. 2, no. 4, Nov. 2006, pp. 455-465.

[60] D. J. Brady and Z. U. Rahman, "Integrated analysis and design of analog and digital processing in imaging systems: introduction to feature issue," Appl. Opt. 41, 2002, pp. 6049-6049.

[61] W. T. Cathey and E. R. Dowski, "New paradigm for Imaging Systems," Appl. Opt. 41, 2002, pp. 6080-6092.

[62] G. Barbastathis and D. J. Brady, "Multidimensional tomographic imaging using volume holography," Proceedings of the IEEE 87, 1999, pp. 2098-2120.

[63] D. L. Marks, R. A. Stack, D. J. Brady, D. C. Munson and R. B. Brady, "Visible Cone beam tomography with a lensless interferometric camera," Science 284, 1999, pp. 1561-1564.

[64] T. Wilson, Confocal Microscopy, Academic Press, London, 1992.

[65] E. E. Fenimore, "Coded aperture imaging – predicted performance of uniformly redundant arrays," Appl. Opt. 17, 1978, pp. 3562-3570.

[66] A. R. Gourlay and J. B. Stephen, "Geometric coded aperture masks," Appl. Opt. 22, 1983, pp. 4042-4047.

[67] H. C. Andrews and B. R. Hunt, Digital Image Restoration. Prentice Hall Inc., 1977.

[68] P. Potuluri, "Multiplex optical sensors for reference structure tomography and compressive spectroscopy," Ph.D. dissertation, Dept. Elect. Eng. Duke Univ., Durham, NC, 2005.

[69] N. Chacka and K. Wilson, "Person tracking using audio-video sensor fusion," in SOW Conference, 2002.

[70] J. Aslam, Z. Butler, F. Constantin, V. Crespi, G. Cybenko, and D. Rus, "Tracking a moving object with a binary sensor network," Proc. 1st ACM Conf. on Embedded Networked Sensor Syst., vol. 1, pp. 150-161, Nov. 2003.

[71] T. Hastie, R. Tibshirani and J. Friedman, "The Elements of Statistical Learning - Data Mining, Inference, and Prediction," Springer Series in Statistics, 2001.

[72] Z. I. Botev, "Nonparametric Density Estimation via Diffusion Mixing," Postgraduate Series, Department of Mathematics, The University of Queensland, November 20, 2007, Available: http://espace.library.uq.edu.au/eserv/UQ:120006/diffusion_estimator.pdf and http://www.mathworks.com/matlabcentral/fileexchange/authors/27236.

[73] Y Hu, J.-g. Lou, H. Chen, and J. Li, "Distributed Density Estimation Using Non-parametric Statistics," Proceedings of International Conference of Distributed Computing Systems (ICDCS'07), 2007.

[74] M. Zhou, W. Qian, X. Gang, and A. Zhou, "Multi-dimensional Data Density Estimation in P2P networks," Distributed And Parallel Databases, Vol. 26, No. 2-3, 261 – 289, 2009.

[75] J.-N. Hwang, S.-R. Lay, and A. Lippman, "Nonparametric Multivariate Density Estimation: A Comparative Study," IEEE Transactions on Signal Processing, Vol 42, No 10, pp. 2795 – 2810, October 1994.

[76] K. Keith, Mathematical Statistics. London, U.K.: Chapman & Hall, 2000.

[77] Y. Xiao and J. Rosdahl, “Throughput analysis for IEEE 802.11a higher data rates,” In IEEE 802.11 Plenary Meeting, St. Louis, MO, Mar. 11–15, 2002, Doc. No. IEEE 802.11-02-138.

[78] Y. Xiao, "Throughput and Delay Limits of IEEE 802.11," IEEE Communications Letters, Vol. 6, No. 8, Aug. 2002, pp. 355-357.

[79] M. Peng and Y. Xiao, “Upper Bound on Network Utilization under Fair-Access in Multi-hop Wireless Grid Sensor Networks with 3-4 Rows,” msn, pp.244-251, 2009 Fifth International Conference on Mobile Ad-hoc and Sensor Networks, 2009.

[80] T. Hastie, R. Tibshirani and J. Friedman, “The Elements of Statistical Learning - Data Mining, Inference, and Prediction,” Springer Series in Statistics, 2001.

[81] A. Baggio and K. Langendoen, “Monte-Carlo Localization for Mobile Wireless Sensor Networks,” Proc. of 2nd International Conference on Mobile Ad-hoc and Sensor Networks Second International Conference(MSN 2006), pp. 317 – 328, Hong Kong, China, December 13-15, 2006.

[82] N. Bulusu, J. Heidemann, and D. Estrin, “GPS-less Low Cost Outdoor Localization for Very Small Devices,” IEEE Personal Communications Magazine, Vol. 7, No. 4, pp. 28 – 34, August 2000.

[83] T. He, C. Huang, B. M. Blum, J. A. Stankovic, and T. Abdelzaher, “Range-free localization Schemes in Large-scale Sensor Networks,” Proc. of the 9th Annual International Conference on Mobile Computing and Networking (MobiCom’03), pp. 81 – 95, 2003.

[84] Loukas Lazos and R. Poovendran, “SeRLoc: Secure Range-Independent Localization for Wireless Sensor Networks,” ACM Transactions on Sensor Networks, Vol. 1, No. 1, pp. 73-100, 2005.

[85] D. Niculescu and B. Nath, “Ad Hoc Positioning System (APS) using AOA,” Proc. of 22nd Annual Joint Conference of the IEEE Computer and Communications Societies (InfoCom’03), Vol. 3, pp. 1734 – 1743, April, 2003.

[86] Y. Shang, W. Ruml, Y. Zhang, and P. J. Fromherz, “Localization from Mere Connectivity,” Proc. of 4th ACM International Symposium on Mobile and Ad Hoc Networking and Computing (MobiHoc’03), pp. 201 – 212, 2003.

[87] Y. Hu, J.-g. Lou, H. Chen, and J. Li, “Distributed Density Estimation Using Non-parametric Statistics,” Proceedings of International Conference of Distributed Computing Systems (ICDCS’07), 2007.